DEPARTMENT OF THE INTERIOR

U.S. GEOLOGICAL SURVEY

THE OLNEY, ILLINOIS, EARTHQUAKE OF 10 JUNE 1987:
A PRELIMINARY REPORT

by

C. J. Langer[1]. Philip S. Powers[1], Arch C. Johnston[2], and G.A. Bollinger[1,3]
(Section I)

and

David Carver[1], Robert A. Williams[1], and Edward Cranswick[1]
(Section II)

Open-File Report 87-623

This report is preliminary and has not been reviewed for conformity with U.S. Geological Survey editorial standards and stratigraphic nomenclature. Any use of trade names is for descriptive purposes only and does not imply endorsement by the USGS.

---

[1]U.S. Geological Survey, Denver Federal Center, Denver, CO
[2]Tennessee Earthquake Information Center, Memphis State Univ., Memphis, TN
[3]Dept. of Geological Sciences, VPI and SU, Blacksburg, VA

1987

CONTENTS

Section I: Overview of the Main Shock, It's Tectonic Environment, and Some
     Aftershock Locations
          C. J. Langer, Philip S. Powers, Arch. C. Johnston, G. A. Bollinger

ILLUSTRATIONS

TABLES

Section II: Digital Seismograms of Locally Recorded Aftershocks and
     Recordings of a Magnitude 4.1_{mbLg} Regional Earthquake at the same
     sites
          David Carver, Robert A. Williams, Edward Cranswick

ILLUSTRATIONS

TABLES

SECTION I

OVERVIEW OF THE MAIN SHOCK, ITS TECTONIC ENVIRONMENT

AND SOME AFTERSHOCK LOCATIONS

1

OVERVIEW OF THE MAIN SHOCK, ITS TECTONIC ENVIRONMENT, AND SOME AFTERSHOCK LOCATIONS

C. J. Langer, Philip S. Powers, Arch C. Johnston, and
G. A. Bollinger

INTRODUCTION

Section 1 of this report briefly describes the preliminary results of some of the investigations as a consequence of the southeastern Illinois earthquake of 10 June 1987. These investigations include determination of the hypocenter and a provisional focal mechanism for the main shock, an estimate of the felt region including some specific intensity observations, and an aftershock study employing portable smoked-paper and digital recording seismic instrumentation. The section concludes with a short discussion of the seismotectonic setting of the earthquake zone. An Appendix is also included which lists parameters of aftershocks located to date.

MAIN SHOCK

Preliminary Determination of Epicenters (PDE) No. 23-87 (25 June 1987) gives the following coordinates for the June 10, 1987 main shock:

Latitude:	38.713° N.	Depth:	10 km
Longitude:	87.954° W.	Origin time:	23:48:54 UTC (6:48 pm CDT)
m_{bLg}:	5.1 (SLM)	m_b:	4.9
		M_s:	4.4

The above location places the epicenter in southeastern Illinois (see figs. 1 and 2), roughly 200 km east of St. Louis, Mo., and about 12 km east of the town of Olney.

A provisional focal mechanism solution was determined from P-wave polarity readings taken from 59 short period seismograms (see fig. 3). The solution is well constrained and indicates right lateral strike-slip on a northeast striking plane (Y) or left-lateral strike-slip on a northwest striking plane (X).

INTENSITY SURVEY

The intensity survey is still in progress. To date, a total of more than 3,000 felt reports have been obtained and are presently being analyzed. It appears that the maximum intensity was VII, based on the following reported effects: "chimneys cracked, bricks fell from chimneys, windows cracked as were stone/brick fences and interior/exterior brick walls, hanging objects swung moderately and springs/well water muddied". PDE No. 23-87 reported minor damage in parts of Illinois, Indiana, and Kentucky and felt reports from parts of 21 states and Canada (see fig. 1).
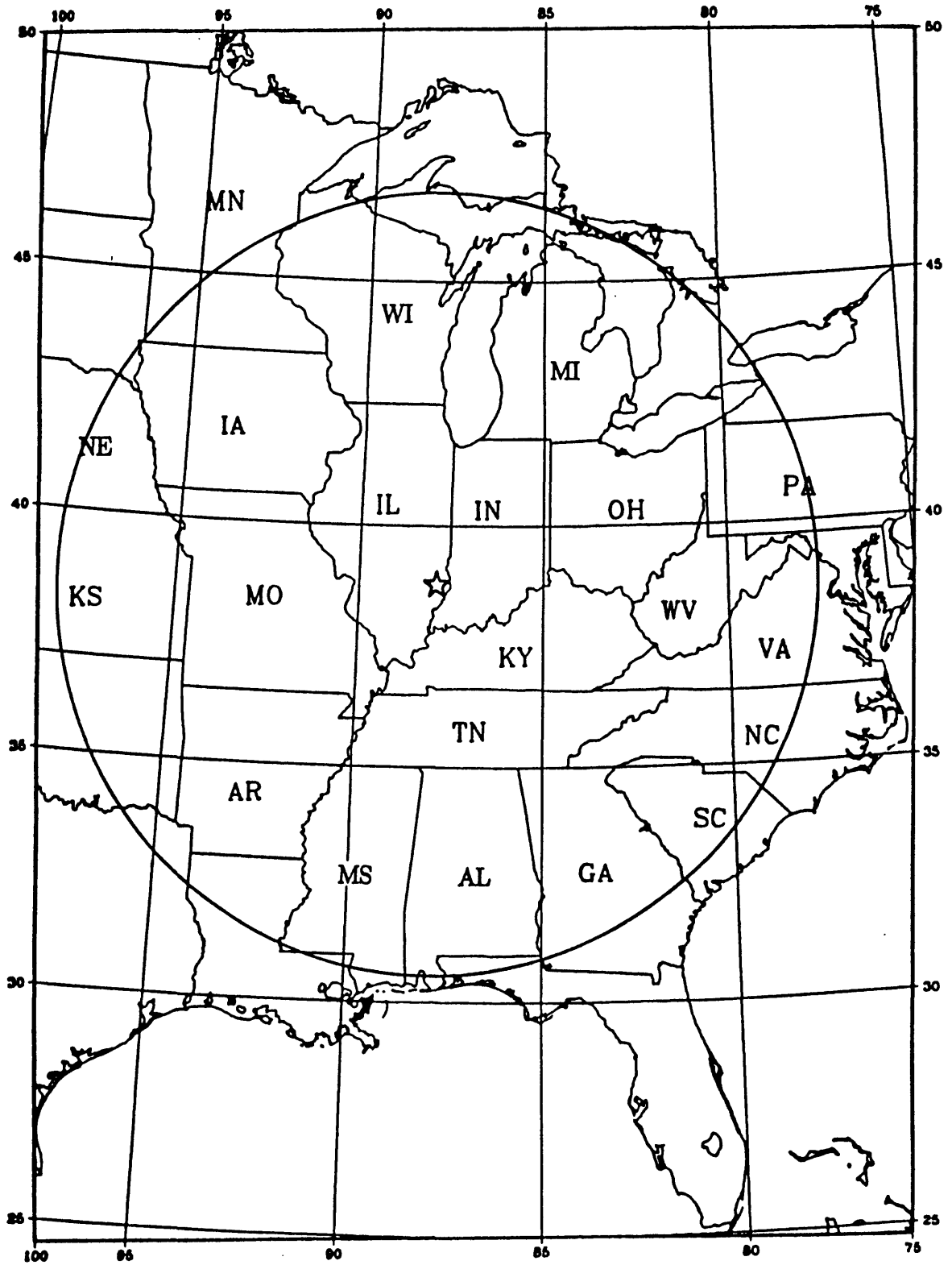
Figure 1.—Map showing area of felt information for 10 June 1987 southern
Illinois earthquake.   The earthquake was felt in at least part of states
indicated by initials.   Circle, with 900 km radius, shows approximate
extent of Postmaster canvass.   Star denotes main shock epicenter.   (Map
provided by B. G. Reagor, U.S. Geological Survey.)
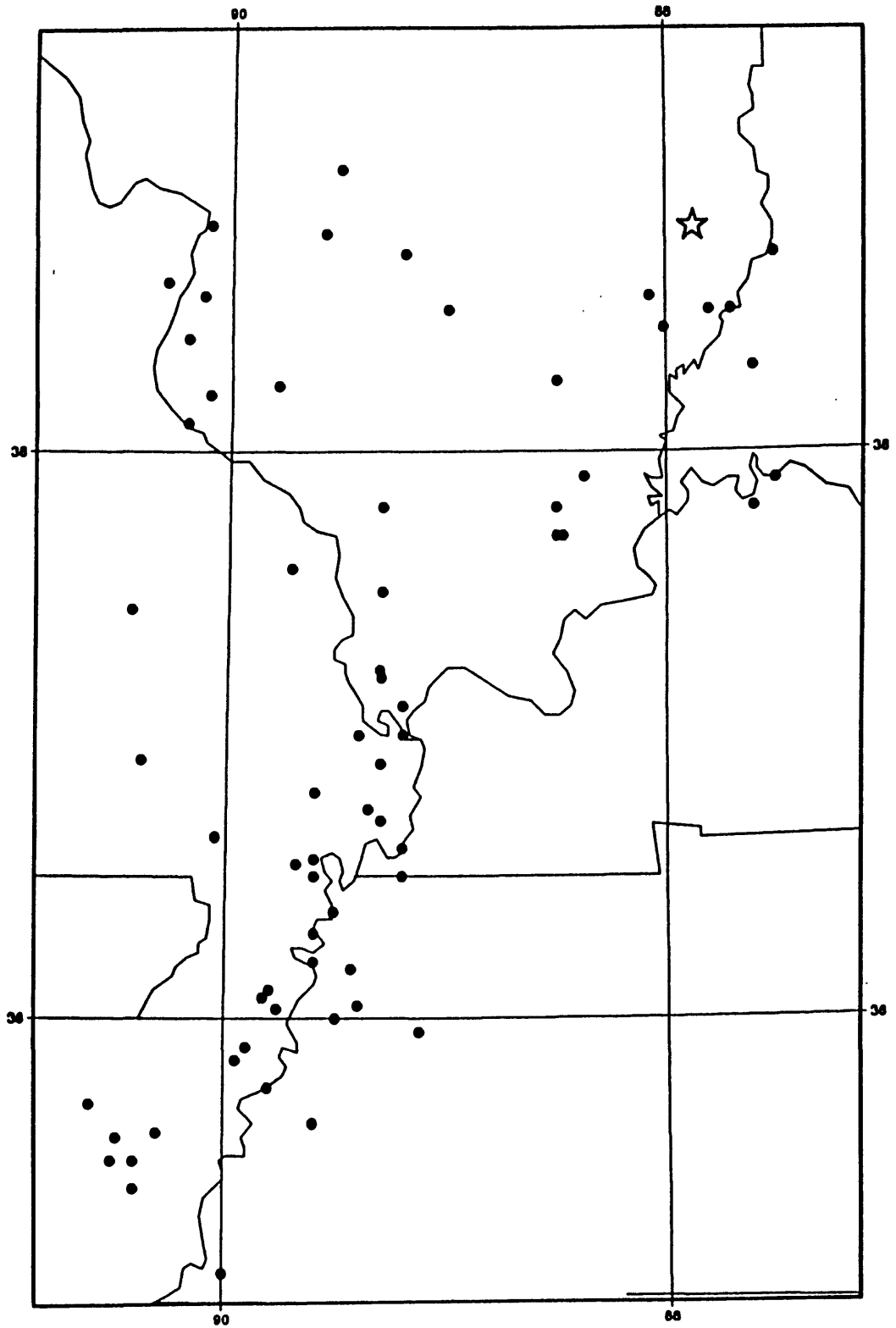
Figure 2.--Map showing historical seismicity of New Madrid fault zone. Dots
    show locations of historical epicenters and star indicates epicenter of
    10 June 1987 earthquake. (From historical data file compiled by
    B. G. Reagor and C. W. Stover, U.S. Geological Survey.)

N

T

△ = COMPRESSIONAL
X = DILATATIONAL
☐ = NODAL

E
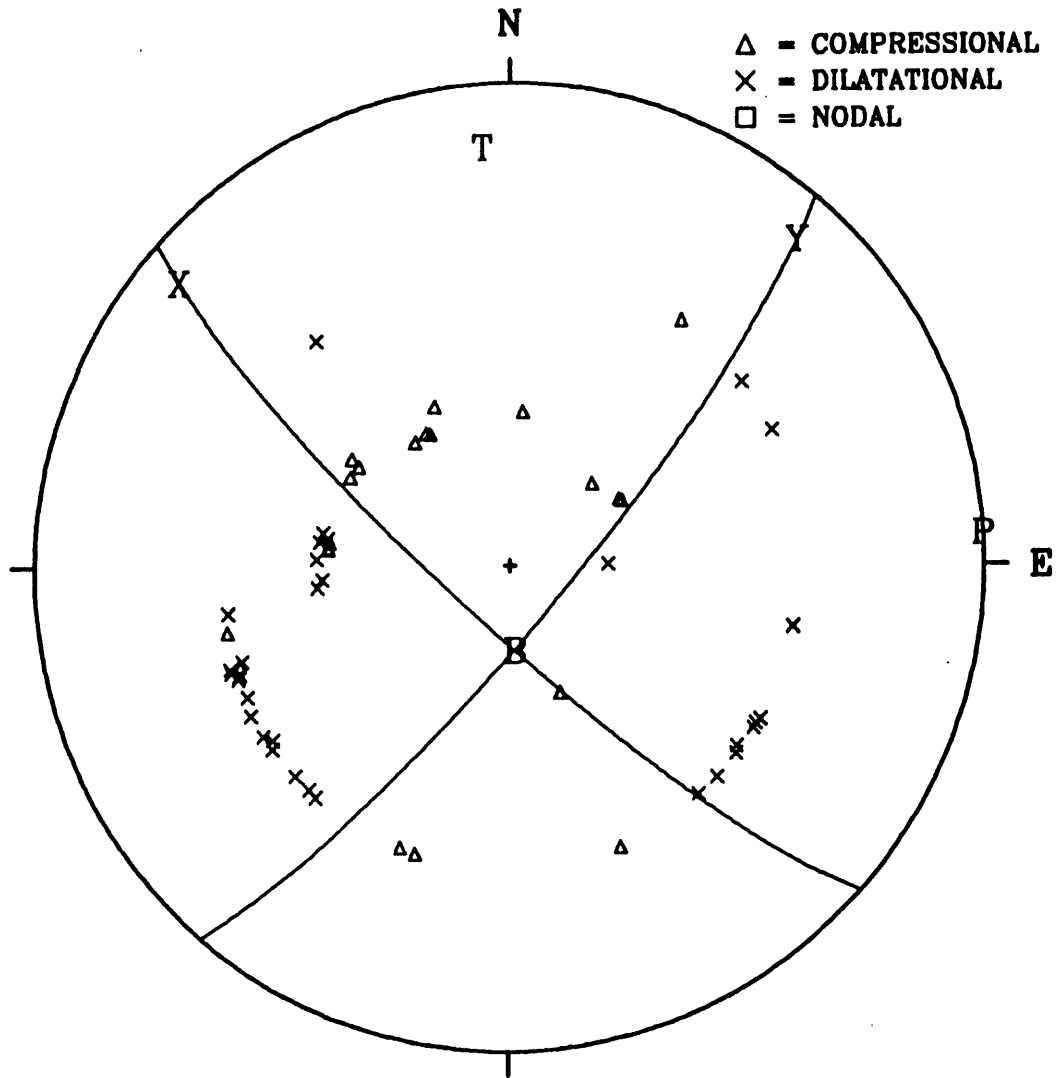
Olney, Illinois Earthquake —— 6/10/87

Figure 3.—Preliminary focal mechanism solution (lower hemisphere, equal-area
projection) for the main shock on 10 June 1987. The X nodal plane strikes
N. 50° W. and dips 80° SW; the Y nodal plane strikes N. 42° E. and dips
80° SE. Axes of maximum and minimum compressive stress shown by P and
T symbols, respectively. Fifty-nine short-period first motion readings
used; there are five inconsistencies. (Data were provided by Dave Gordon
and Russ Needham, U.S. Geological Survey, and by the Center for Earthquake
Research and Information, Memphis State University.)

Table 1. Main shock focal mechanism -- Station data for 1987 Olney, Illinois, earthquake.

Station	Distance (deg)	Azimuth (deg)	dt/d W (sec/deg)	JB Focal Angle(deg)	Quality, Direction, & Source of Earth Motion			
SMKY	1.399	157.52	14.28	52.29	I	C	SP	P
ELC	1.753	215.59	14.27	127.76	I	C	SP	P
FVM	2.082	250.11	14.27	52.24	I	D	SP	P
IN1	2.414	40.44	14.26	127.81	E	D	SP	P
IN4	2.515	69.33	14.26	127.81	E	D	SP	P
UTM	2.551	198.34	14.26	52.19	I	C	SP	P
AN11	3.123	52.85	14.24	127.91	E	D	SP	P
AN10	3.207	55.83	14.24	127.91	E	D	SP	P
AN8	3.217	60.60	14.24	127.91	I	D	SP	P
AN9	3.322	52.15	14.24	52.09	I	D	SP	P
AN4	3.475	63.16	14.23	52.04	E	D	SP	P
POW	3.634	226.14	14.22	51.98	E	D	SP	P
BHT	3.736	139.21	14.22	128.02	E	D	SP	P
CCVA	4.001	120.58	14.21	51.93	E	D	SP	P
ACM	4.235	21.44	14.20	128.12	E	C	SP	P
GBTN	4.265	134.47	14.20	51.88	E	D	SP	P
OLY	4.270	222.32	14.20	51.88	E	D	SP	P
ETT	4.391	139.41	14.19	51.83	E	D	SP	P
RICH	4.952	122.79	14.16	51.68	E	D	SP	P
RBNC	5.198	128.70	14.16	51.68	E	D	SP	P
BRBC	5.409	121.63	14.13	51.52	E	D	SP	P
NAV	5.821	101.71	14.10	51.37	E	D	SP	P
BLA	6.135	101.88	14.10	51.37	I	D	SP	P
RLO	6.180	247.81	14.10	51.37	I	D	SP	P
TUL	6.851	248.26	14.03	51.02	I	D	SP	P
JSC	6.975	127.40	14.03	51.02	I	D	SP	P
BHO	7.053	234.24	14.03	51.02	I	D	SP	P
VVO	7.086	243.94	14.03	51.02	E	D	SP	P
SIO	7.299	248.58	13.98	50.76	E	D	SP	P
PCO	7.443	257.02	13.98	50.76	I	C	SP	P
OCO	8.250	250.19	13.89	50.31	E	C	SP	P
ACO	9.102	260.66	13.84	50.07	E	D	SP	P
QZO	9.869	250.80	13.73	49.53	I	D	SP	P
GLA	22.460	263.68	9.87	33.15	E	D	SP	P
NOP	22.516	272.21	9.87	33.15	E	D	SP	P
TNP	22.911	277.62	9.78	32.81	E	D	SP	P
NEW	23.094	303.86	9.78	32.81	I	C	SP	P
KVN	23.429	280.34	9.70	32.51	E	D	SP	P
MNA	23.574	278.84	9.70	32.51	E	C	SP	P
PLM	23.934	265.99	9.62	32.21	E	D	SP	P
CMB	25.371	278.72	9.43	31.50	E	D	SP	P
LON	25.979	298.99	9.39	31.35	E	C	SP	P
LLA	26.129	275.76	9.39	31.35	E	C	SP	P
ARN	26.410	277.62	9.34	31.16	E	C	SP	P
MHC	26.496	277.65	9.34	31.16	E	C	SP	P
PRS	26.535	275.34	9.34	31.16	E	C	SP	P
MCW	26.905	303.10	9.29	30.98	E	C	SP	P
RSNT	28.785	334.36	9.05	30.09	E	C	SP	P
FBA	43.029	327.28	8.11	26.70	E	C	SP	P
PMR	43.333	322.36	8.08	26.59	E	C	SP	P

Table 1. Main shock focal mechanism — station data for 1987 Olney, Illinois earthquake...Continued.

Station	Distance (deg)	(Azimuth) (deg)	dt/d W (sec/deg)	JB Focal Angle(deg)	Quality, Direction, & Source of Earth Motion			
FBA	43.029	327.28	8.11	26.70	I	C	SP	P
ALE	44.752	4.62	8.00	26.31	E	C	SP	P
IMA	45.583	328.62	7.97	26.20	E	C	SP	P
ZOBO	57.760	157.35	7.04	22.96	I	C	SP	P
LPB	58.016	157.42	7.04	22.96	E	C	SP	P
EPLA	61.038	60.27	6.81	22.17	I	C	SP	P
GUD	62.066	58.90	6.73	21.89	I	C	SP	P
KBA	69.515	45.69	6.11	19.79	I	C	SP	P
KIC	80.763	89.25	5.26	16.94	I	D	SP	P

Table 2.

Operational List for Portable Aftershock Network of Analog Seismographs

Station Code	Installed-Date/Time(UTC)		Removed-Date/Time(UTC)	
ART	6/12	17:50	6/16	18:06
BUG	6/12	15:43	6/16	15:47
JOE	6/12	19:21	6/16	19:01
KEL	6/12	13:12	6/16	19:53
LOY	6/13	21.16	6/16	19:10
OBB	6/12	22:57	6/16	18:32
PAL	6/13	12:48	6/16	16:05
SAR	6/13	15:54	6/16	14:05
SCH	6/13	14:02	6/16	15:15
TIC	6/12	21:27	6/16	13:49
ROS	6/12	17:10	6/16	14:00
MUD	6/12	18:00	6/16	04:30
BON	6/12	19:35	6/16	14:30
HAR	6/12	20:00	6/16	15:30
TIK	6/15	18:50	6/16	15:00

(On and off times for ROS, MUD, BON, HAR, and TIK are approximate.)

AFTERSHOCK SURVEY

Within 1-1/2 days following the main shock, the installation of a portable network of analog and digital seismographs was in progress. Table 2 presents an operational log for the ten USGS analog stations (smoked-paper recording systems); the digital stations and their results are described in a separate report included herein (Carver and others, Section II). Network operation continued for about four days and the results described in the following discussion include data from five additional analog stations operated by personnel from the Tennessee Earthquake Information Center.

Approximately 100 aftershocks were recorded of which about half (55) have been located thus far using HYPOELLIPSE. Most solution Quality measures are A/A, average GAP Z 68 deg and average DMIN Z 3 km (see Table A-1 for a full listing of hypocentral parameters). In fact, there were usually about ten stations whose epicentral distances were less than the computed focal depths. These parameters attest to the high quality of the computed hypocentral locations. The velocity model utilized was the St. Louis University Uplands Model (see Appendix) with a V_p/V_s of 1.77 (refer to fig. 4).

Figures 5 through 10 present the station distribution along with map view epicentral plots and vertical section focal depth plots including associated standard error measures [ERH ellipses (ave = 0.4 km) or ERZ bars (ave = 1.0 km)]. The hypocentral zone is very small indeed and occupies a volume, somewhat elongate to the northeast: the zone is about 1.5 km long, 1.0 km wide, with some 4 km of vertical extent between about 8 and 12 km in depth. Explanation of this unusual, but not rare, nearly cylindrical aftershock distribution will be a primary objective in our ongoing studies of this important shock.

Focal mechanism solutions for the aftershocks are being developed. Some very preliminary single-event solutions and a cursory examination of the P-wave first motion patterns in general seem to indicate either reverse displacement on north- to northeasterly striking planes, right-lateral strike-slip motion on planes striking northeast to east-northeast, or a combination thereof.

SEISMOTECTONIC SETTING

The June 10th earthquake occurred in the Wabash Valley seismic zone in southeastern Illinois and southwestern Indiana as identified by Nuttli and Herrmann (1978) and Nuttli (1979). That zone has a record of seismic activity dating back to 1860 and includes six shocks with 5.0FMF5.5 in the last 88 yrs. Interestingly, those earthquakes, which are rather large for the midwest, occur with a modest amount of regularity every 18±16 years (table 3). The identification of the zone was based primarily on the historical seismicity record, but the presence of the north-northeasterly trending Wabash Valley fault system in the southern half of the 200-km-long zone was noted. It was also noted that the seismicity data were too sparse to determine whether it was one continuous zone or a series of discontinuous smaller zones. Gordon (1987) relocated eight earthquakes (1958-1980) and found four of them to have focal depths in excess of 20 km (see table 4).
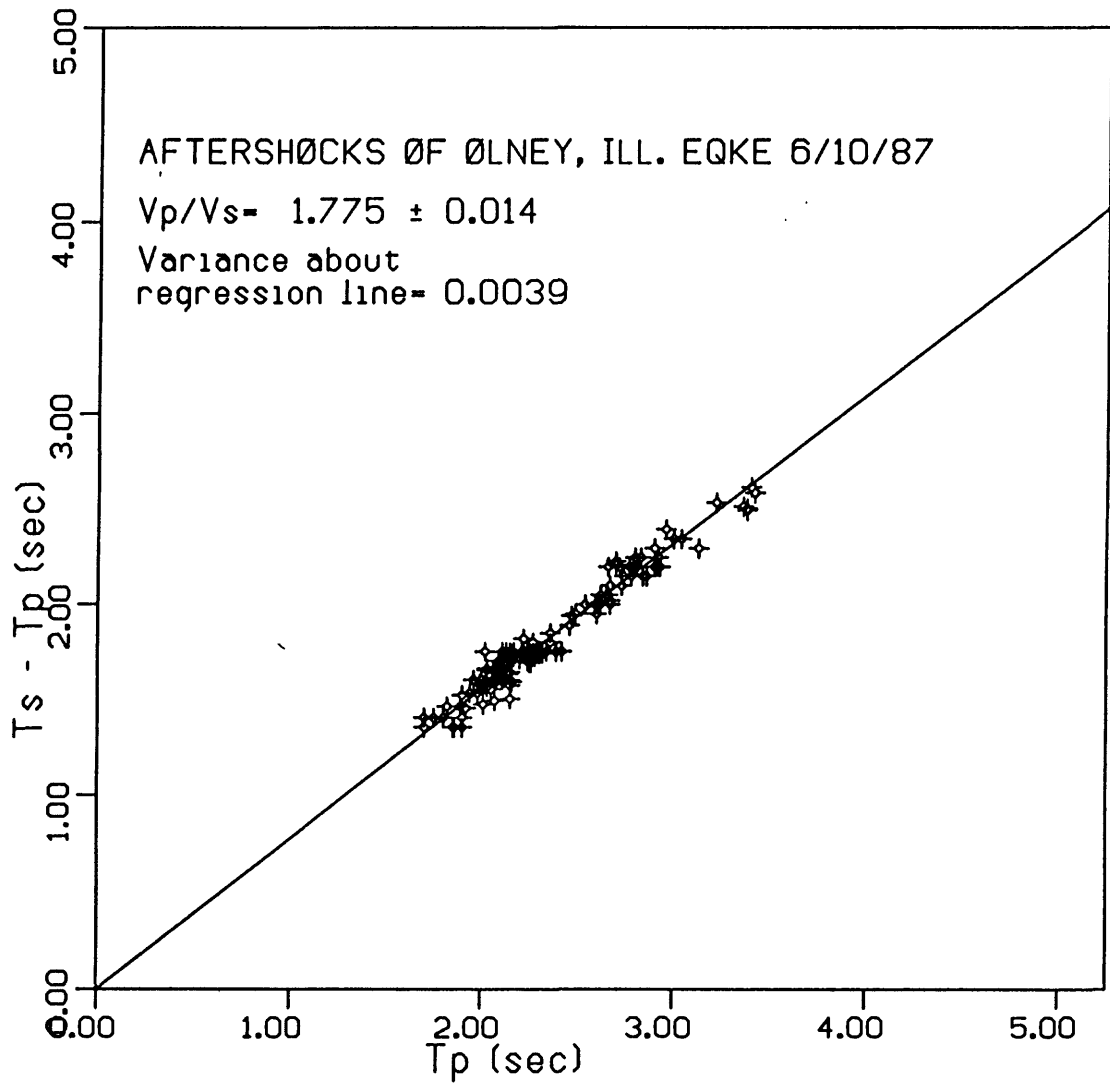
Figure 4.--Wadati plot (Ts - Tp vs. Tp) using only s readings with travel-time residuals ≤ .05 sec.
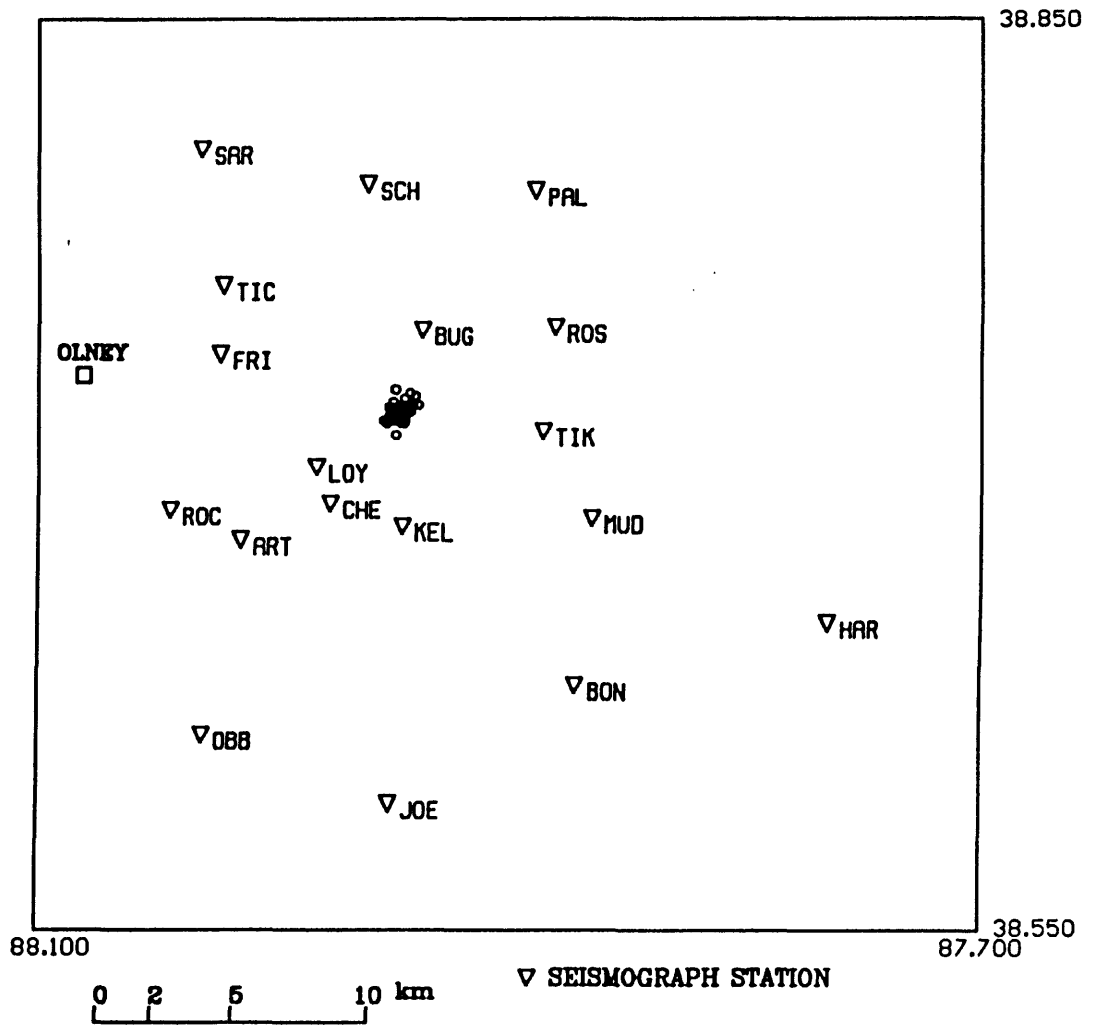
Figure 5.--Plot of aftershock epicenters (small circles) and seismograph
stations (inverted triangles with 3-letter codes). Town of Olney,
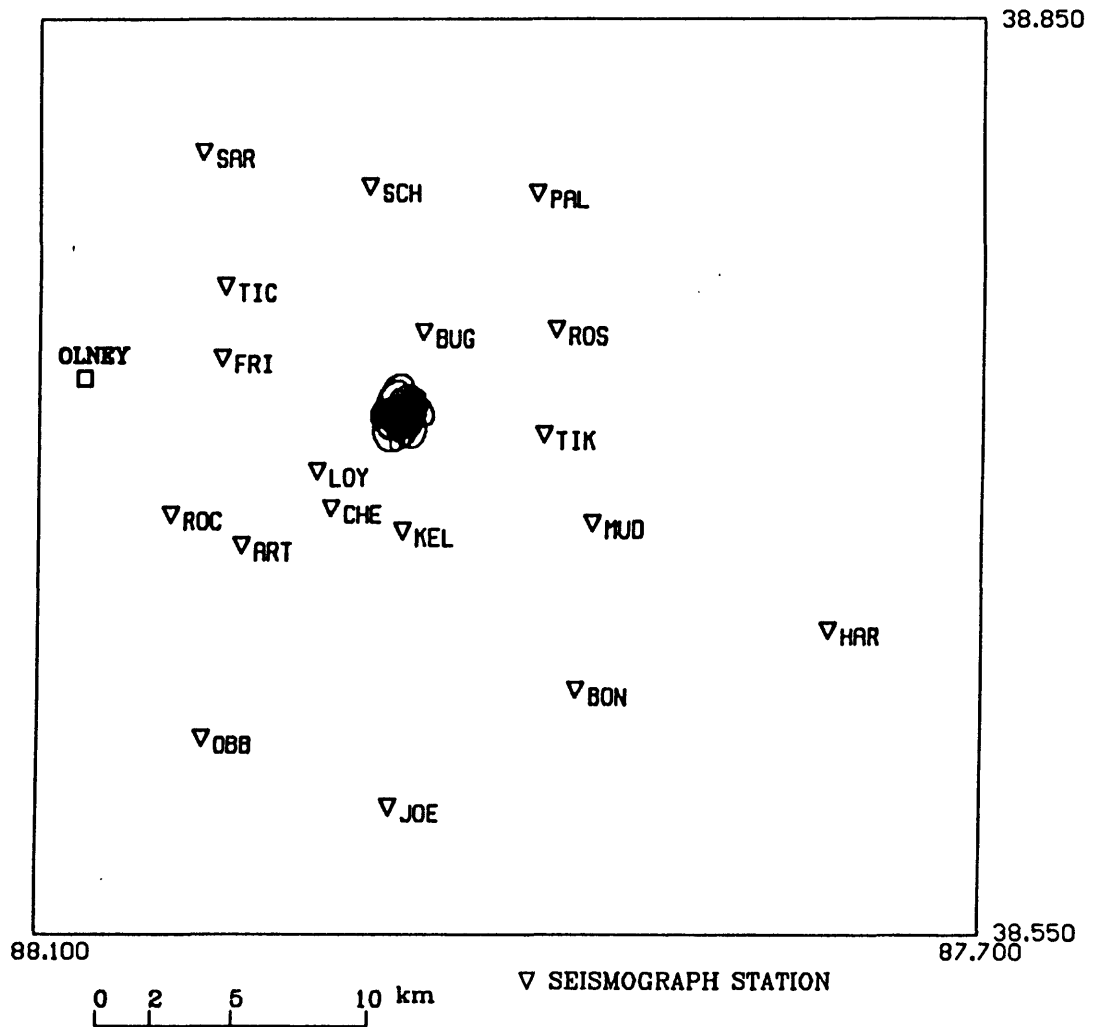Illinois, shown by square symbol.

Figure 6.—Plot of aftershock epicenters with associated 94 percent
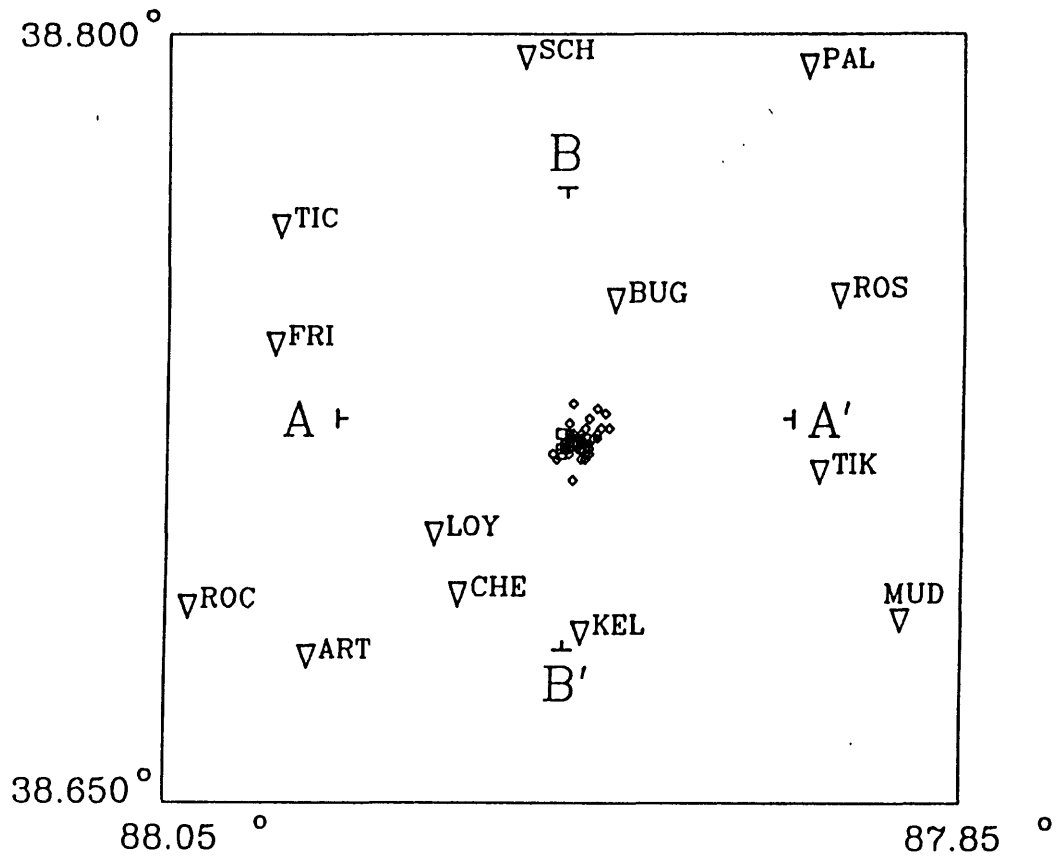 confidence ellipses. Symbols same as fig. 5.

12

Figure 7.--Enlarged plot of aftershocks showing detail in epicentral and
    magnitude distributions, also key for vertical sections A-A' and
    B-B'; refer to sections for distance scale. Magnitude symbols:
    diamond = $0.0 \leq Md \leq 0.99$, square = $1.0 \leq Md \leq 1.99$, circle
    (only one) = $2.0 \leq Md \leq 2.99$.   See table A-1 for definition of
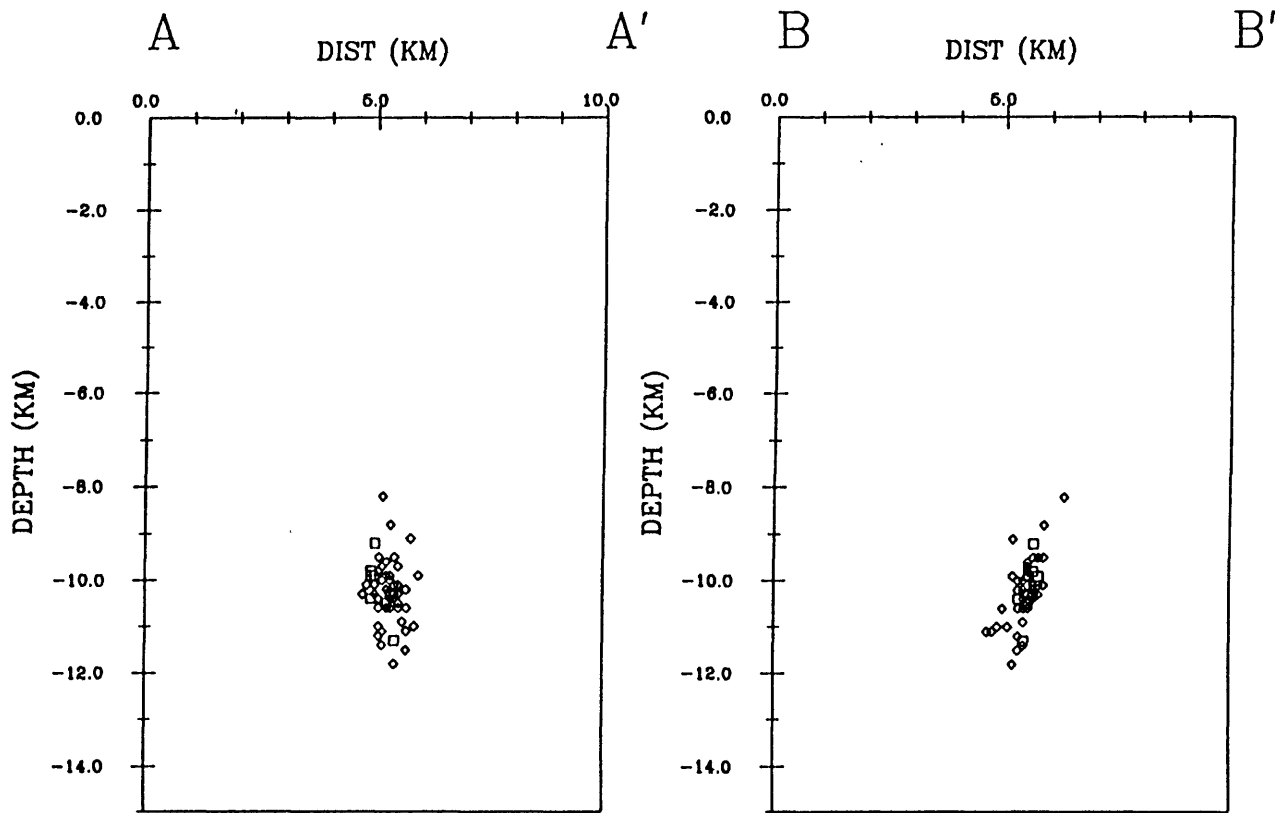   Md.

Figure 8.--East-west (A-A') and north-south (B-B') vertical section plots
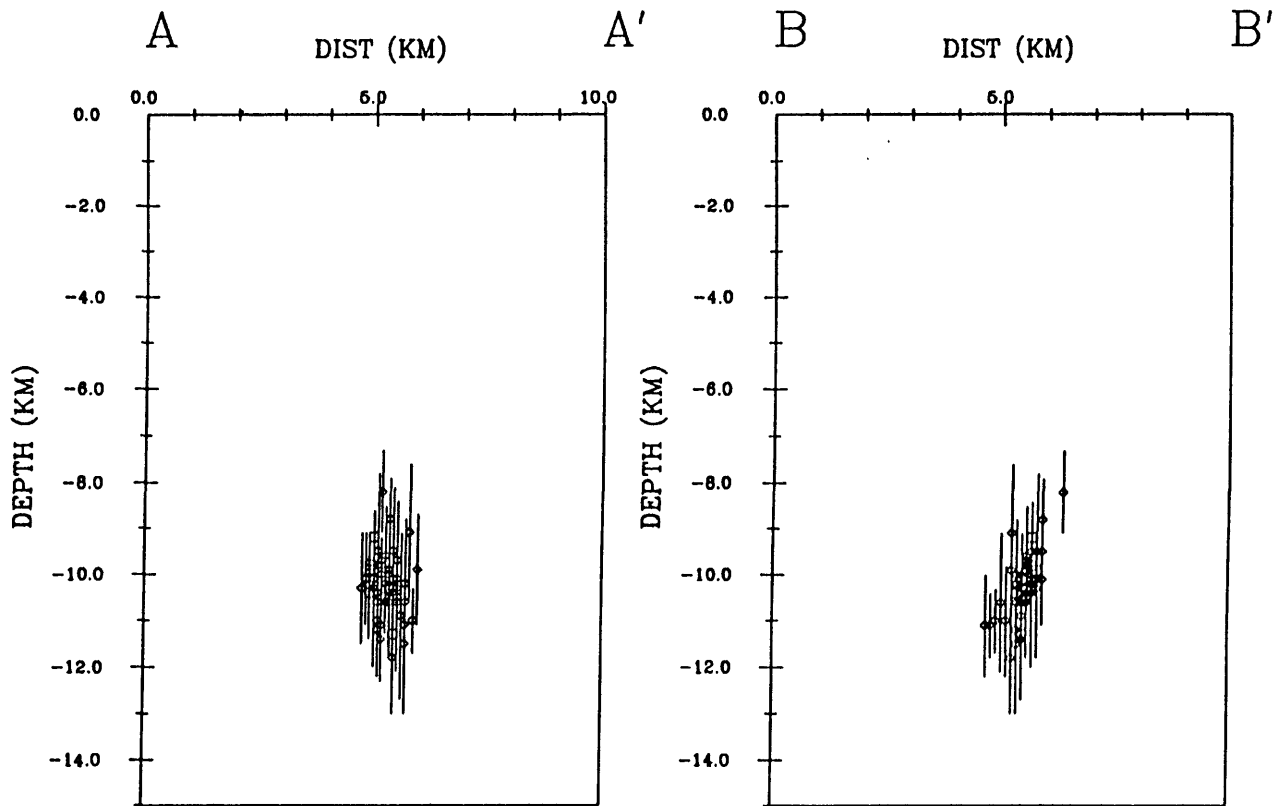   keyed to fig. 7, no vertical exaggeration. Symbols same as fig. 7.

Figure 9.--Vertical section plots, same as fig. 8, with vertical error (ERZ) bars (94 percent confidence limits).
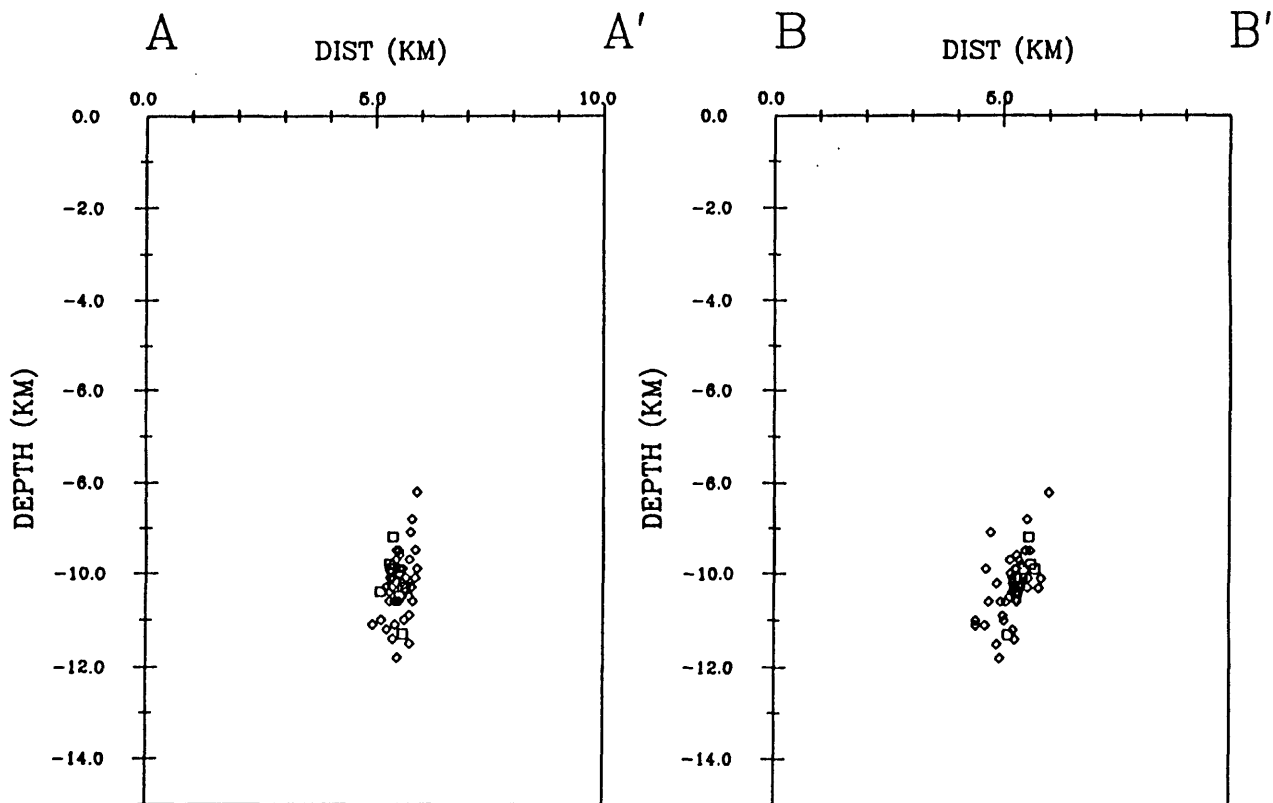
Figure 10.--Vertical section plots, same as fig. 8, rotated 40° clockwise from east-west, north-south alignment.

16

Table 3.

Magnitude 5 or greater earthquakes in the Wabash Valley Seismic Zone (Nuttli and Herrmann, 1978)

Date Yr-Mo-Dy	Lat deg N	Long deg W	m_b	MMI_o	Time Interval Yrs.
1899.04.30	38.8	87.0	5.0	VII	
					10.4
1909.09.27	39.5	87.4	5.3	VII	
					13.2
1922.11.27	37.8	88.5	5.0	VII	
					2.3
1925.04.27	38.3	87.6	5.0	VII[*]	
					43.5
1968.11.09	38.0	88.5	5.5	VII	
					18.6
1987.06.10	38.7	88.0	5.1[**]	VII	
				AVERAGE	17.6 ± 15.6 yrs.

[*]Listed as an intensity VI in Seismicity Map of the State of Indiana by Stover and others, 1979, Misc. Map MF-1145.

[**]m_{blg}

Table 4.

Relocated historic earthquakes in the Wabash Valley seismic zone (Gordon, 1987)

Date (Yr-Mo-Dy)	Lat. (deg N)	Long. (deg W)	Depth (km)	Magnitude
58.11.08	38.436	88.008	4.9	4.4
62.06.27	37.900	88.638	6.8	3.9
68.11.09	37.911	88.373	21.2	5.5
71.02.12	38.497	87.847	15.0	3.1
74.04.03	38.549	88.072	13.5	4.7
78.06.02	38.412	88.464	20.4	3.2
78.12.05	38.557	88.373	23.4	3.5
80.03.13	37.895	88.436	20.3	3.0
*(87.06.10	38.713	87.954	10	5.1)

*Study earthquake, this report.

Six focal mechanism solutions have been reported thus far from the zone (Nuttli, 1979; Herrmann, 1979). Four show reverse faulting and two are strike slip; all have northerly trending nodal planes that are subparallel to the strike of the Wabash Valley fault system. Note that the same subparallelism is true for the previously mentioned focal mechanism solution for the recent shock.

Braile and others (1982) have suggested that the Wabash Valley seismic zone may be related genetically to the larger, more active New Madrid seismic zone about 150 km to the southwest, as an offset continuation of the Reelfoot rift. The southwest boundary of the northeast-trending Wabash Valley zone is defined geologically by the east-southeast-striking Cottage Grove-Rough Creek fault zones and geophysically by a prominent east-southeast-trending magnetic lineament. The northeast boundary is set arbitrarily at 39° N. lat. where the gravity and magnetic expression of the zone is lost (Thenhaus, 1983).

The Wabash Valley fault zone is situated in the southern half of the seismic zone, which is geologically part of the Illinois Basin. The fault zone is about 100 km long, trends north-northeast and is characterized by generally parallel, high-angle, normal faults that bound horsts and grabens. Maximum displacements are up to 146 m, and the faulting is post Pennsylvanian and pre-Pleistocene in age (Bristol and Treworgy, 1979). Sixty-eight kilometers of seismic-reflection profiles across the northern end of the fault zone (f50 km south of Olney, Ill.) imaged a series of northeasterly trending grabens in the Precambrian basement (Sexton and others, 1986). The interpretation developed from those data was that the Wabash Valley faults resulted from a post-Pennsylvanian reactivation of late Precambrian rift structures. Because the major graben features are at depths between about 4 and 7 km and the hypocentral locations for the main shock and aftershocks are at depths of about 8-12 km, there is an implied association between the current seismicity and a northern extension of the basement rift system rather than the Wabash Valley faults exposed at the surface some 30-40 km to the southeast. The near east-west orientation of the axis of maximum compressive stress for the midcontinent region (Zoback and Zoback, 1980; Dart, 1985), is favorably directed so that reverse and/or right-lateral strike slip fault displacement (the same as indicated by our aftershock focal mechanisms) can occur, respectively, along preexisting north to northeast striking zones of weakness (the ancient rift structures). A similar association between basement rift structures and seismicity is seen in the Reelfoot rift to the southwest.

ACKNOWLEDGMENTS

REFERENCES AND BIBLIOGRAPHY

Bell, A.H., Atherton, E., Bushbach, T.C., and Swann, D.H., 1964, Deep oil possibilities of the Illinois basin: Illinois State Geological Survey Circular 368, 38 p.

Braile, L.W., Hinze, W.J., Sexton, J.L., Keller, G.R., and Lidiak, E.G., 1979, An integrated geophysical and geological study of the tectonic framework of the 38th parallel lineament in the vicinity of its intersection with the extension of the New Madrid Fault Zone: U.S. NUCLEAR REGULATORY COMMISSION NUREG/CR-9014, 191 p.

Braile, L.W., Hinze, W.J., Keller, G.R., Lidiak, E.G., 1982, The northeastern extension of the New Madrid Seismic Zone: in, McKeown, F. A., and Pakiser, L. C., ed., Investigations of the New Madrid, Missouri, earthquake region: U.S. Geological Survey Professional Paper 1236, p. 175-184.

Braile, L.W., Hinze, W.J., Sexton, J.L., Keller, G.R., and Lidiak, E.G., 1984, Tectonic development of the New Madrid seismic zone: in, Gori, P.L. and Hays, W.W., ed., Proceedings of the Tectonic symposium of the "New Madrid seismic zone", U.S. Geological Survey Open-File Report 84-770, p. 204-233.

Bristol, Hubert M., and Treworgy, J.D., 1979, The Wabash Valley Fault System in Illinois: Illinois State Geological Survey Division Circular 509, 19 p.

Clark, S.K., and Royds, J.S., 1948, Structural trends and fault systems in eastern interior basin: Bulletin of American Association of Petroleum Geologists, v. 32, pp. 1728-1749.

Dart, Richard, 1985, Horizontal stress directions in the Denver and Illinois Basins from the orientations of borehole breakouts: U.S. Geological Survey Open-File Report 85-733, 41 p.

Dewey, J.W., Hill, D.P., Ellsworth, W.L., and Engdahl, E.R., 1987, Earthquakes, faults, and the seismotectonic framework of the contiguous United States: in, Pakiser, L.C., and Mooney, W.D., eds., Geophysical Framework of the Continental United States, G.S.A. Memoir, in review.

Docekal, Jerry, 1971, Earthquakes of the stable interior with emphasis on the midcontinent: University of Nebraska Dept. of Geology, PhD Dissertation.

Gordon, D.W., 1987, Revised instrument hypocenters and correlation of earthquake locations and tectonics in the Central United States: U.S. Geological Survey Professional Paper 1364, 183 p., in press.

Gori, P.L., and Hays, W.W., ed., 1984, Proceedings of the symposium on "The New Madrid Seismic Zone," Nov. 26, 1984, Reston, VA: U.S. Geological Survey Open-File Report 84-770, 468 p.

Herrmann, Robert B., 1979, Surface wave focal mechanisms for eastern North American earthquakes with tectonic implications: Journal of Geophysical Research, v. 84, p. 3543-3552.

Heyl, Jr., A.V., and Brock, M.R., 1961, Structural framework of the Illinois-Kentucky mining district and its relation to mineral deposits: U.S. Geological Survey Short Papers in the Geodetic and Hydrology Sciences., Articles 293-435; 294, p. D-3 to D-6 (USGS Prof. Paper 424-D).

Kolata, D.R., Treworgy, J.D., and Masters, J.M., 1981, Structural framework of the Mississippi embayment of southern Illinois: Illinois State Geological Survey Circular 516, 38 p.

Lahr, J.C., 1979, HYPOELLIPSE/VAX: a computer program for determining local earthquake hypocentral parameters, magnitude, and first motion pattern: U.S. Geological Survey Open-File Report 84-519, 233 p.

Lee, W.H.K., Bennett, R.E., and Meagher, K.L., 1972, A method of estimating magnitude of local earthquakes from signal duration: U.S. Geological Survey Open-File Report 72-223, 28 p.

McKeown, F.A., and Pakiser, L.C., ed., 1982, Investigations of the New Madrid, Missouri, earthquake region: U.S. Geol. Survey Professional Paper 1236, 201 p.

Nelson, W.J., and Krausse, H.F., 1981, The Cottage Grove fault system in southern Illinois: Illinois State Geological Survey Circular 522, 65 p.

Nuttli, Otto W., and Herrmann, Robert B., 1978, State-of-the-Art for assessing earthquake hazards in the United States; Report 12, Credible Earthquakes for the Central United States: U.S. Army Engineers Waterways Experimental Station Misc. Paper S-73-1, 103 p.

Nuttli, Otto W., 1979, Seismicity of the central United States: Reviews in Engineering Geology, v. IV, Geological Society of America, p. 67-93.

Plumb, R.A., and Cox, J.W., 1987, Stress directions in eastern North America determined to 4.5 km from borehole elongation measurements: Journal of Geophysical Research, v. 92, p. 4805-4816.

Sexton, J.L., Bracle, L.W., Hinze, W.J., and Campbell, M.J., 1986, Sesimic reflection profiling studies of a buried Precambrian rift beneath the Wabash Valley fault zone: Geophysics, v. 51, p. 640-660.

Stover, C.W., Reagor, B.G., and Algermissen, S.T., 1979, Seismicity map of the State of Indiana: U.S. Geological Survey Map MF-1145.

Stover, C.W., Reagor, B.G., and Algermissen, S.T., 1979, Seismicity map of the State of Illinois: U.S. Geological Survey Map MF-1143, scale

Taylor, K.B., and Herrmann, R.B., 1987, Illinois earthquake of June 10, 1987: EERI Newsletter, v. 21, n. 9, p. 1-3.

Thenhaus, Paul C., ed., 1983, Summary of Workshops concerning regional seismic source zones of parts of the conterminous United States convened by the U.S. Geological Survey 1979-1980, Golden, CO.: U.S. Geological Survey Circular 898, 36 p.

Zoback, M. L., and Zoback, M., 1980, State of stress in the conterminous United States, Journal of Geophysical Research, v. 85, p. 6113-6156.

						1	**2**	**3**	**4**	**5**	**6**	**7**	**8**	**9**	**10**	**11**
EQ NO	DATE (YMD)	ORGN TIME (UTC)	LAT (deg)	LONG (deg)	DEPTH (km)	DMIN (km)	MAG (Md)	NO	GAP (deg)	RMS (sec)	ERZ (km)	AZ1 (deg)	ERH1 (km)	AZ2 (deg)	ERH2 (km)	QUA
1	870613	0217 51.18	38.722N	87.946W	9.93	3.1	0.88	13	69	0.05	1.32	-37.	0.53	-127.	0.40	A
2	870613	0304 48.22	38.723N	87.946W	11.83	2.8	0.48	11	73	0.03	1.17	-47.	0.47	43.	0.33	A
3	870613	0514 05.11	38.717N	87.944W	10.05	3.4	0.53	11	72	0.05	1.72	-44.	0.65	-134.	0.46	A
4	870613	0521 33.56	38.723N	87.933W	9.86	2.7	0.11	11	69	0.04	1.23	-37.	0.47	-127.	0.34	A
5	870613	0616 13.13	38.722N	87.946W	9.79	3.3	0.84	12	71	0.03	0.97	-23.	0.45	-113.	0.30	A
6	870613	0632 00.51	38.718N	87.949W	9.52	3.4	0.40	11	76	0.06	1.68	38.	0.69	-62.	0.57	A
7	870613	0639 54.40	38.718N	87.949W	9.40	3.4	0.10	9	76	0.02	1.07	-19.	0.41	-109.	0.28	A
8	870613	0809 21.98	38.722N	87.948W	11.06	2.4	0.35	11	81	0.04	1.06	36.	0.48	-54.	0.39	A
9	870613	0840 31.45	38.722N	87.947W	9.61	3.2	1.00	10	75	0.03	1.14	-13.	0.42	-103.	0.29	A
10	870613	0848 03.68	38.722N	87.950W	9.95	3.3	2.27	12	72	0.04	1.25	-24.	0.58	-114.	0.39	A
11	870613	0926 30.20	38.722N	87.950W	10.32	3.3	0.31	11	77	0.04	1.67	-17.	0.72	-107.	0.49	A
12	870613	1229 54.40	38.724N	87.949W	10.95	2.9	——	10	77	0.04	1.23	-135.	0.56	-45.	0.45	A
13	870613	1420 11.93	38.721N	87.947W	10.49	3.2	1.29	13	59	0.02	0.65	-65.	0.27	35.	0.19	A
14	870613	1529 23.53	38.717N	87.946W	8.84	3.5	0.22	11	73	0.03	0.94	-69.	0.35	39.	0.28	A
15	870613	1601 30.18	38.722N	87.943W	10.90	3.0	0.40	12	72	0.04	1.84	-105.	0.53	-15.	0.40	A
16	870613	1929 32.15	38.722N	87.946W	10.63	3.0	0.87	16	74	0.04	0.44	-92.	0.32	-2.	0.26	A
17	870613	1959 41.96	38.721N	87.946W	11.27	3.0	1.38	17	58	0.05	0.62	-68.	0.37	22.	0.33	A
18	870614	0250 39.66	38.722N	87.942W	10.24	2.9	——	12	70	0.06	1.35	-74.	0.58	16.	0.43	A
19	870614	0253 00.37	38.724N	87.944W	10.61	2.7	0.03	10	105	0.04	1.47	-88.	0.61	2.	0.43	A
20	870614	0314 09.21	38.723N	87.941W	9.12	2.8	0.27	13	87	0.06	1.51	-78.	0.53	12.	0.40	A
21	870614	0410 39.17	38.722N	87.944W	10.48	3.2	0.07	13	66	0.04	1.25	-102.	0.42	-12.	0.33	A
22	870614	0418 43.91	38.719N	87.946W	10.43	3.3	0.69	14	64	0.05	1.37	-66.	0.41	24.	0.39	A
23	870614	0428 29.91	38.718N	87.945W	10.30	3.4	——	13	66	0.03	1.01	-71.	0.37	19.	0.24	A
24	870614	0430 42.66	38.722N	87.946W	10.09	3.1	0.54	15	64	0.05	1.10	-68.	0.45	32.	0.35	A
25	870614	0455 41.81	38.722N	87.944W	9.67	3.1	0.40	15	66	0.04	0.80	-57.	0.32	33.	0.25	A
26	870614	0508 52.71	38.722N	87.946W	10.28	3.2	1.78	15	63	0.03	0.74	-65.	0.28	35.	0.24	A
27	870614	0824 16.71	38.719N	87.947W	10.21	3.3	0.11	14	69	0.04	0.92	-85.	0.39	5.	0.33	A
28	870614	0946 01.55	38.721N	87.942W	10.61	3.0	——	13	66	0.04	1.11	-105.	0.37	-15.	0.30	A
29	870614	1218 24.12	38.722N	87.946W	10.43	3.1	0.09	12	84	0.05	1.23	-97.	0.56	-7.	0.47	A
30	870614	1348 47.91	38.721N	87.947W	10.21	3.2	0.88	15	62	0.05	1.06	-66.	0.41	34.	0.35	A
31	870614	1355 54.01	38.718N	87.946W	9.48	3.5	——	13	67	0.05	1.38	-70.	0.50	20.	0.32	A
32	870614	1555 38.95	38.717N	87.951W	10.14	3.1	0.44	15	71	0.04	0.97	-99.	0.39	-9.	0.33	A
33	870614	1741 55.22	38.721N	87.946W	10.01	3.1	0.65	16	58	0.02	0.49	-75.	0.20	15.	0.18	A
34	870614	1859 37.13	38.722N	87.947W	9.93	3.2	0.54	17	59	0.03	0.59	-80.	0.25	10.	0.22	A
35	870614	2052 42.81	38.722N	87.947W	10.58	3.2	0.27	16	69	0.03	0.86	-79.	0.29	11.	0.22	A
36	870615	0337 56.55	38.719N	87.944W	10.31	3.2	0.67	16	56	0.04	0.82	-86.	0.37	4.	0.29	A
37	870615	0443 30.55	38.722N	87.949W	11.19	3.0	0.11	13	73	0.04	0.66	-84.	0.43	6.	0.30	A
38	870615	0551 17.34	38.722N	87.948W	9.97	3.0	0.72	18	53	0.04	0.76	-84.	0.31	6.	0.27	A
39	870615	0705 30.19	38.721N	87.948W	11.37	3.1	0.18	16	53	0.05	0.94	-95.	0.42	-5.	0.35	A
40	870615	0838 42.34	38.725N	87.940W	11.00	2.5	0.79	18	55	0.04	0.69	-84.	0.28	6.	0.25	A
41	870615	0857 20.15	38.722N	87.942W	11.40	2.9	0.17	15	65	0.07	1.40	-89.	0.66	1.	0.55	A
42	870615	0931 19.93	38.722N	87.951W	10.44	3.1	1.62	18	51	0.05	0.99	-86.	0.42	4.	0.36	A
43	870615	0945 04.51	38.719N	87.946W	10.31	3.3	1.42	16	58	0.03	0.63	-76.	0.28	14.	0.23	A
44	870615	1140 42.86	38.721N	87.949W	10.36	3.1	0.71	15	73	0.02	0.55	-78.	0.19	12.	0.14	A
45	870615	1922 23.54	38.719N	87.950W	10.25	3.4	0.76	18	80	0.03	0.53	-69.	0.20	31.	0.18	A
46	870615	1935 35.34	38.722N	87.950W	10.14	3.3	0.50	17	72	0.05	0.69	-104.	0.39	-14.	0.32	A
47	870615	1954 48.17	38.718N	87.953W	10.33	3.1	0.28	16	75	0.05	1.23	-77.	0.42	13.	0.33	A
48	870616	0113 31.07	38.713N	87.949W	8.23	3.2	——	15	63	0.04	0.88	-115.	0.29	-25.	0.24	A
49	870616	0321 30.83	38.718N	87.951W	9.87	3.3	1.56	18	61	0.03	0.64	-69.	0.24	31.	0.22	A
50	870616	0456 01.36	38.719N	87.950W	10.12	3.4	0.01	14	71	0.05	1.21	-70.	0.46	20.	0.33	A

Table A-1. Appendix: Listing of aftershock parameters....Continued

EQ NO	DATE (YMD)	ORGN TIME (UTC)	LAT (deg)	LONG (deg)	DEPTH (km)	1 DMIN (km)	2 MAG (Md)	3 NO	4 GAP (deg)	5 RMS (sec)	6 ERZ (km)	7 AZ1 (deg)	8 ERH1 (km)	9 AZ2 (deg)	10 ERH2 (km)	11 QUA
51	870616	0458 47.76	38.722N	87.948W	9.66	3.3	----	14	70	0.02	0.47	-94.	0.20	-4.	0.14	A
52	870616	0614 02.45	38.719N	87.950W	9.23	3.3	1.36	17	61	0.03	0.58	-62.	0.22	28.	0.19	A
53	870616	0724 24.25	38.722N	87.942W	11.12	2.3	0.04	14	68	0.04	0.70	-91.	0.42	-1.	0.34	A
54	870616	0856 15.29	38.719N	87.951W	9.84	3.3	1.38	17	61	0.03	0.63	-64.	0.25	26.	0.21	A
55	870616	0922 47.55	38.721N	87.949W	10.64	3.2	0.06	13	78	0.04	1.12	-69.	0.43	21.	0.26	A
AVERAGES					10.24	3.1	0.56	14.0	68.	0.04	1.00	-68.	0.41	-10.	0.32	

No. of rows is 55.
No. of GAP values (<=180) indicating location inside net: 55; GAP values outside net: 0.
     Average GAP for inside locations only.

1 —Distance to closest seismograph station.
2 —Local magnitude estimate based on duration (coda length) of earthquake (Lee, et al., 1972).
3 —Number of observations (P and S) used to compute hypocentral solution.
4 —Largest azimuthal separation in degrees between stations as viewed from the epicenter.
5 —Root mean square errors of travel time residuals.
6-10—Error estimates based on 94% confidence ellipsoid (see Lahr, 1979, pp 31-32).
11 —A measure that is intended to indicate the general reliability of the hypocentral
     solution where;
     A = excellent epicenter, good focal depth;
     B = good epicenter, fair focal depth;
     C = fair epicenter, poor focal depth.

* * * NORMAL TRIAL DEPTH * * *
9.0000
1.7700

LAYER	VELOCITY KM/SEC	DEPTH, KM	THICKNESS KM
1	5.600	0.000	2.000
2	6.150	2.000	18.000
3	6.700	20.000	20.000
4	8.180	40.000	57.000
5	8.370	97.000	1000.000

SECTION II

DIGITAL SEISMOGRAMS OF LOCALLY RECORDED AFTERSHOCKS AND RECORDINGS
OF A MAGNITUDE 4.1_{mbLg} REGIONAL EARTHQUAKE AT THE SAME SITES

DIGITAL SEISMOGRAMS OF LOCALLY RECORDED AFTERSHOCKS AND RECORDINGS OF A MAGNITUDE 4.1$_{mbLg}$ REGIONAL EARTHQUAKE AT THE SAME SITES

David Carver, Robert Williams, and Edward Cranswick

INTRODUCTION

The digital seismograms presented in this section were recorded by PADS's (Portable Autonomous Digital Sesimograph) which were deployed as part of the USGS field program (12 Jun to 17 Jun UTC) summarized in the previous section. Over the course of the five-and-a-half-day monitoring period, six PADS's were deployed for various durations at a total of 8 station locations (see Figure 1), three of which were colocated with smoked-paper recorders previously discussed. All the time series of this dataset were recorded by PADS's of the same model which were operated in the same signal-conditioning/digitizing mode. At the writing of this report, we have identified 31 earthquakes which have been well-recorded by one to five PADS stations (see Table I). Most of these events are microearthquake aftershocks at epicentral ranges of 5-10 km, but three are larger earthquakes at regional distances. The regional events include a magnitude 4.1$_{mbLg}$ (NEIS) earthquake which occurred roughly 270 km to the southwest at 164+21:17 UTC. In this section, for consistency with the digital records, time will be specified as: [Julian Day]+[Hour]:[Minute].

We will review the field operations (conducted by D.C. and R.W.), characterize the site conditions of the PADS stations, describe the timing and the response of the instrumentation, and present a summary and illustration of the dataset as a whole. The records of the 164+21:17 event will be presented and discussed in terms of the variations of site/propagation response which they exhibit. The Appendix of this section outlines the computer processing of the dataset with particular emphasis on the issue of the completeness of the resulting sample of the aftershock sequence.

FIELD PROGRAM

The first PADS, station OLN, was deployed on arrival to the epicentral area at 163+05:00 which was within 30 hours of the mainshock. OLN recorded several events the first night, but none of its seismograms have been included in this first-pass of the dataset (see the Appendix for a description of the criteria used for event selection). Stations ART, BUG, CHE, KEL, ROC and RUS were deployed on the first day in the field, commencing about 163+12:00, and OLN was shut down. ART, BUG, and KEL were the sites of co-located smoked-paper recorders referred to above.

Several thunderstorms played havoc with the PADS stations: the combination of rain/thunder/lightning was responsible for many "false" or "nonseismic" triggers which exhausted the digital recording cassettes (tapes). As a consequence of intense storms on two successive nights all the PADS stations, except for ROC, were "triggered-out" (i.e., effectively dead, see Appendix) for the periods of roughly 164+01:00 T 164+18:00 and 165+00:00 T 165+16:00. Within hours after it had been established, KEL was struck by lightning (as observed by C. Langer) which damaged the PADS deployed there. KEL subsequently had no digital recording capability until the third day (at roughly 165+15:00) when station RUS was shut down, and its PADS was redeployed
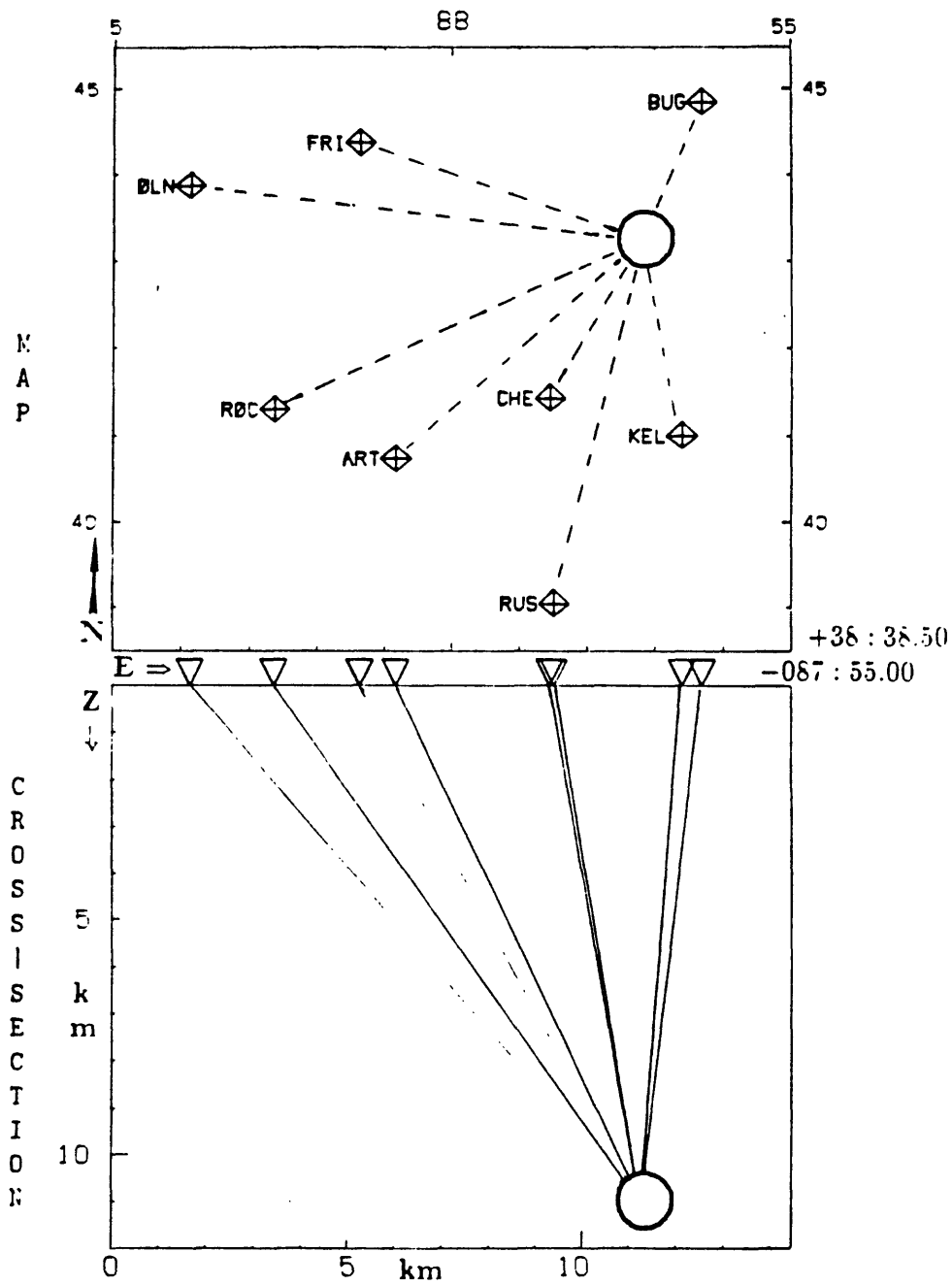
FIGURE 1: Map and East-West cross-section (including whole latitude range of the map) of hypocentral zone showing the locations of the the PADS (Portable Autonomous Digital Seismograph) stations and the locus of aftershock activity (C. Langer and others, 1987; see Section I). The map locations of the stations have been projected down to the top of the cross-section. The cross-section has no vertical exaggeration, and the distance scale of both the map and cross-section is defined by the kilometer ticks of the cross-section. The ideal raypaths appropriate for a homogeneous halfspace velocity structure have been drawn between the stations and the source volume to indicate the azimuthal coverage and the approximate apparent angles of incidence. **NOTE** that the true angle of incidence of the closest station, CHE, is approximately equal to the apparent angle of incidence at Station ART in the cross-section.

at KEL. In the same afternoon, the PADS at station BUG was shut down and re-deployed at a new site, station FRI. All stations except for ROC and KEL were shut down on the fifth day (by 167+15:00), and these two stations remained deployed until the sixth day (at 168+12:00). Consequently, ROC operated the longest of any station and nearly the whole duration of the field program.

RECORDING SITES

The epicentral area is underlain by several thousand meters of Paleozoic sedimentary rock which overlie Precambrian crystalline basement. The Paleozoic is poorly exposed because it is generally overlain by Pleistocene glacial deposits. ROC and KEL were sited on Paleozoic outcrops, but all the other stations were sited on glacial drift (till). Based on information from the property owners of these latter sites about the depth-to-bedrock in their water wells, the thickness of the low-velocity surficial layer of glacial drift is estimated to vary between 15-30 m. Station ROC was sited on an outcrop of relatively well-cemented sandstone which had been exposed by the downcutting erosion of a creek.

PADS INSTRUMENTATION

Each PADS consisted of a Dyneer-Sprengnether DR-200 self-triggering digital recorder equipped with an S-6000 triaxial geophone. The recorder clocks characteristically had a drift rate of approximately 10 ms/day. They were initially set to and calibrated against (on a daily basis in general) a portable master clock whose time drift was calibrated against WWV radio time-code. Each orthogonal component of vector (3-component) ground motion signal was generated by a velocity transducer with a natural frequency of 1.7 Hz (damping coefficient = 0.7, effective motor constant = 1.18 volts/cm/s). Signals were low-cut filtered at 0.2 Hz and high-cut (anti-aliasing) filtered at 50Hz, amplified by a factor of 100 (40 dB), and digitally sampled at 200 sps by a gain-ranged 12-bit A/D (analog-to-digital converter). Low-frequency (near the 1.7 Hz corner of the geophones) calibration of the combined recorder/sensor system was performed using the DR-200's built-in step-response test. The high-frequency (near the 50 Hz corner of the anti-aliasing filters) response was estimated by recording a broad-band foot-stomp (i.e., a NIKE delta function) at approximately 10 m distance from the geophone. The latter procedure also tested the sensitivity of the PADS trigger which consisted of an STA/LTA algorithm (STA = 0.2 s, LTA = 6.4 or 12.8 s, ratio = 6 or 9 dB). The pre-event memory was f6 s, and total record durations are typically 20-30 s.

All earthquakes have been recorded on-scale, and even though the local aftershocks were small, the relatively quiet recording sites and the low internal noise and gain-ranging of the digital recorders produced excellent records (For example, when the velocity time series of the 164+21:17 event recorded at station ROC are integrated to displacement, the resulting traces exhibit very little long-period "drift" even after being high-cut filtered at 2 Hz).

27

LOCAL AFTERSHOCKS

Figure 2 (includes 30 pages) display 10.0 s of all channels (three components at all stations) recorded from a series of 30 earthquakes in the timespan, 163+20:05 T167+20:59 (including 2 regional events but not the magnitude $4.1_{mbLg}164+21:17$ regional earthquake). Table I below lists the number of events recorded according to the number of stations which recorded them. Table II of Figure 2 is a chronological list of the events which indicates the stations which recorded each event.

Table I

Stations/Event	Events
5	3
4	2
3	7
2	7
1	11

All of the local events are characterized by S-minus-P times between 1.0 and 2.0 s. Because of the source/receiver geometry diagrammed in Figure 1, angles of incidence at the various stations were usually steep. Many of the arrivals therefore exhibit an effective segregation of the P- and S-waves into vertical and horizontal components respectively. In general, the waveforms are relatively simple and impulsive, but there are many examples of distinct phases arriving between the P- and S-phases. The vector records demonstrate that the second large phase on the vertical components usually leads the S-waves on the horizontal components by several tenths of a second which indicates that this second phase is an SV-to-P converted phase. Many of the time series and spectra (not shown) exhibit strong surface-resonance modes (reverberations).

Some of the time series of different events recorded at the same station are virtually identical in shape (after normalizing the traces by peak amplitude) which suggests that they represent sources with very similar mechanisms and locations. However, some events look very different at the same station, and this variation may be related to a change in event location as a function of time that is observed in the distribution of hypocenters. The peak ground motion of all the records of local events in Figure 2 is approximately 5×10^{-3} cm/s (velocity).

28

TABLE II

Event	Stations						No.
163+20:05	ART	BUG	—	—	—	—	2
164+02:17	—	—	—	—	—	ROC	1
06:16	—	—	—	—	—	ROC	1
08:48	—	—	—	—	—	ROC	1
14:20	—	—	—	—	—	ROC	1
19:29	ART	BUG	CHE	—	—	—	3
19:59	ART	BUG	CHE	—	—	ROC	4
165+04:18	—	—	—	—	—	ROC	1
04:30	—	—	—	—	—	ROC	1
04:55	—	—	—	—	—	ROC	1
05:08	—	—	—	—	—	ROC	1
13:48	—	—	—	—	—	ROC	1
17:41	ART	—	CHE	—	—	ROC	3
18:59	ART	—	CHE	—	—	ROC	3
20:52	ART	—	—	—	—	—	1
166+03:37	ART	—	CHE	FRI	—	—	3
05:51	ART	—	CHE	FRI	KEL	ROC	5
07:05	ART	—	—	FRI	—	—	2
08:38	ART	—	CHE	FRI	KEL	ROC	5
08:57	ART	—	—	—	—	—	1
09:31	ART	—	CHE	FRI	KEL	ROC	5
09:45	ART	—	CHE	—	KEL	ROC	4
16:26	ART	—	—	—	KEL	ROC	3
19:22	—	—	CHE	—	KEL	ROC	3
19:31	—	—	CHE	—	KEL	ROC	3
19:35	—	—	CHE	—	KEL	—	2
167+03:21	—	—	CHE	—	—	ROC	2
06:14	—	—	CHE	—	—	ROC	2
08:56	—	—	CHE	—	—	ROC	2
20:59	—	—	—	—	KEL	ROC	2

FIGURE 2: Table II lists the approximate origin-times of 30 earthquakes (not including the 164+21:17 regional event) which are contained in the first pass of the PADS dataset that is presented in this report. This includes all events which either triggered 2 or more PADS within a 30 s window or those correlated with a first-pass inspection of the smoked-drum records immediately after the field program (C. Langer, 1987, written communication). Each of the next 30 pages (labeled "FIGURE 2 continued") corresponds to one earthquake, and each displays 10.0 seconds of the three components of all stations which recorded the event. The origin (on the *left*) of the time-axes at the top and bottom of the figure corresponds to the time plotted *below* the arrow in the *right-hand* margin of the page. All traces are plotted to the same absolute amplitude scale that is graphically defined by the arrow and by the peak velocity (cm/s; annotated above the arrow) which was recorded for each event (each page). The arrow's length equals the maximum trace amplitude which corresponds to the peak value, and the arrow points in the direction of positive ground motion for all components. Each trace is identified on the *right* by its station and velocity-component — .V1 is vertical Z; .V2 is horizontal N; .V3 is horizontal E — and the peak velocity (cm/s) of the trace is annotated in the *left-hand* margin.
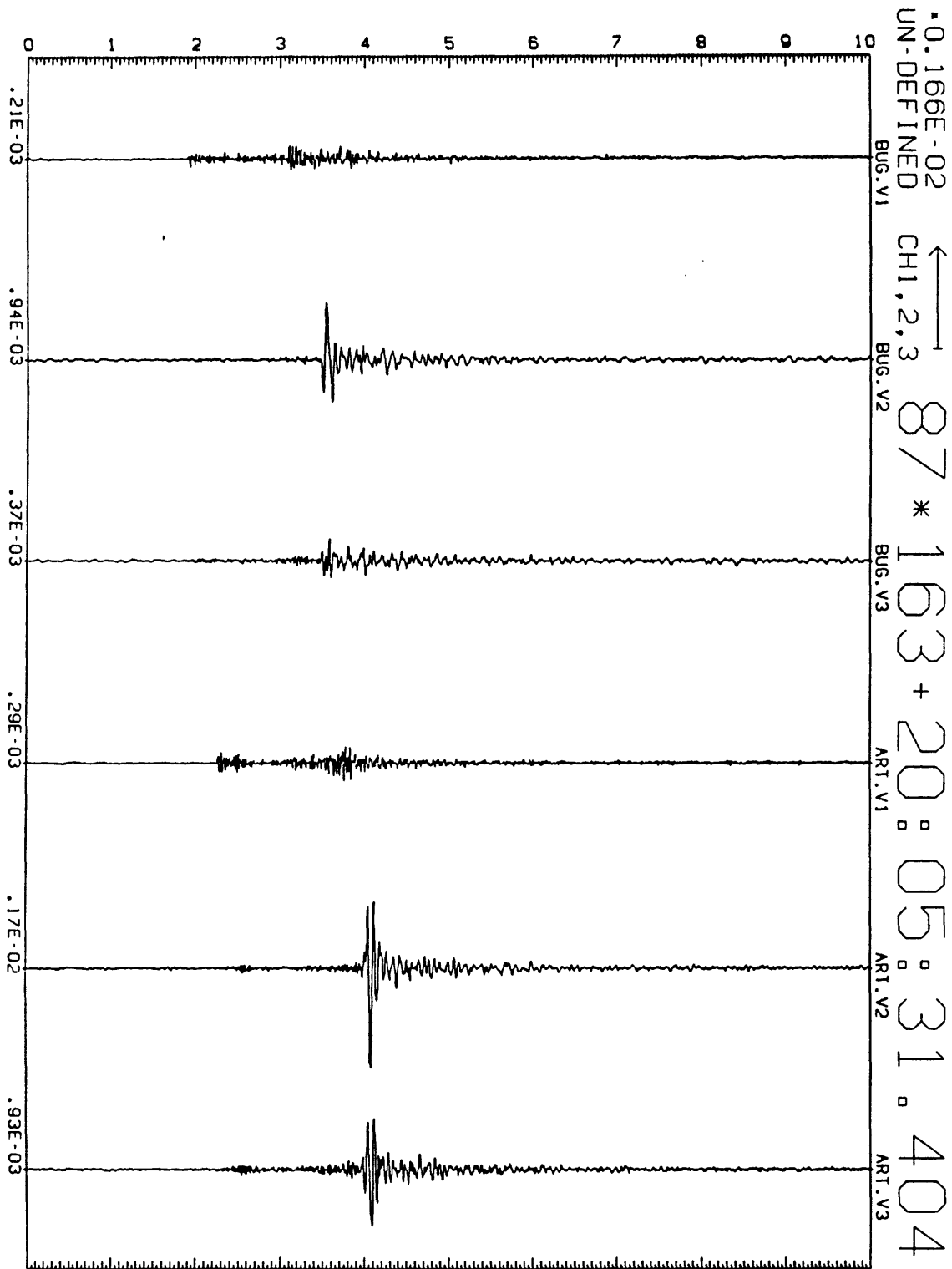
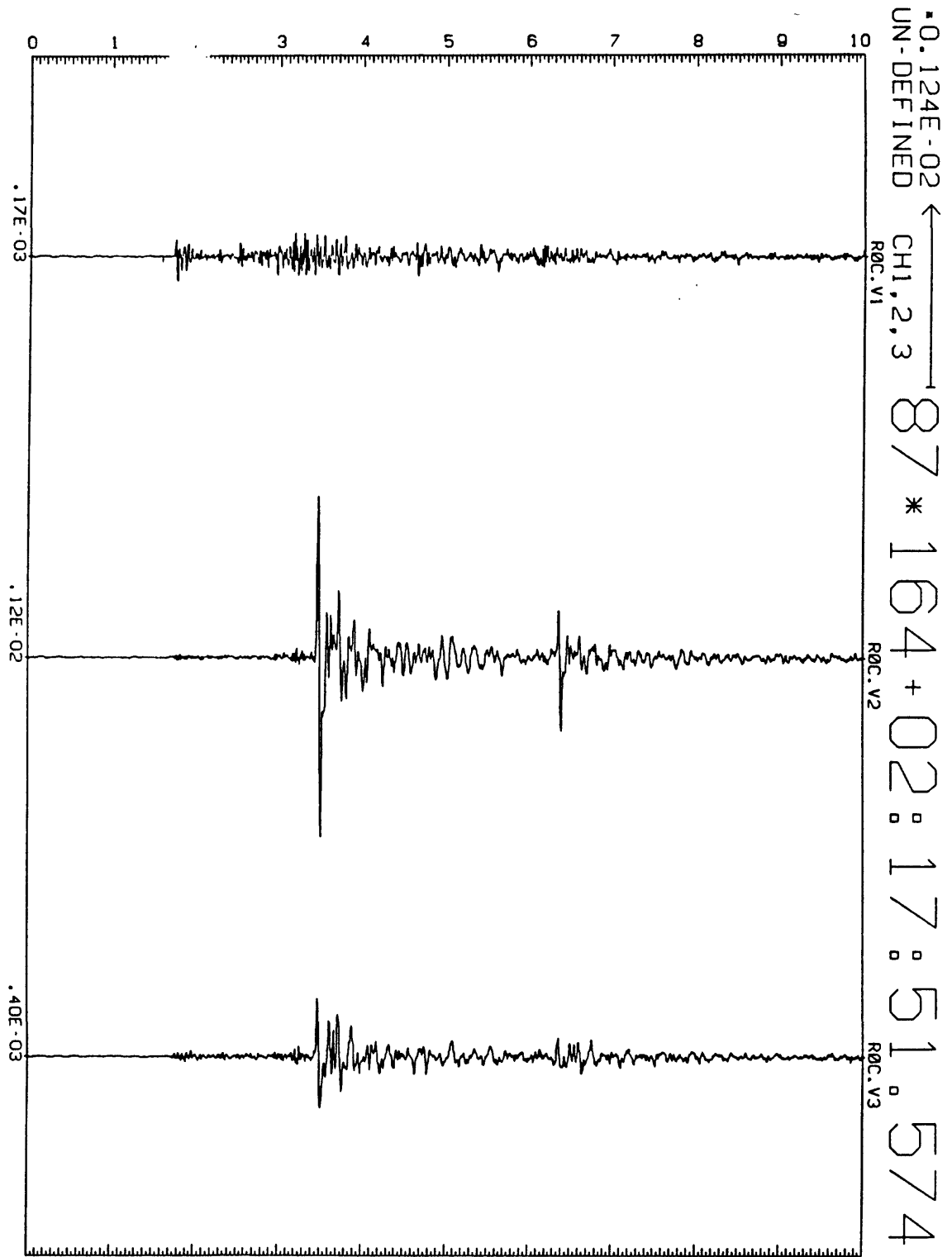**FIGURE 2 continued:** See Figure 2 caption on page 29 for a description of labeling conventions.

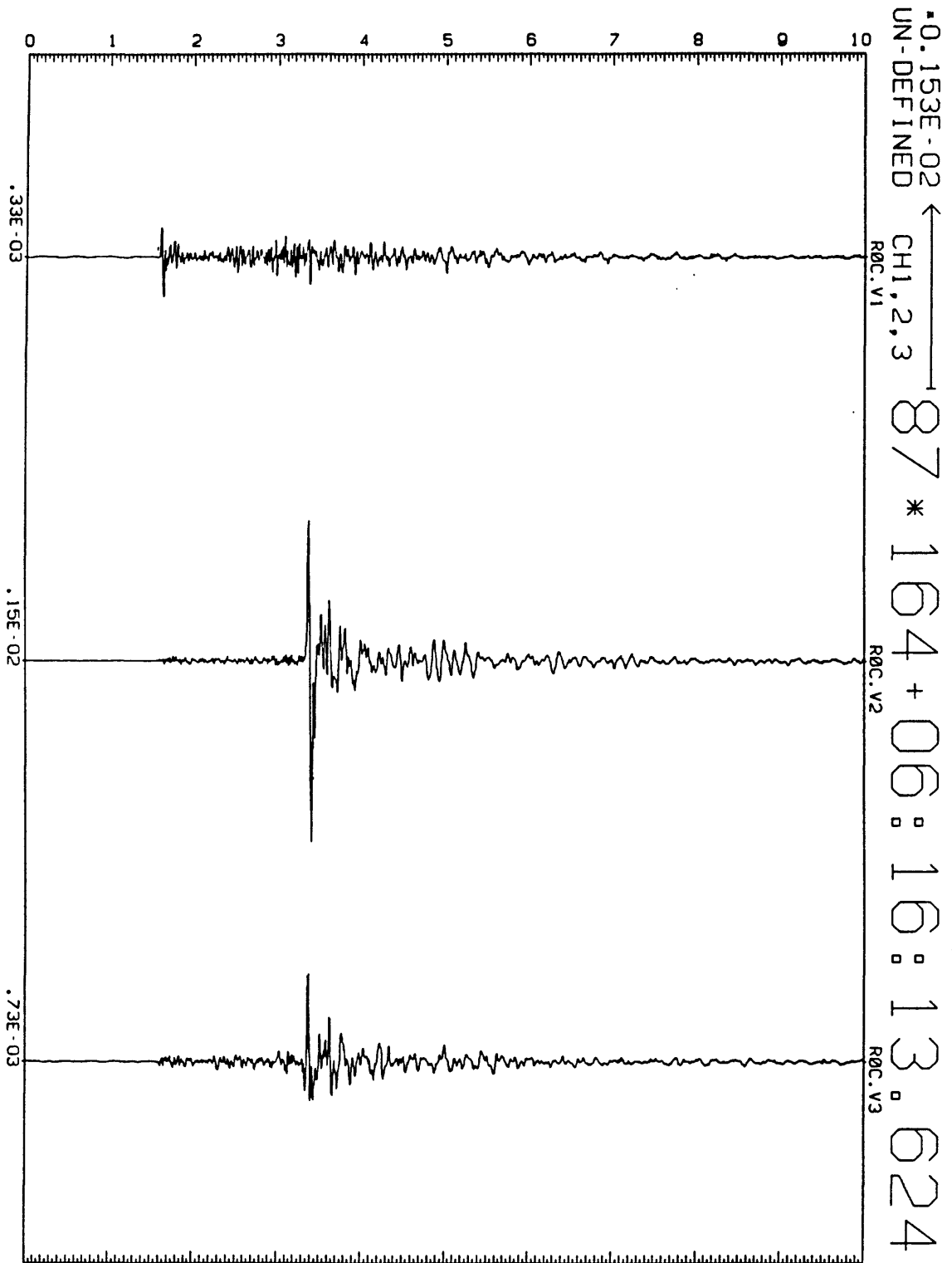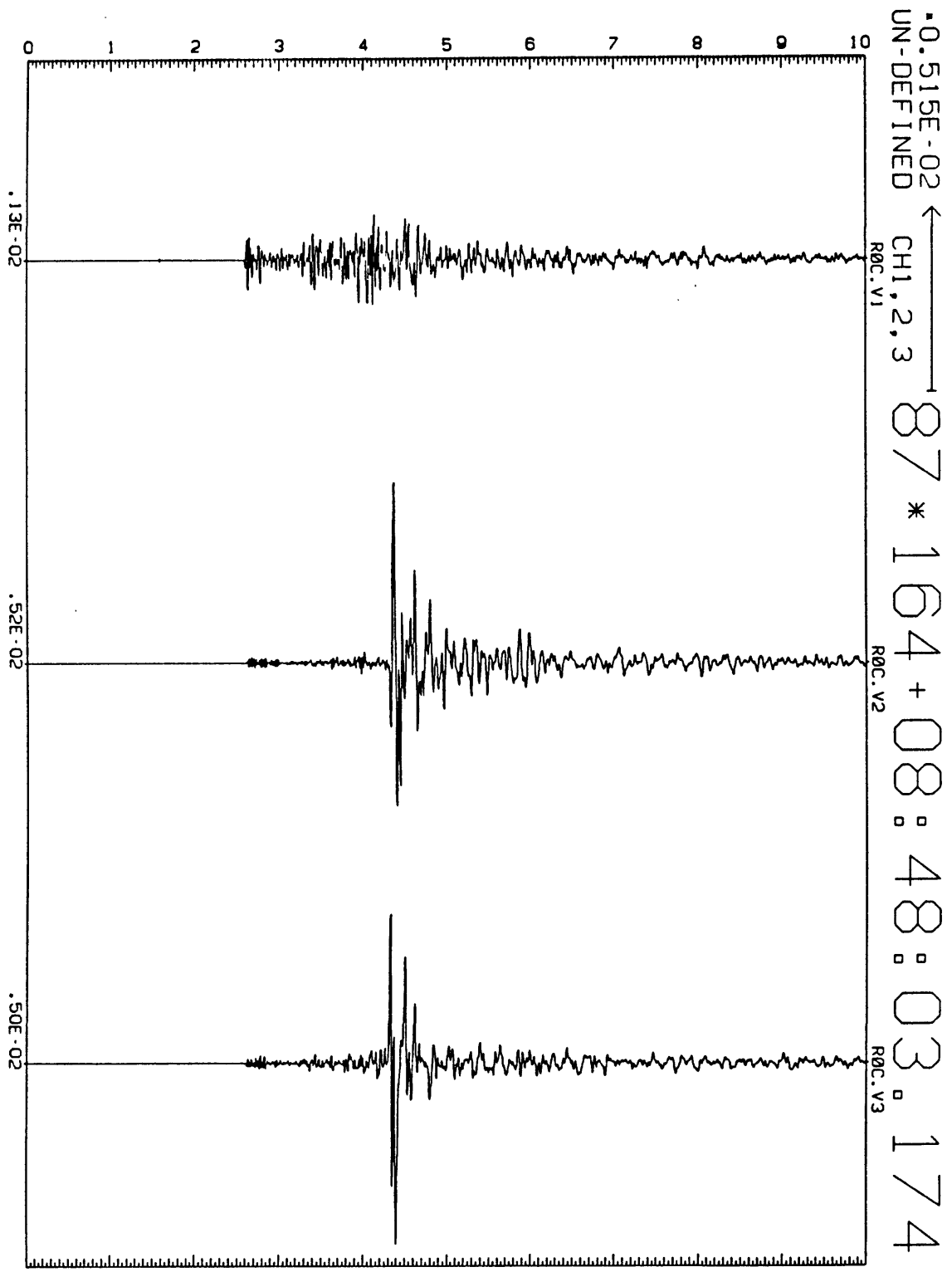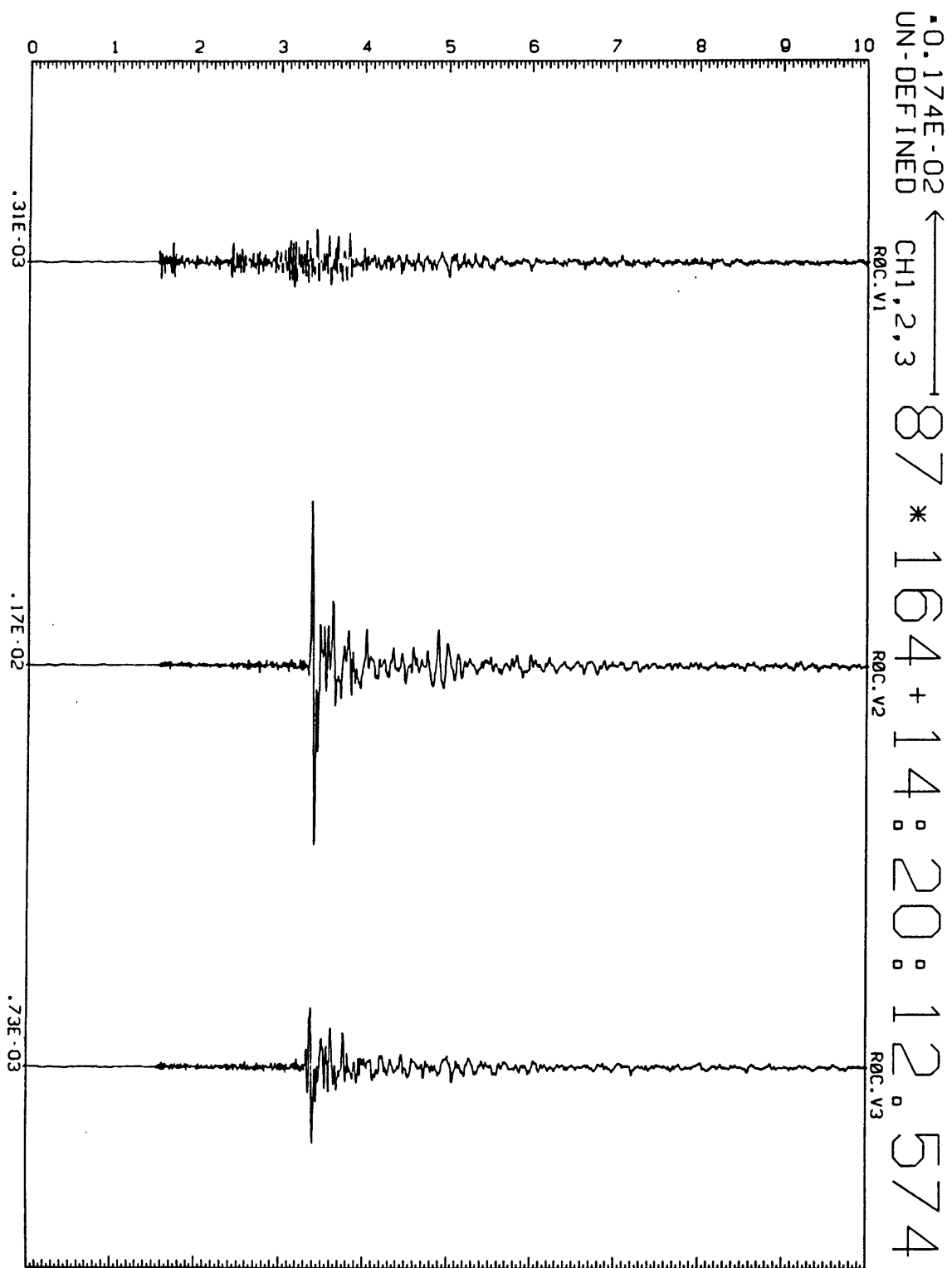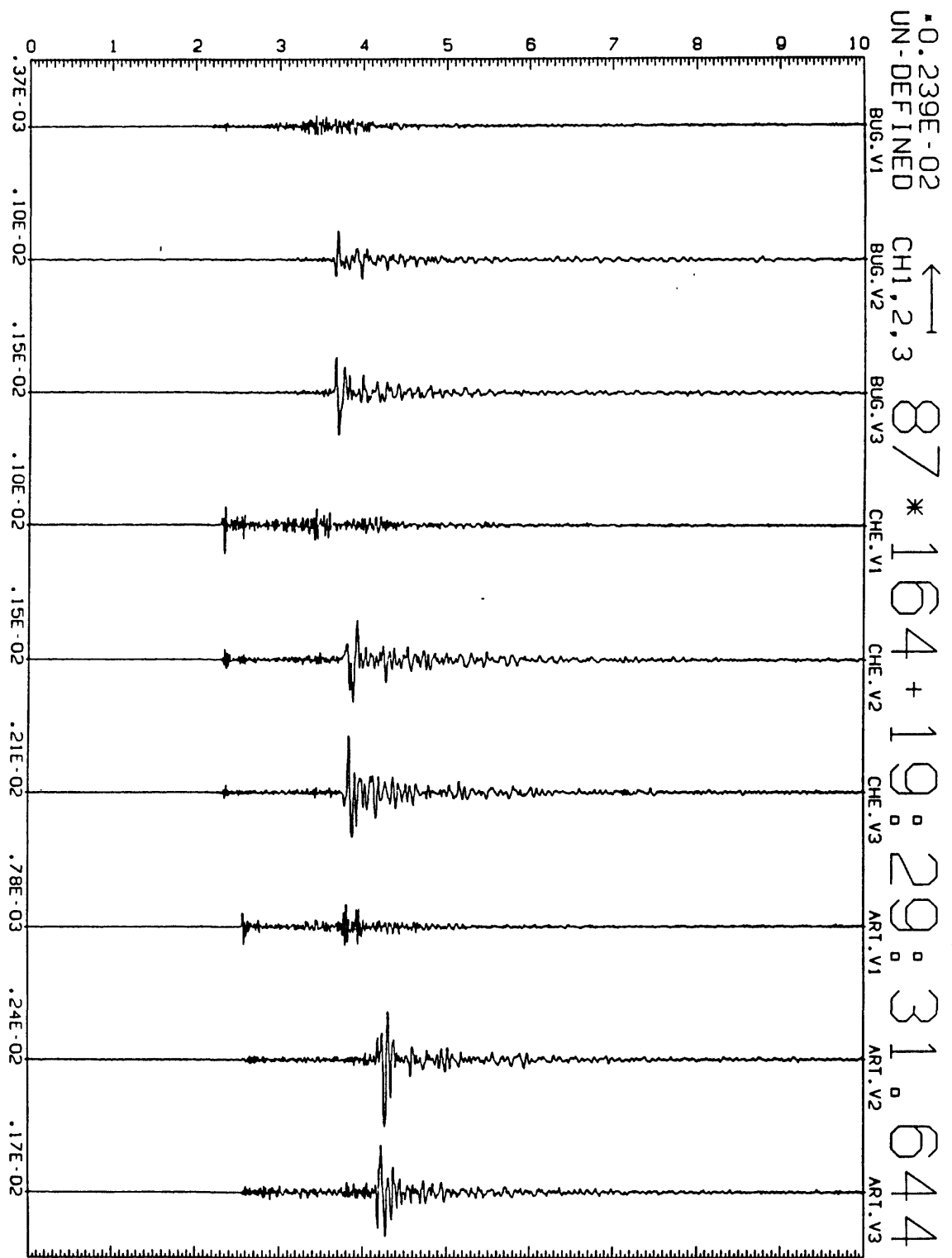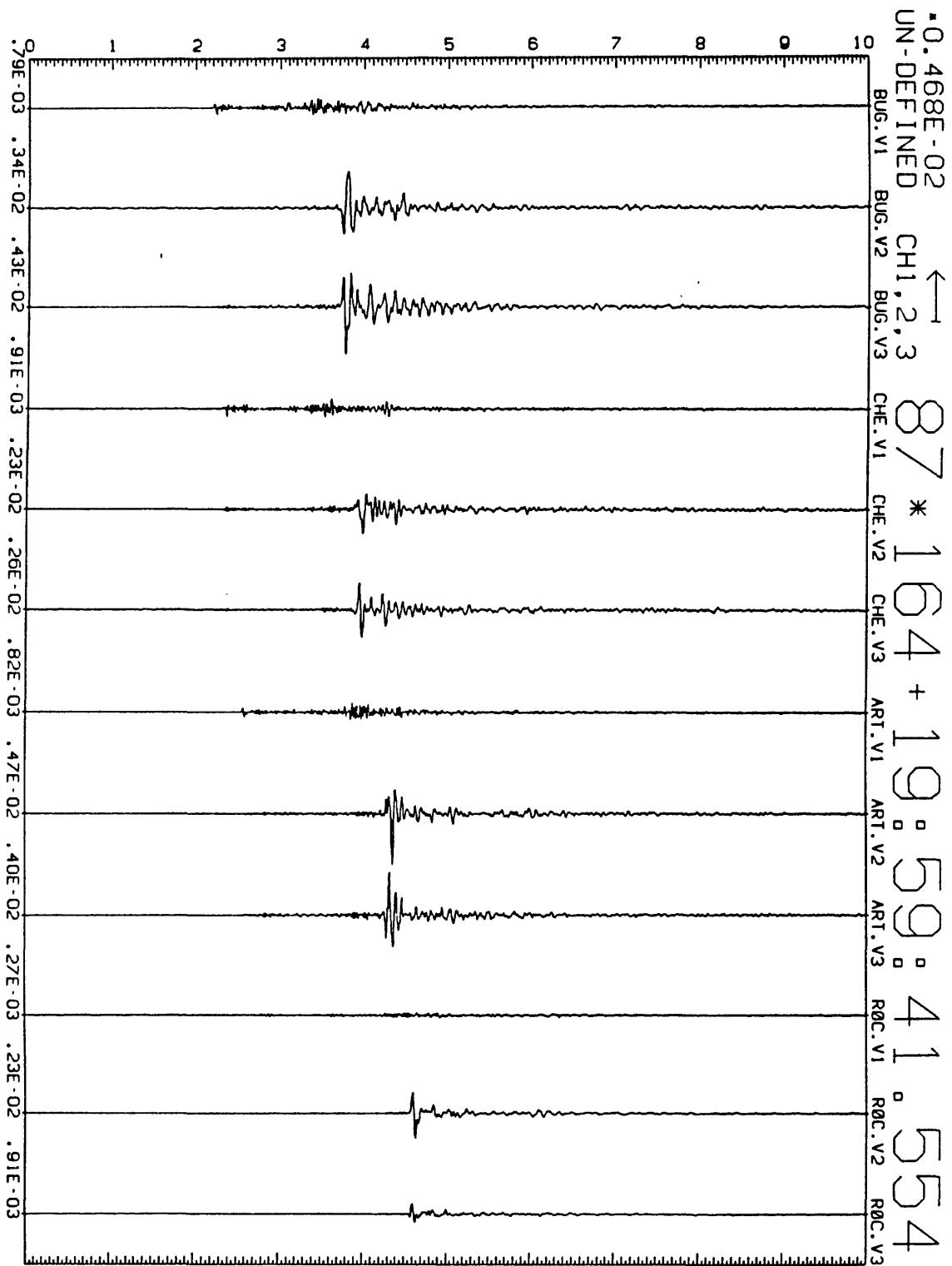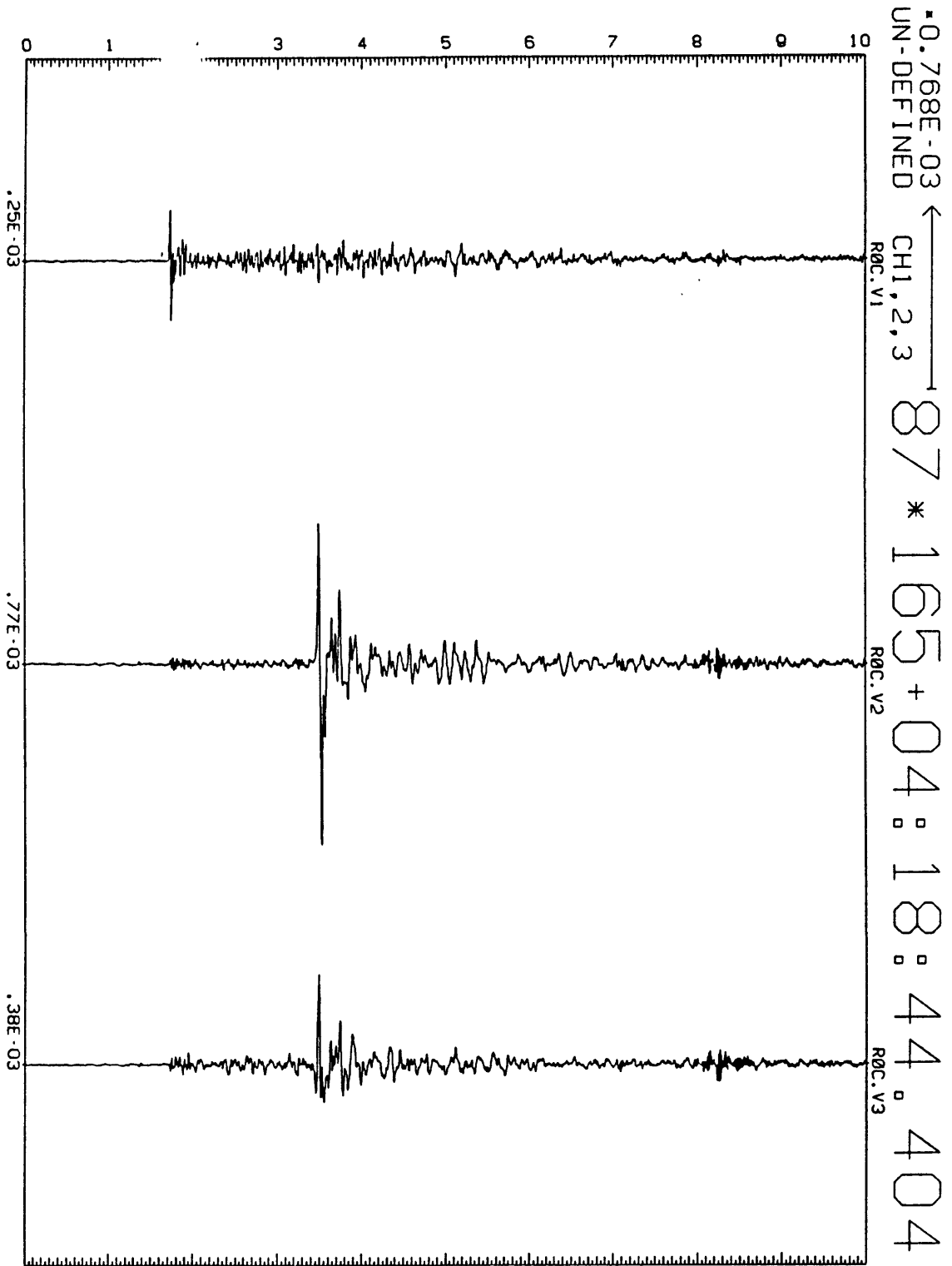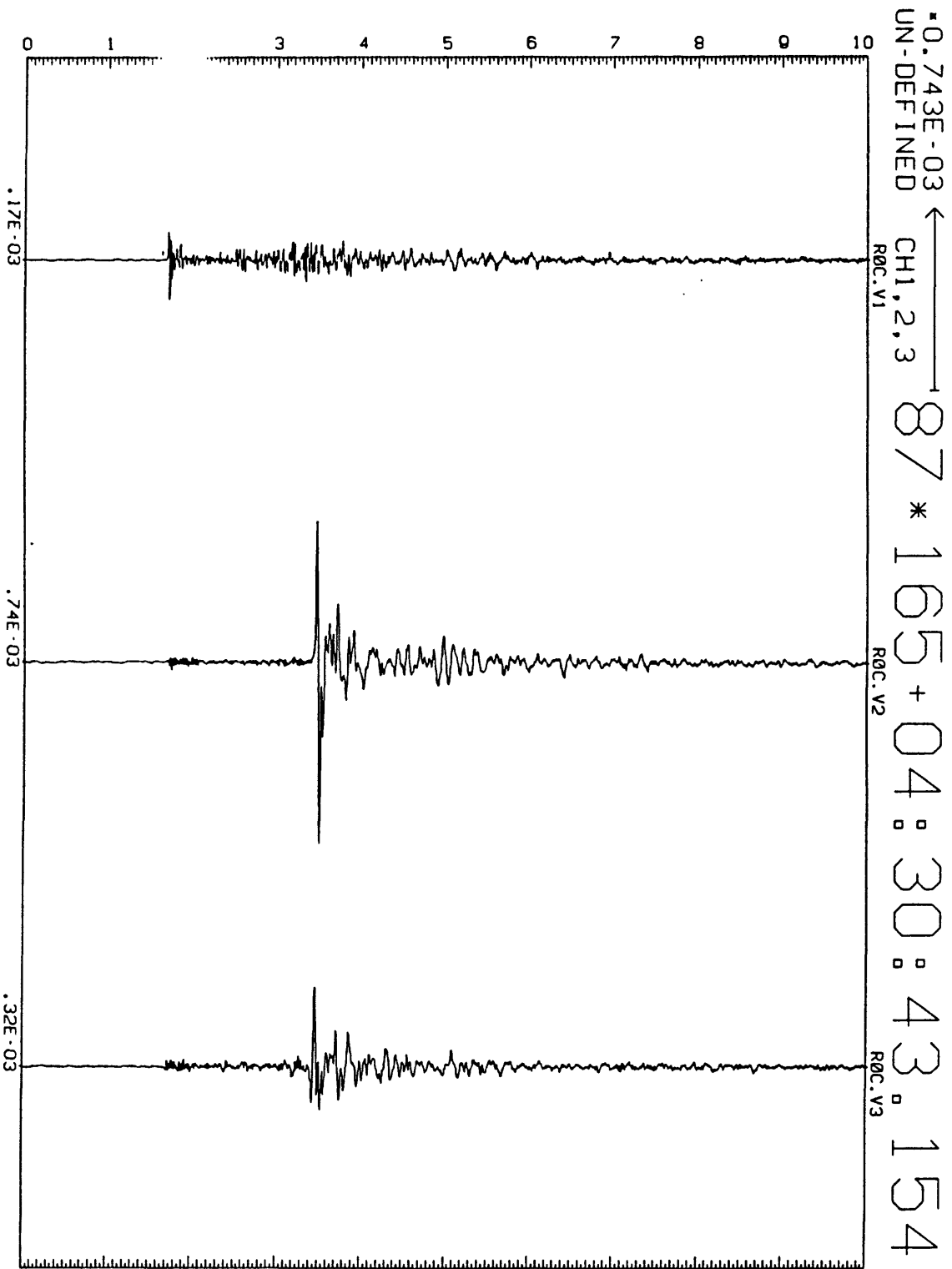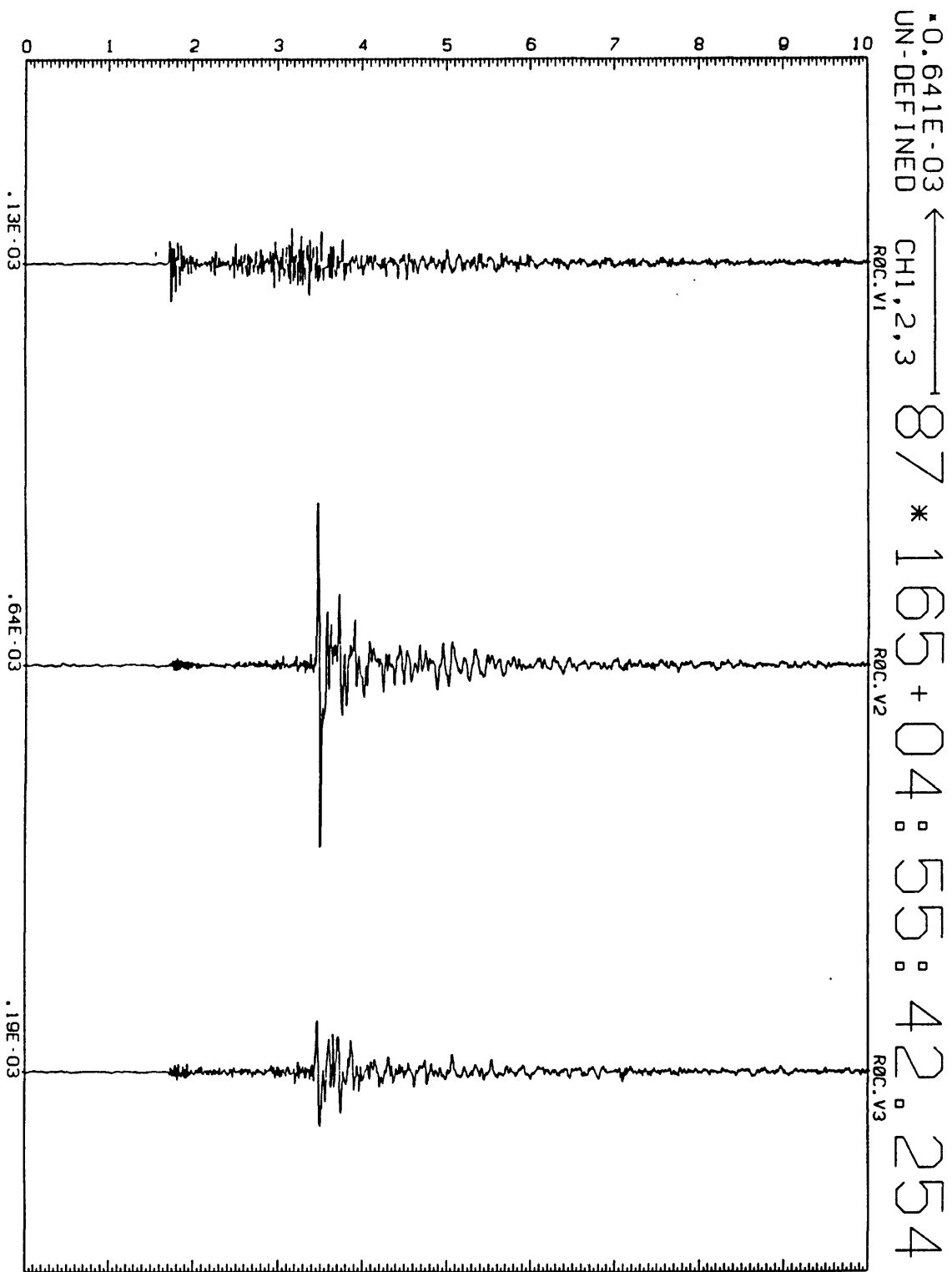**FIGURE 2 continued:** See Figure 2 caption on page 29 for a description of labeling conventions.
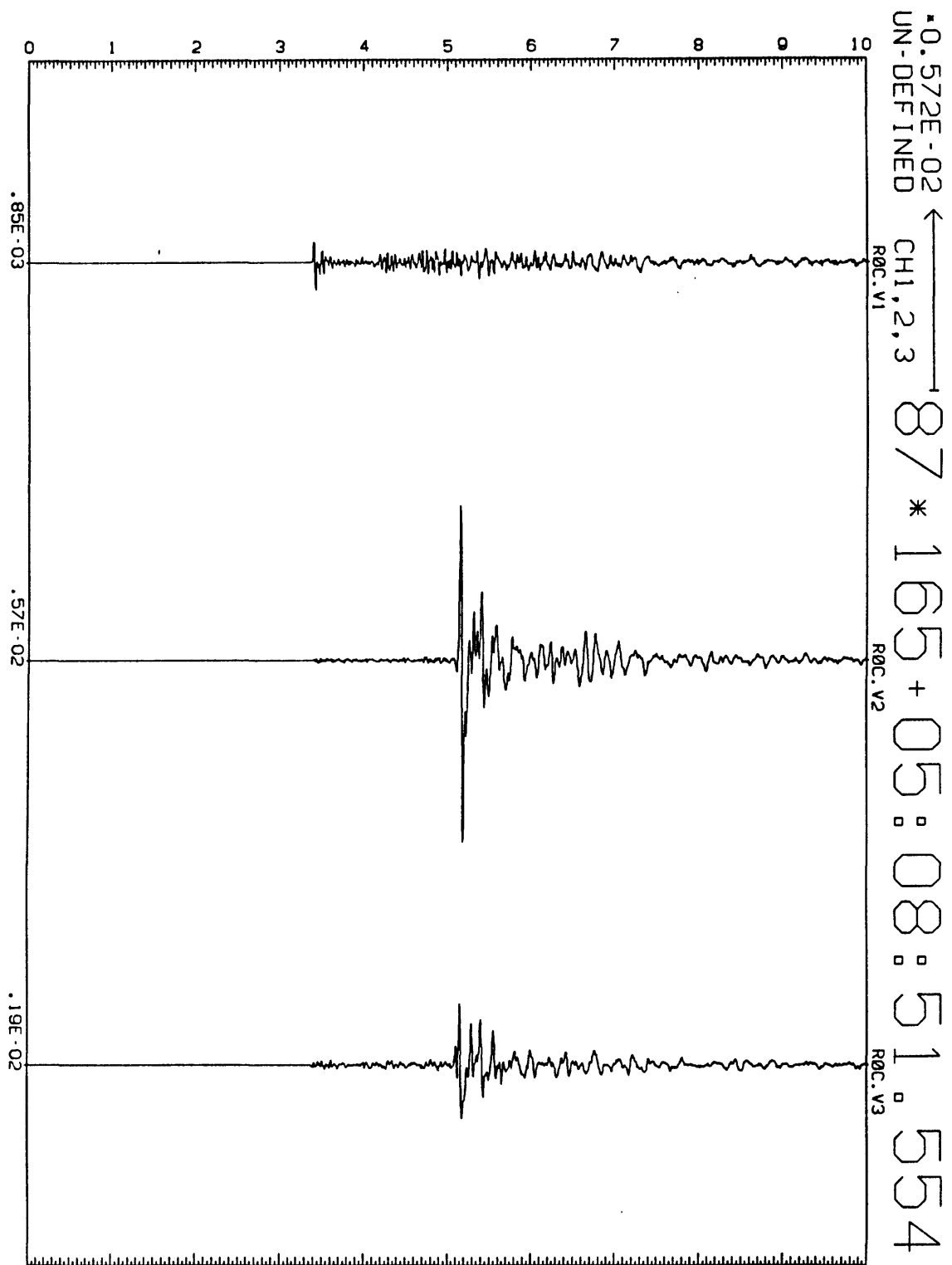
FIGURE 2 continued: See Figure 2 caption on page 29 for a description of labeling conventions.

32

FIGURE 2 continued: See Figure 2 caption on page 29 for a description of labeling conventions.

33

FIGURE 2 continued: See Figure 2 caption on page 29 for a description of labeling conventions.

FIGURE 2 continued: See Figure 2 caption on page 29 for a description of labeling conventions.
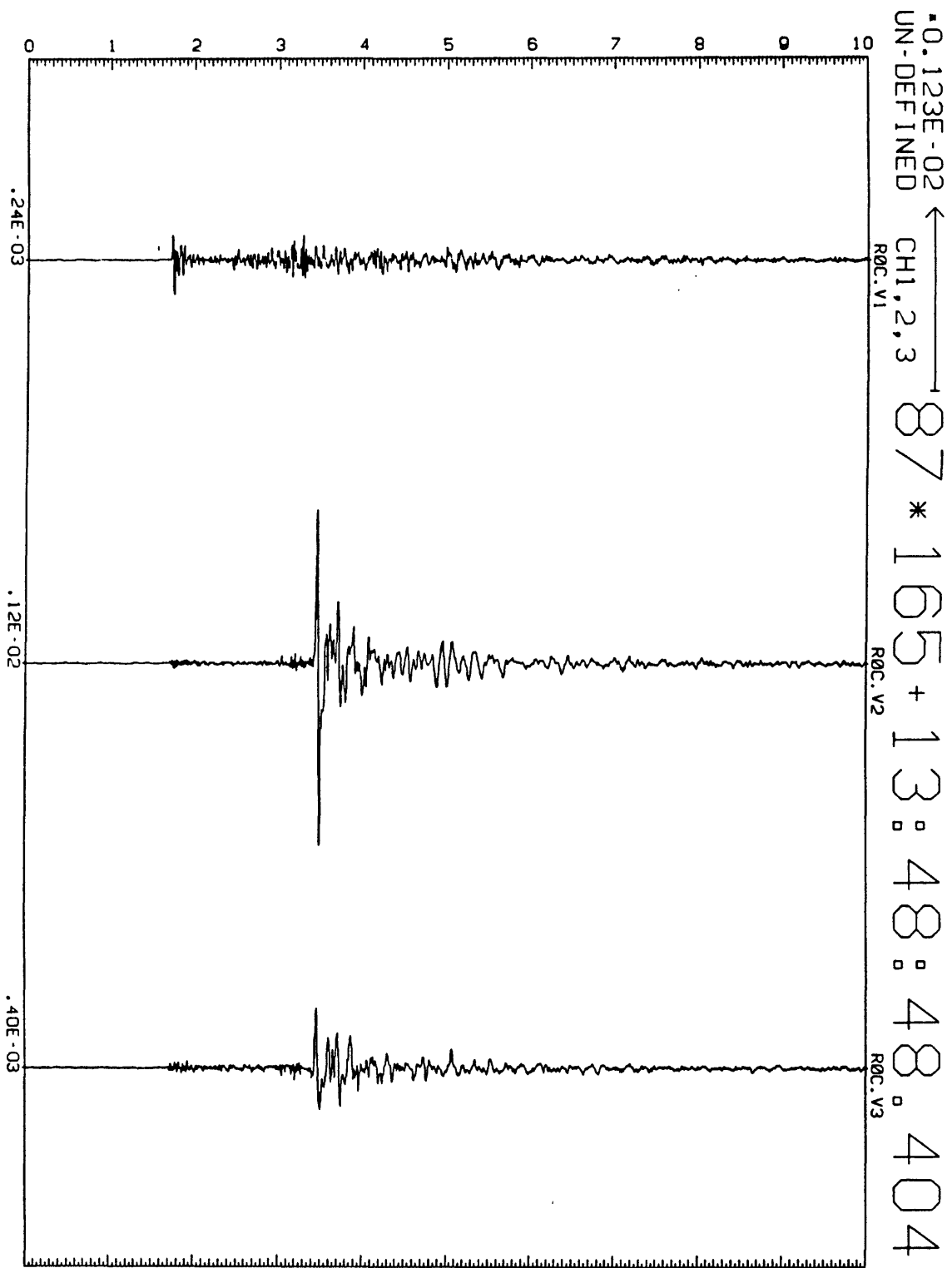
FIGURE 2 continued: See Figure 2 caption on page 29 for a description of labeling conventions.

FIGURE 2 continued: See Figure 2 caption on page 29 for a description of labeling conventions.
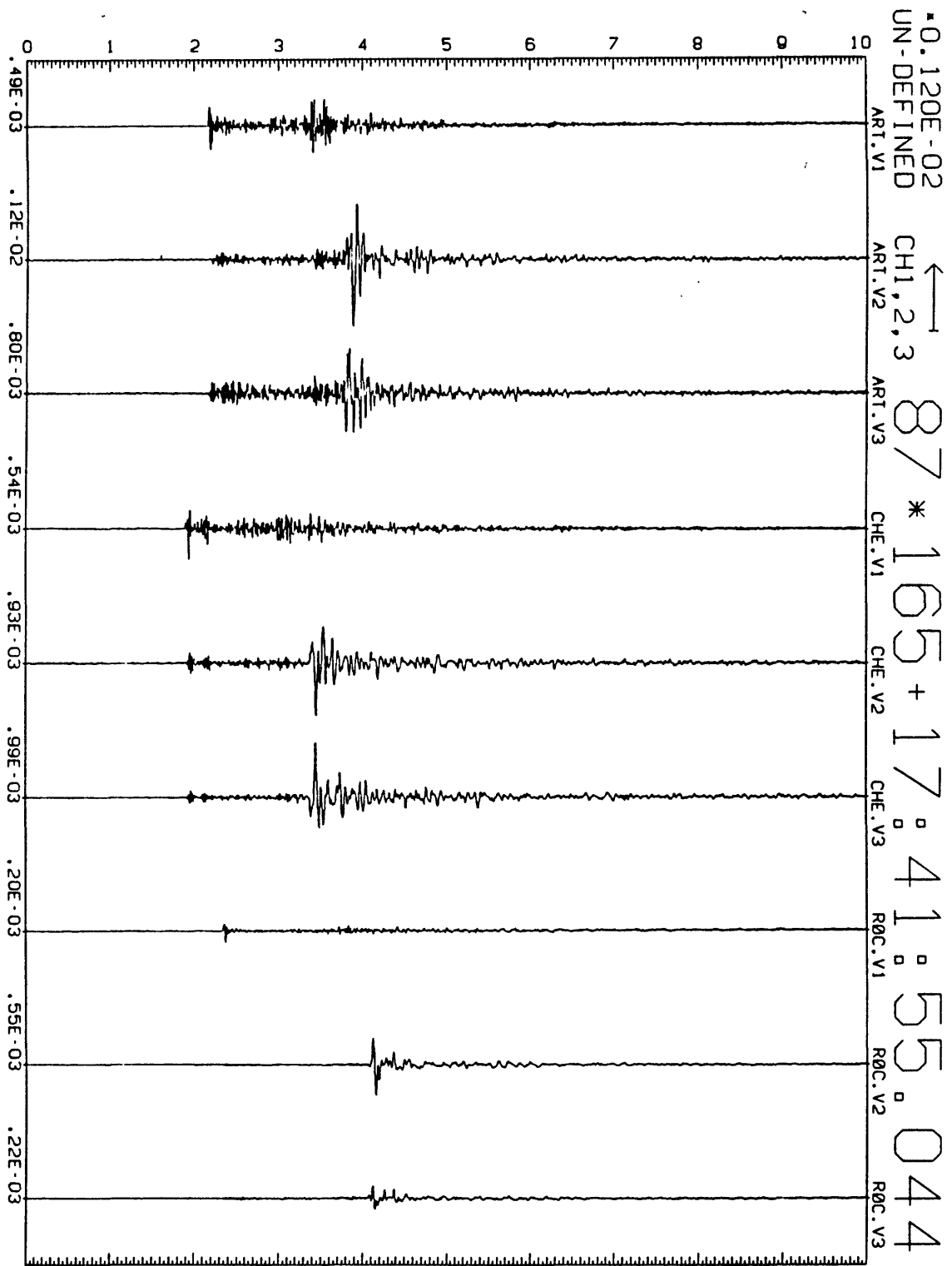
FIGURE 2 continued: See Figure 2 caption on page 29 for a description of labeling conventions.

FIGURE 2 continued: See Figure 2 caption on page 29 for a description of labeling conventions.

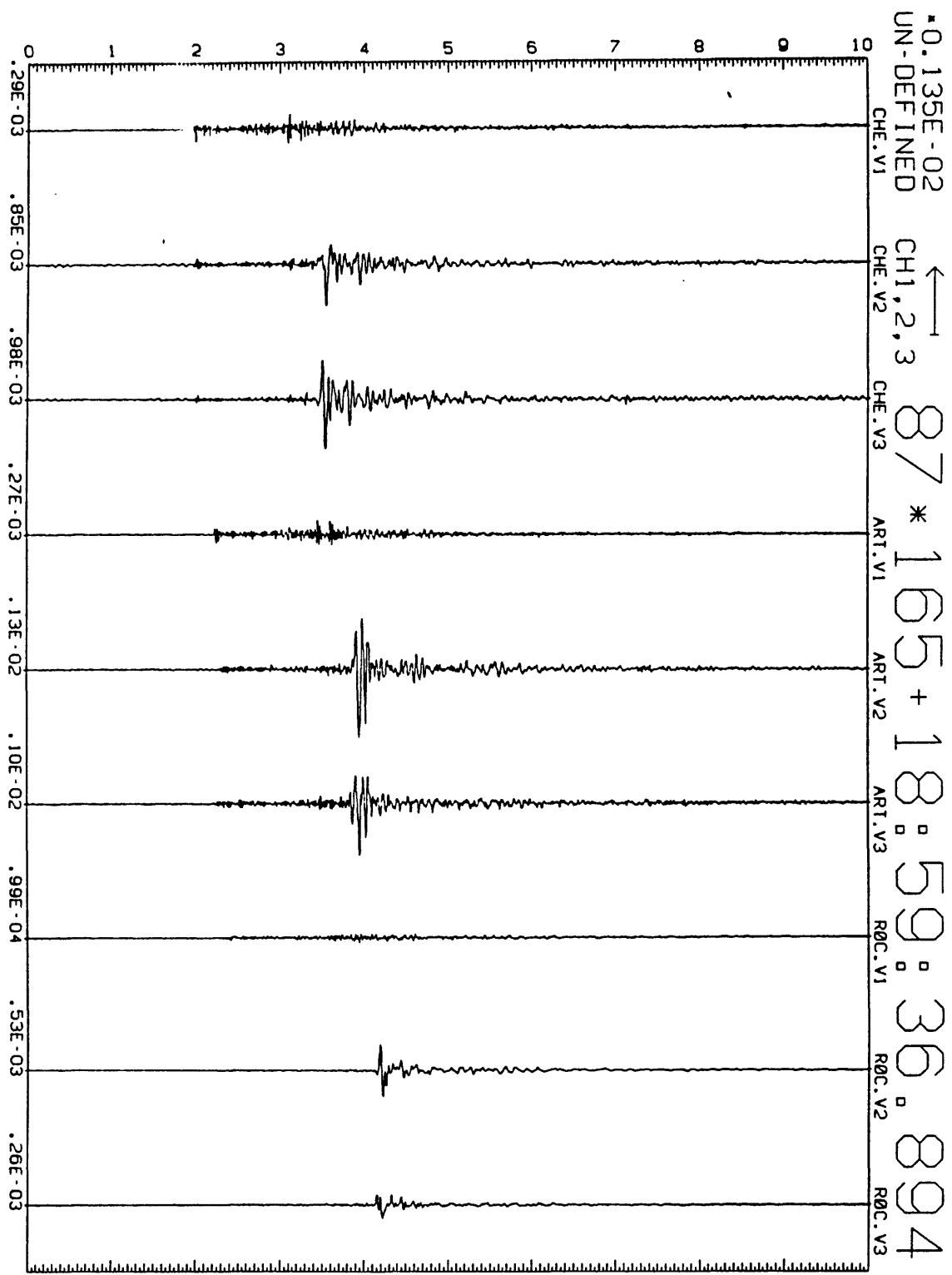FIGURE 2 continued: See Figure 2 caption on page 29 for a description of labeling conventions.

FIGURE 2 continued: See Figure 2 caption on page 29 for a description of labeling conventions.

FIGURE 2 continued: See Figure 2 caption on page 29 for a description of labeling conventions.
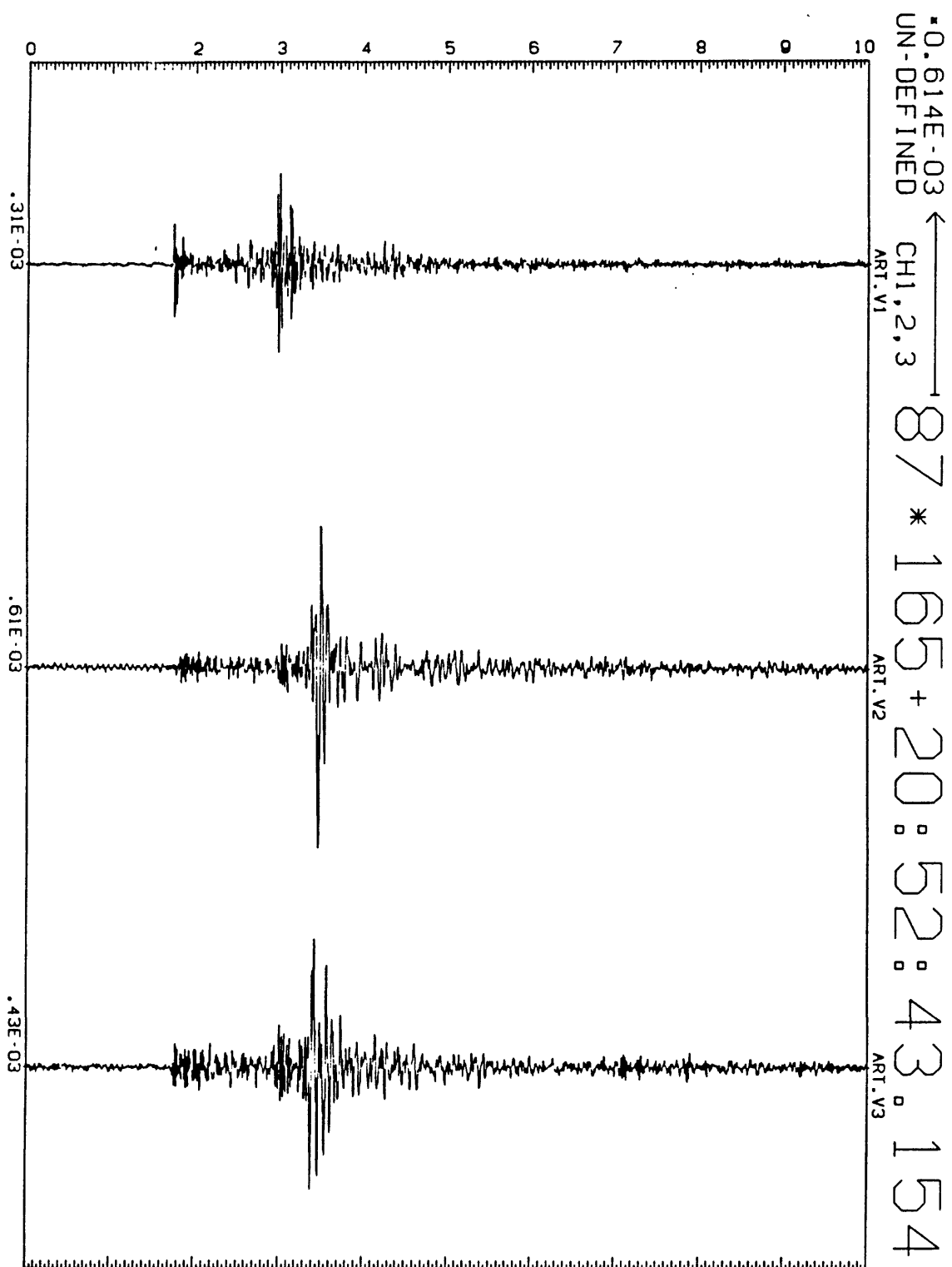
FIGURE 2 continued: See Figure 2 caption on page 29 for a description of labeling conventions.

FIGURE 2 continued: See Figure 2 caption on page 29 for a description of labeling conventions.

FIGURE 2 continued: See Figure 2 caption on page 29 for a description of labeling conventions.
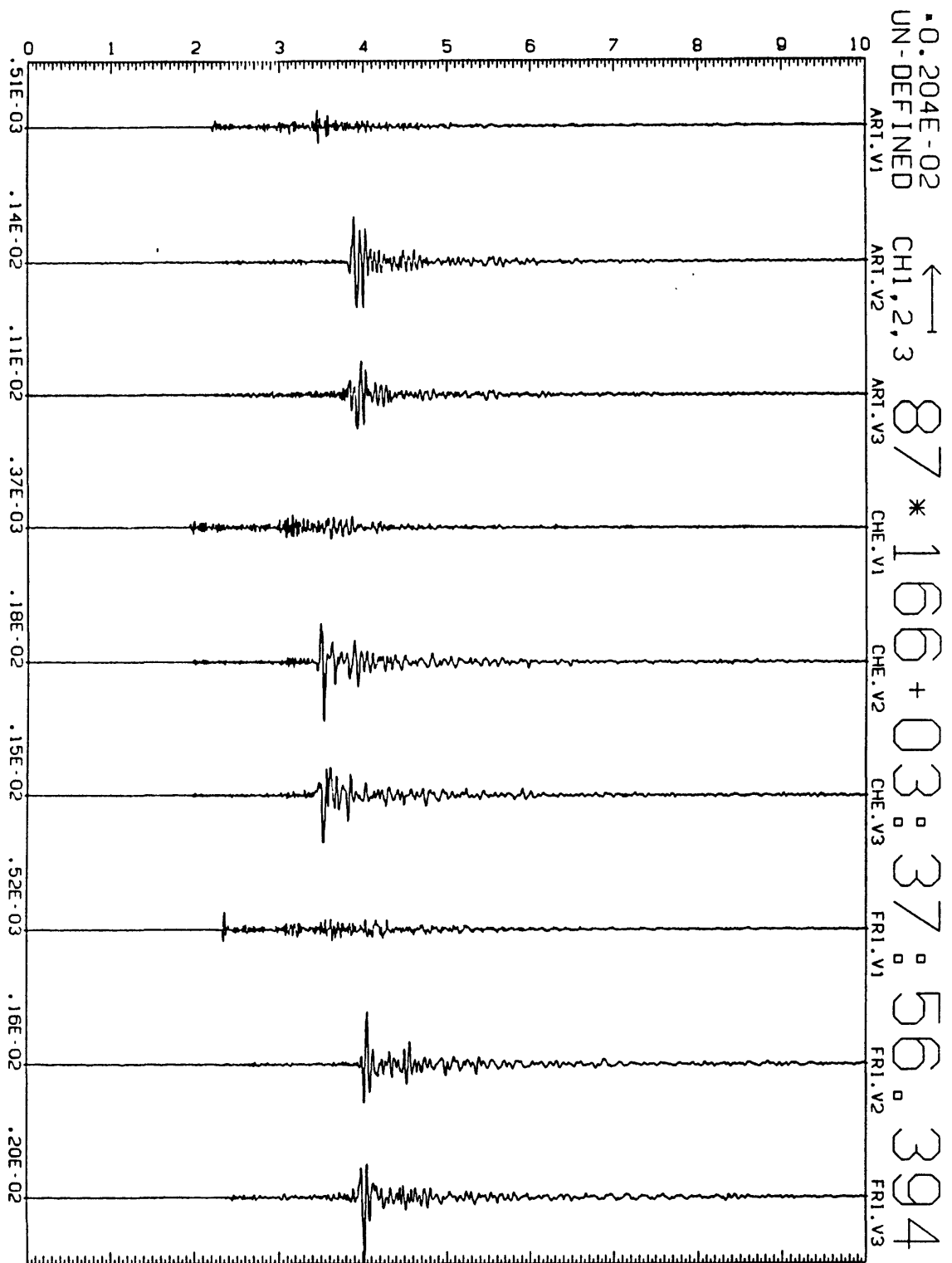
45

FIGURE 2 continued: See Figure 2 caption on page 29 for a description of labeling conventions.

FIGURE 2 continued: See Figure 2 caption on page 29 for a description of labeling conventions.

47

FIGURE 2 continued: See Figure 2 caption on page 29 for a description of labeling conventions.
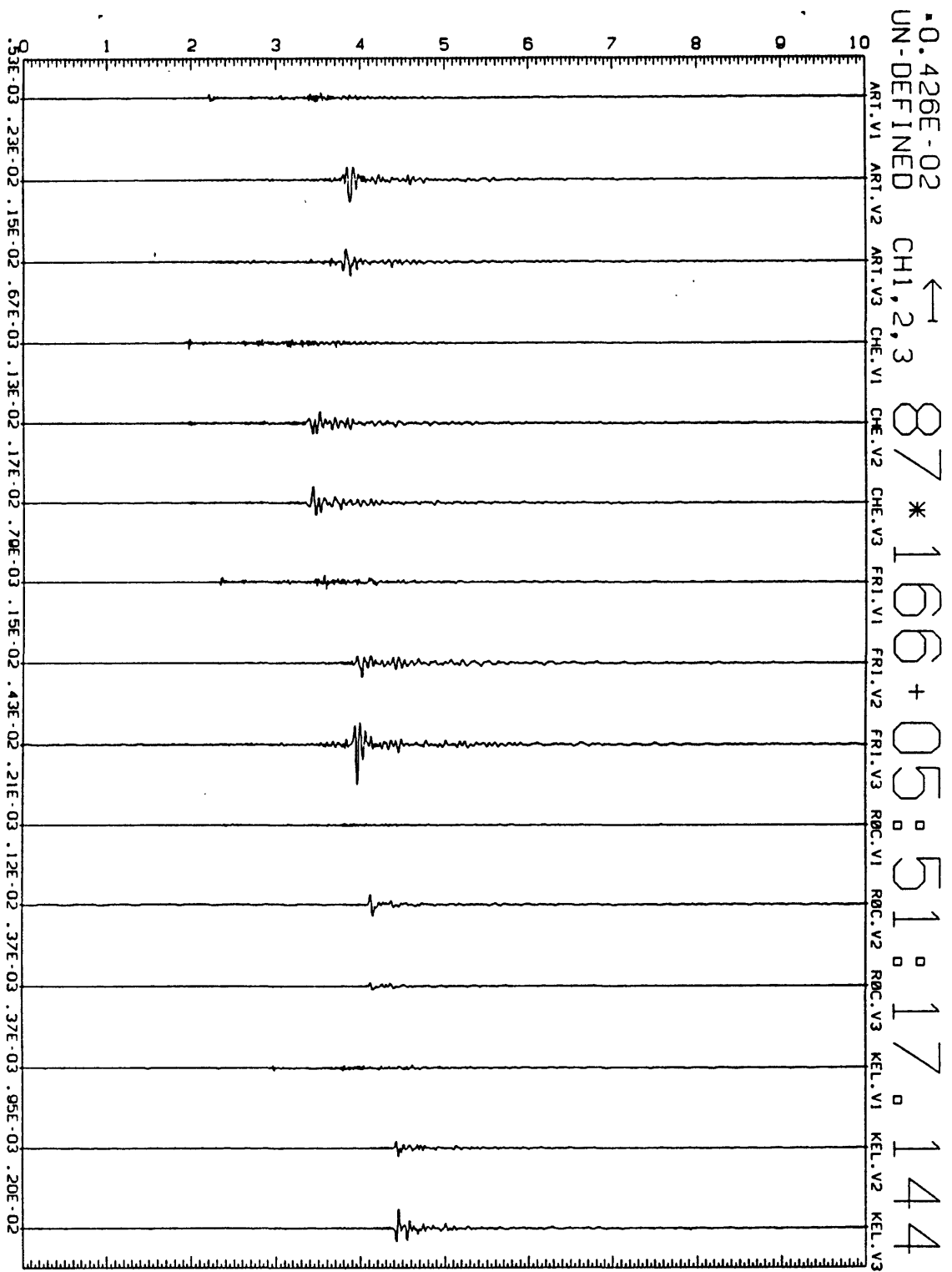
48

FIGURE 2 continued: See Figure 2 caption on page 29 for a description of labeling conventions.

49

FIGURE 2 continued: See Figure 2 caption on page 29 for a description of labeling conventions.

FIGURE 2 continued: See Figure 2 caption on page 29 for a description of labeling conventions.

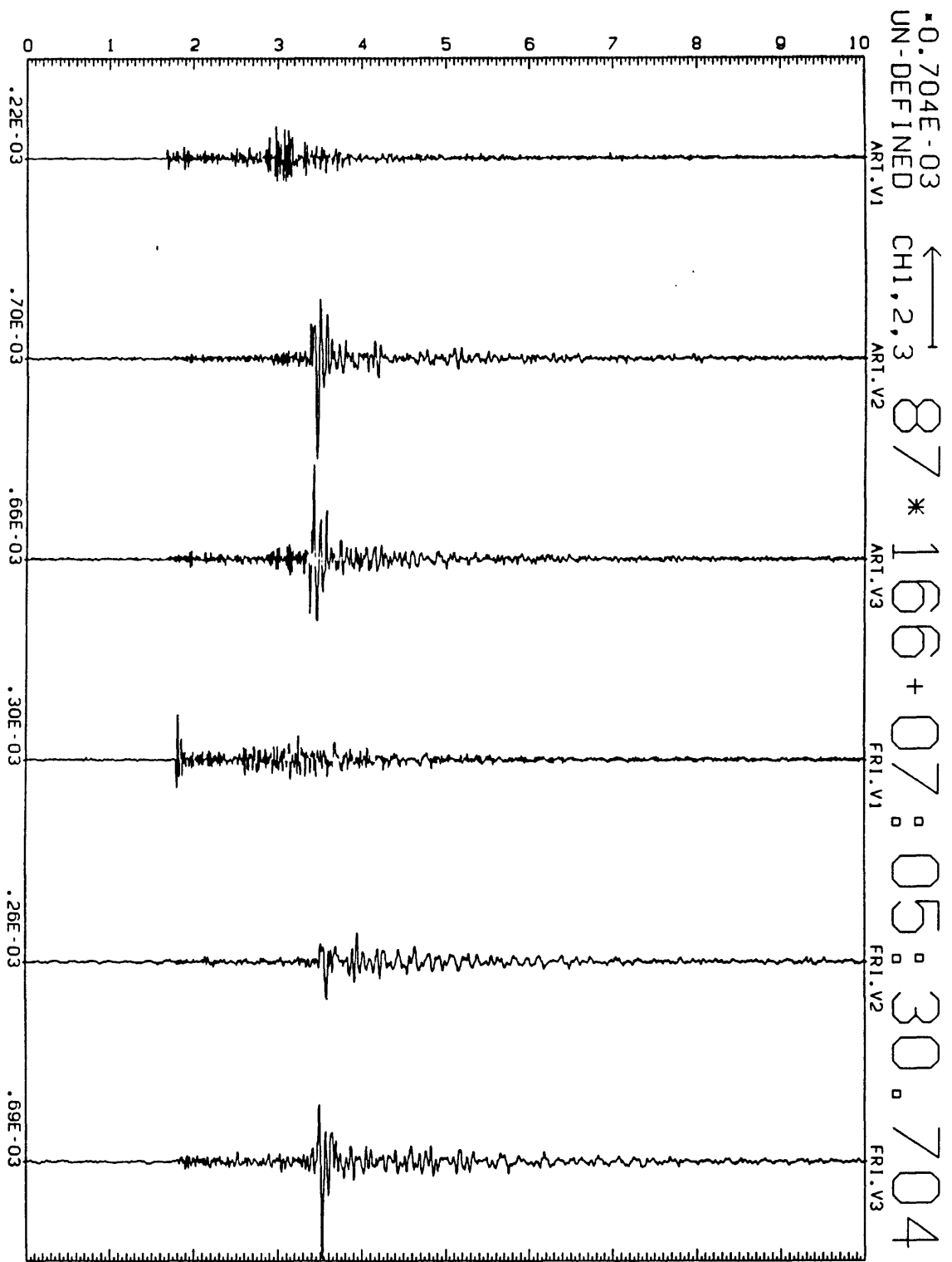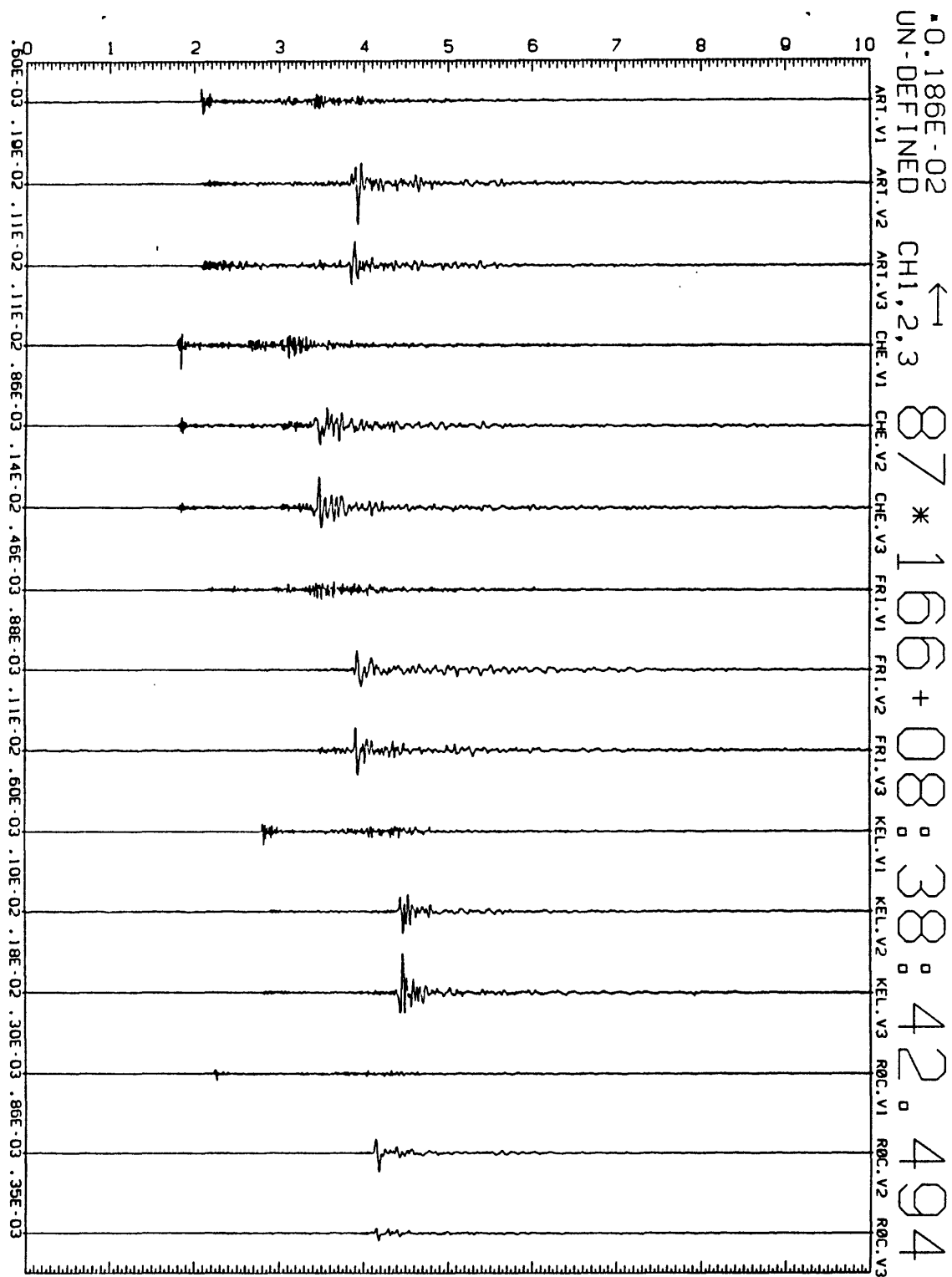FIGURE 2 continued: See Figure 2 caption on page 29 for a description of labeling conventions.

52

FIGURE 2 continued: See Figure 2 caption on page 29 for a description of labeling conventions.

FIGURE 2 continued: See Figure 2 caption on page 29 for a description of labeling conventions.

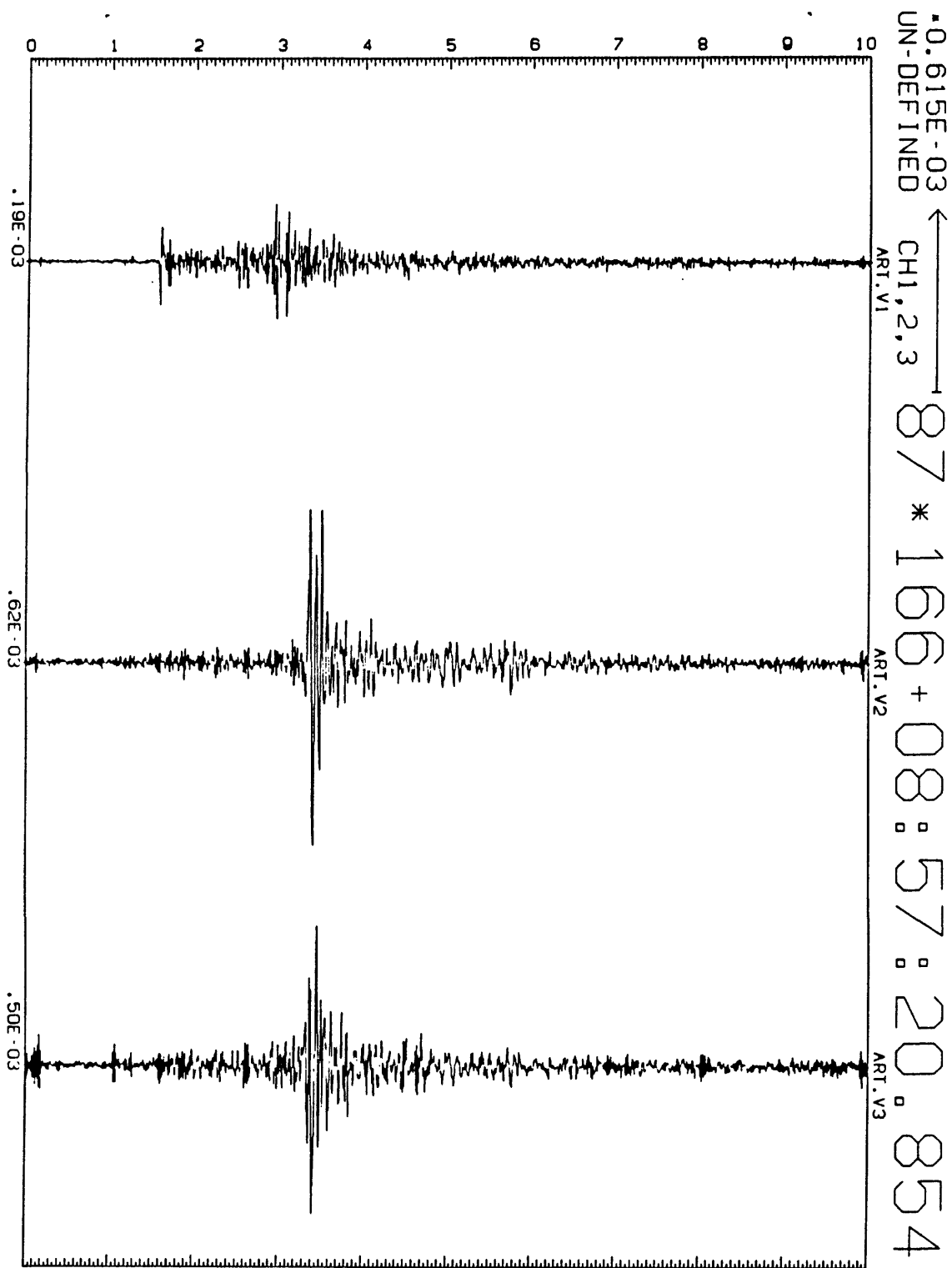FIGURE 2 continued: See Figure 2 caption on page 29 for a description of labeling conventions.

FIGURE 2 continued: See Figure 2 caption on page 29 for a description of labeling conventions.
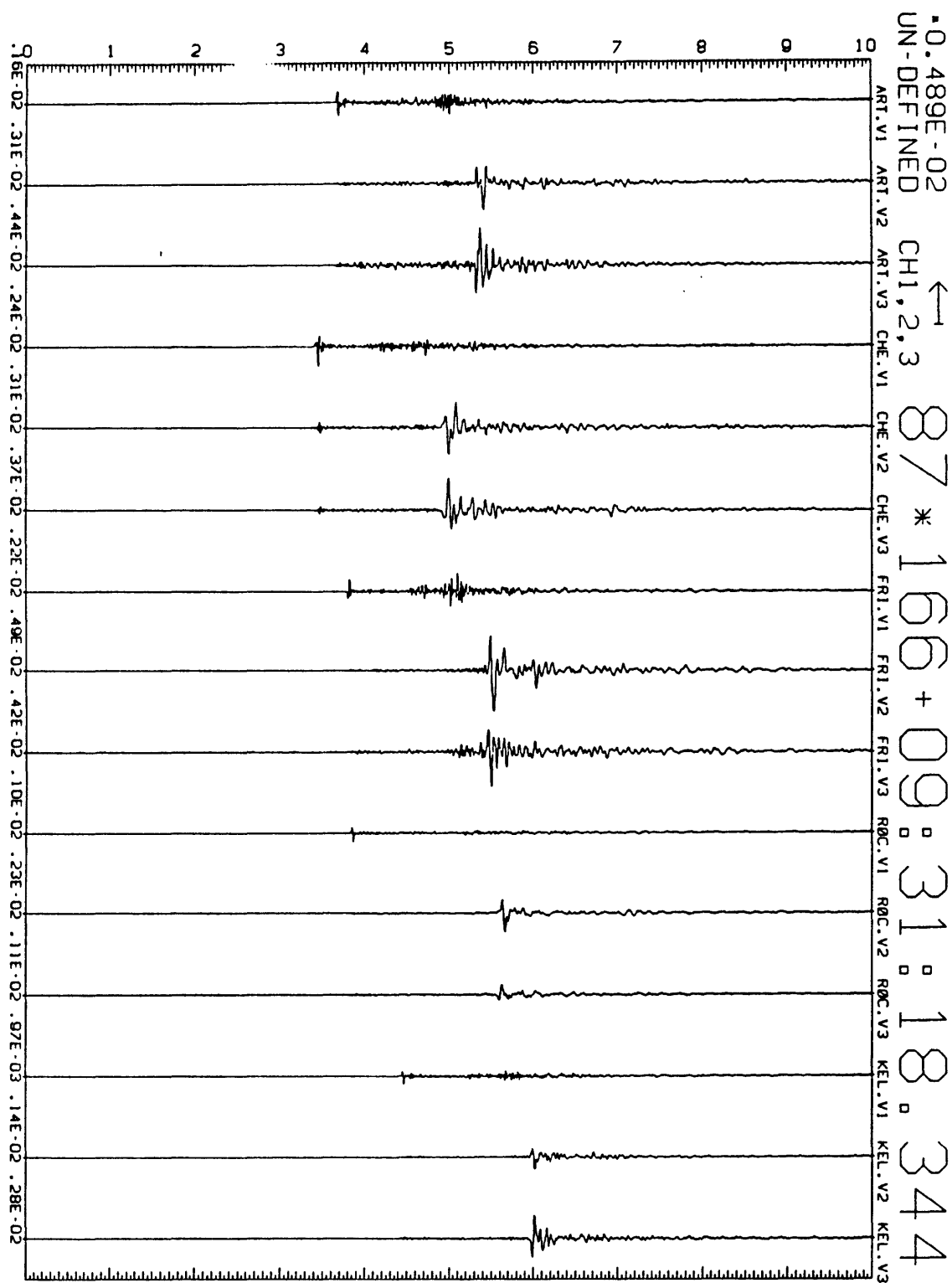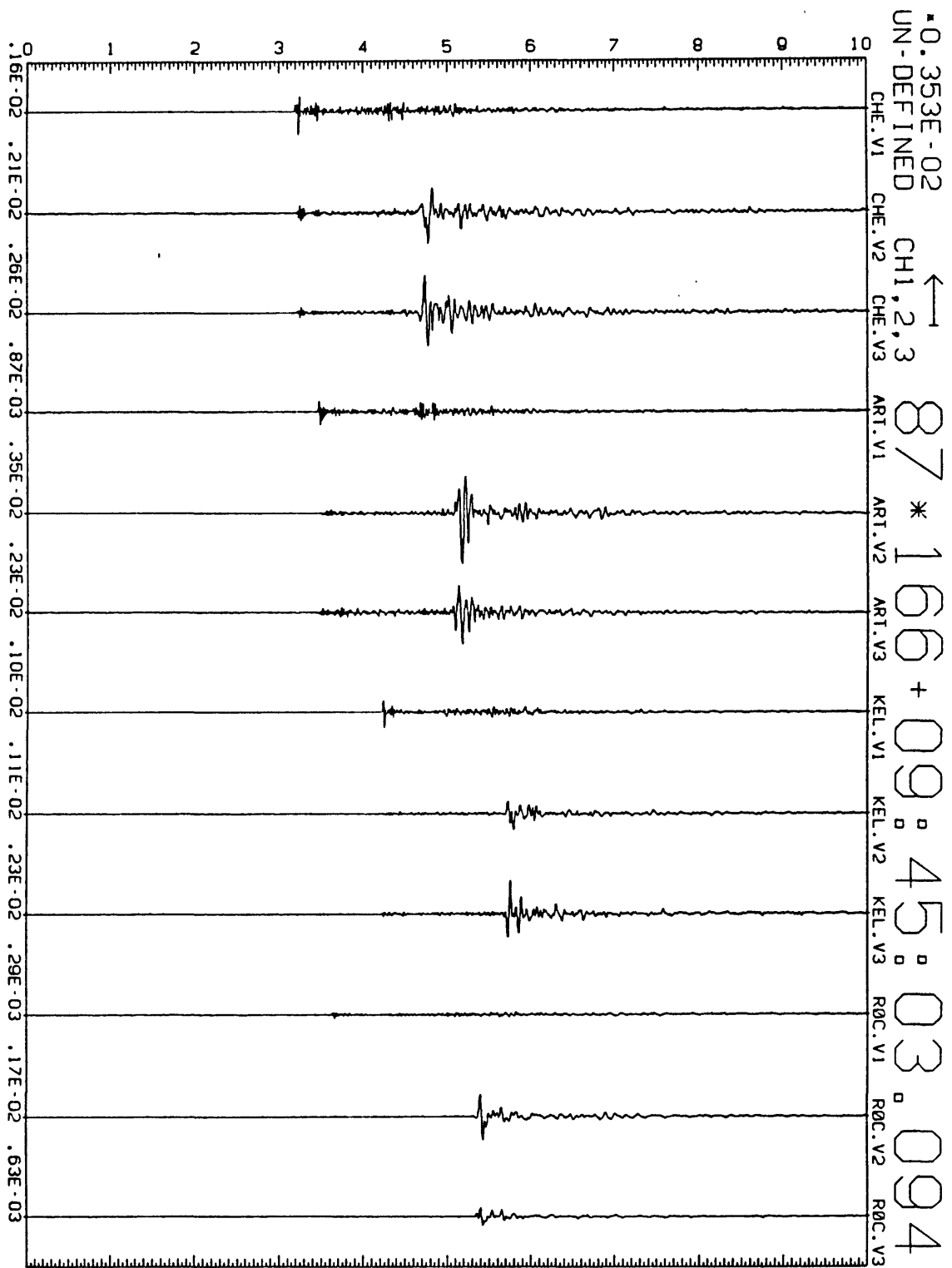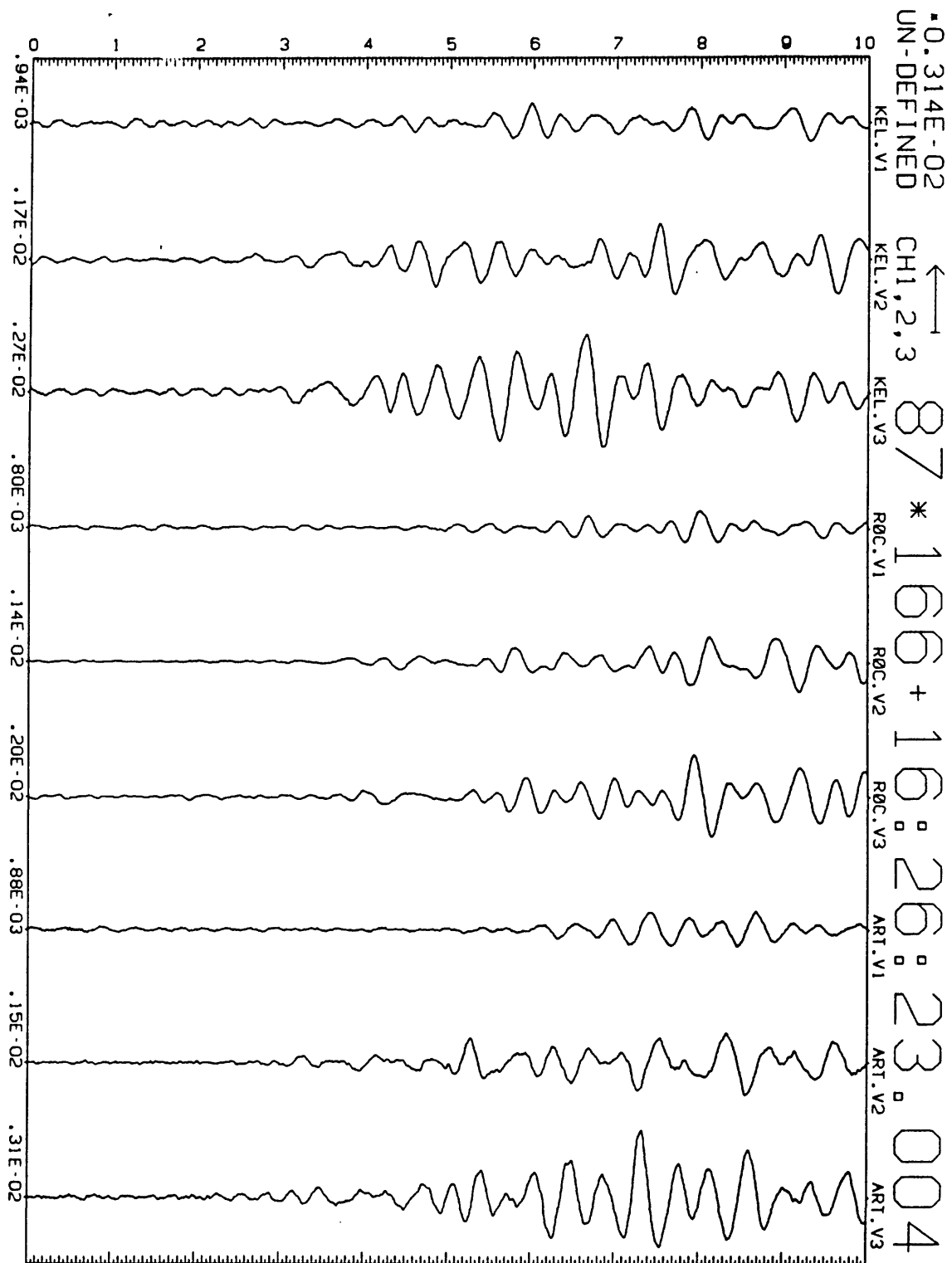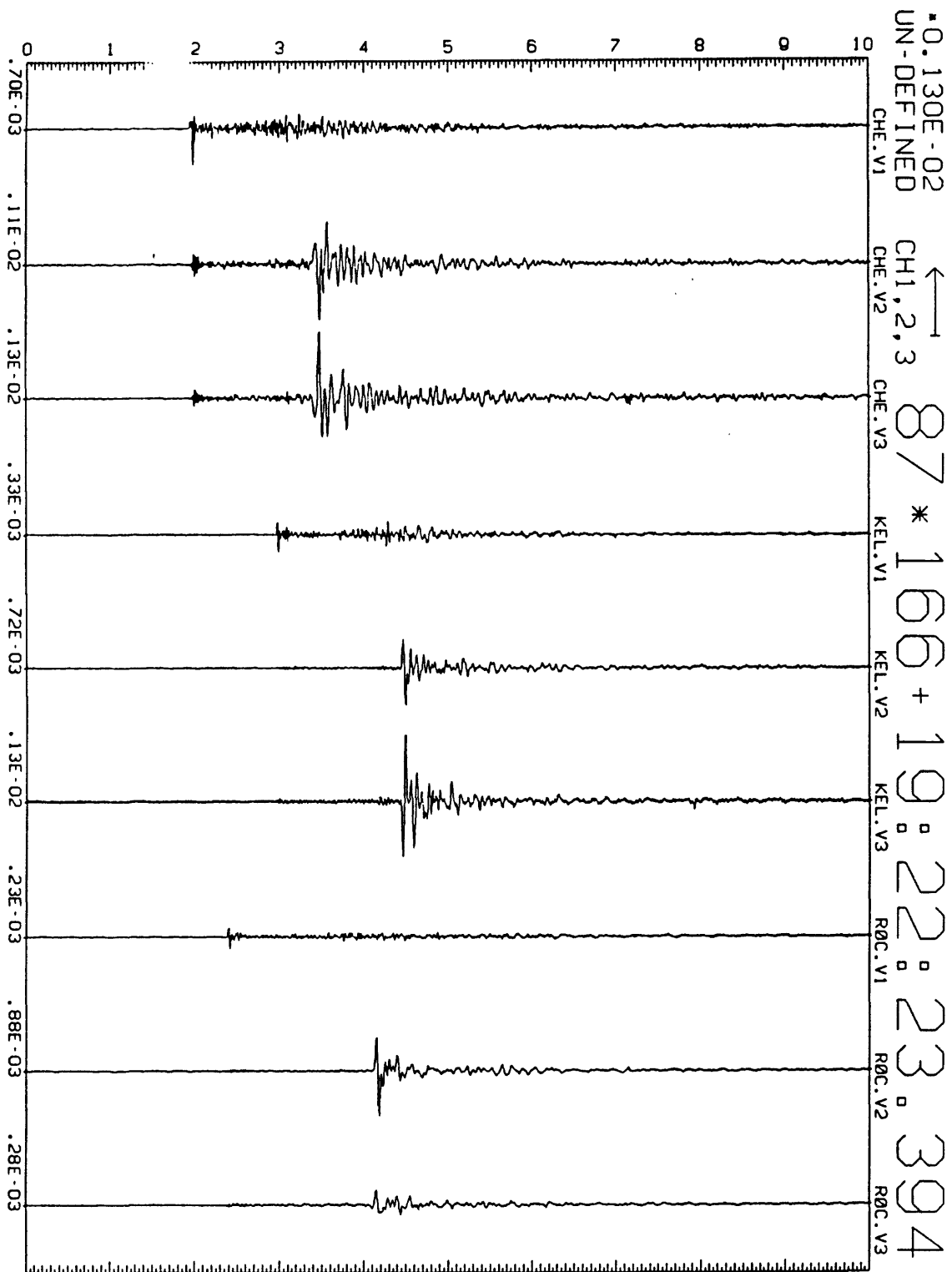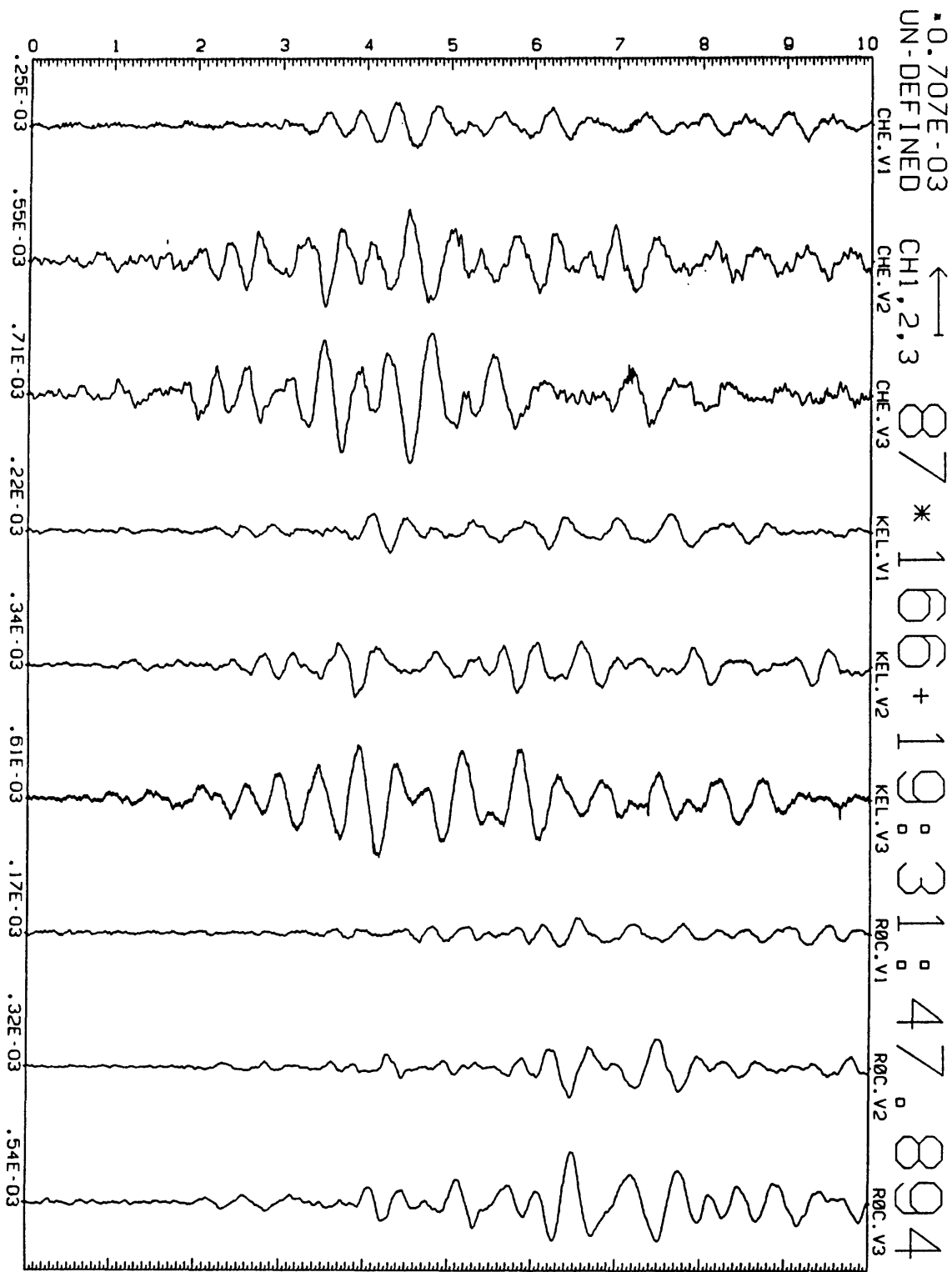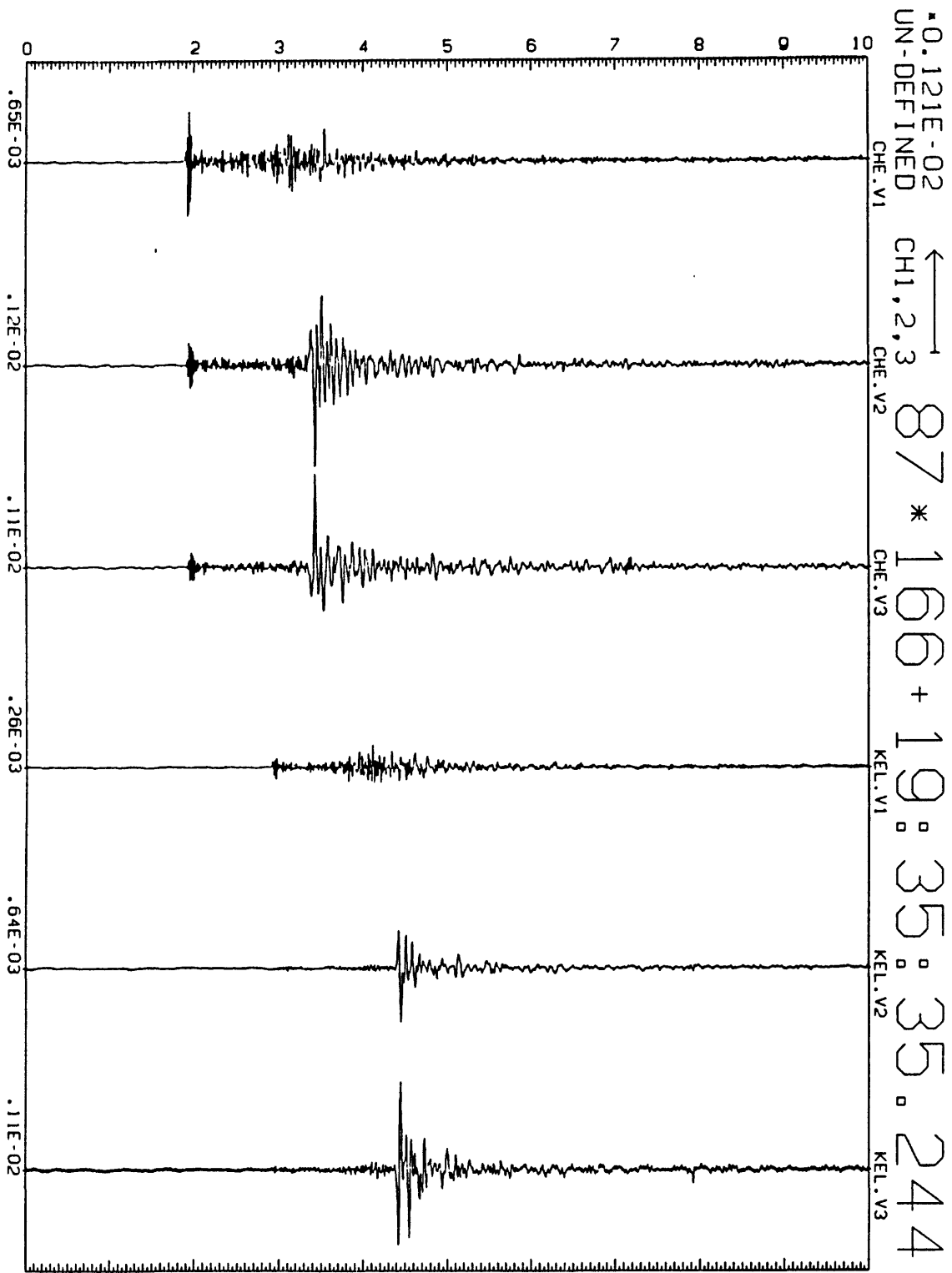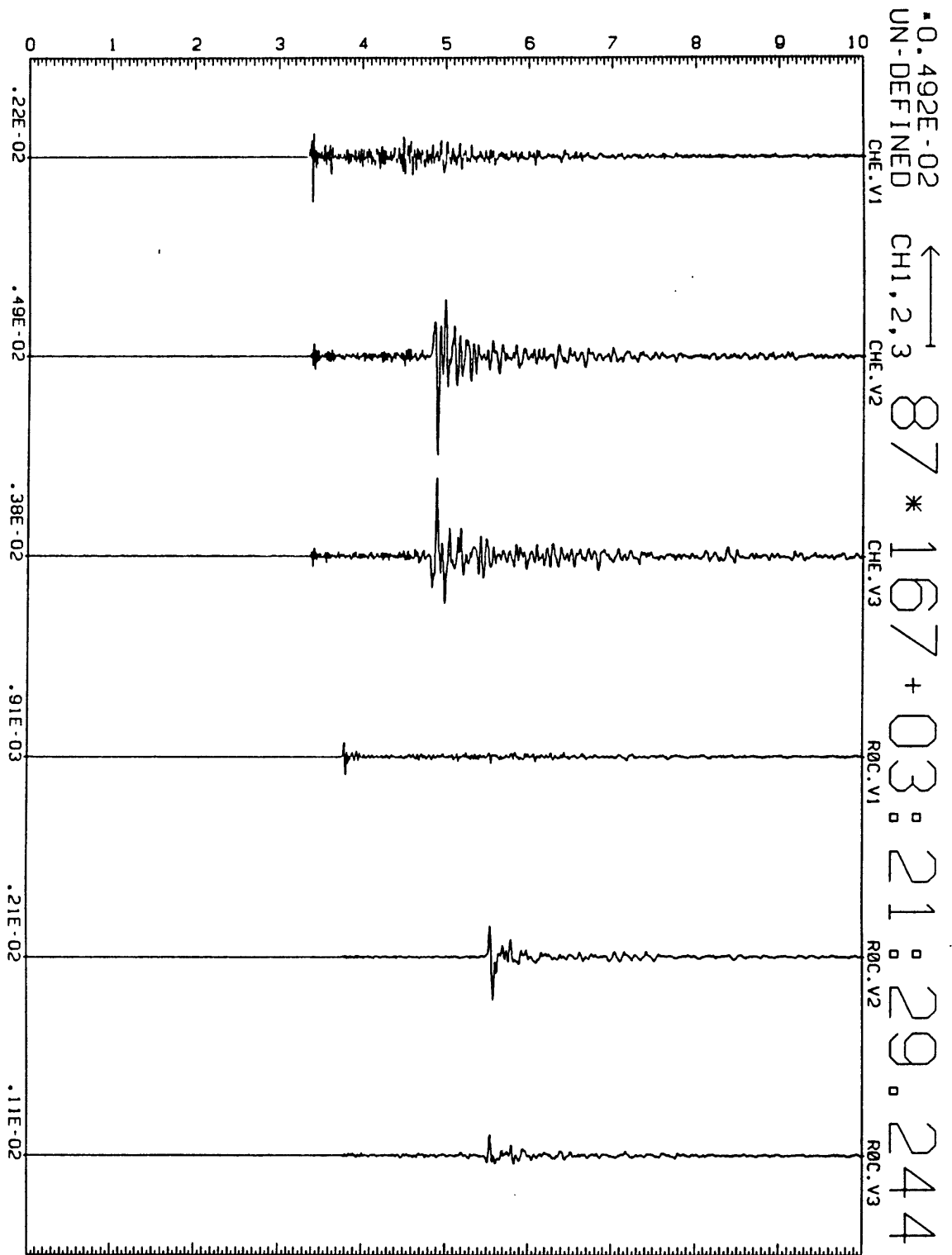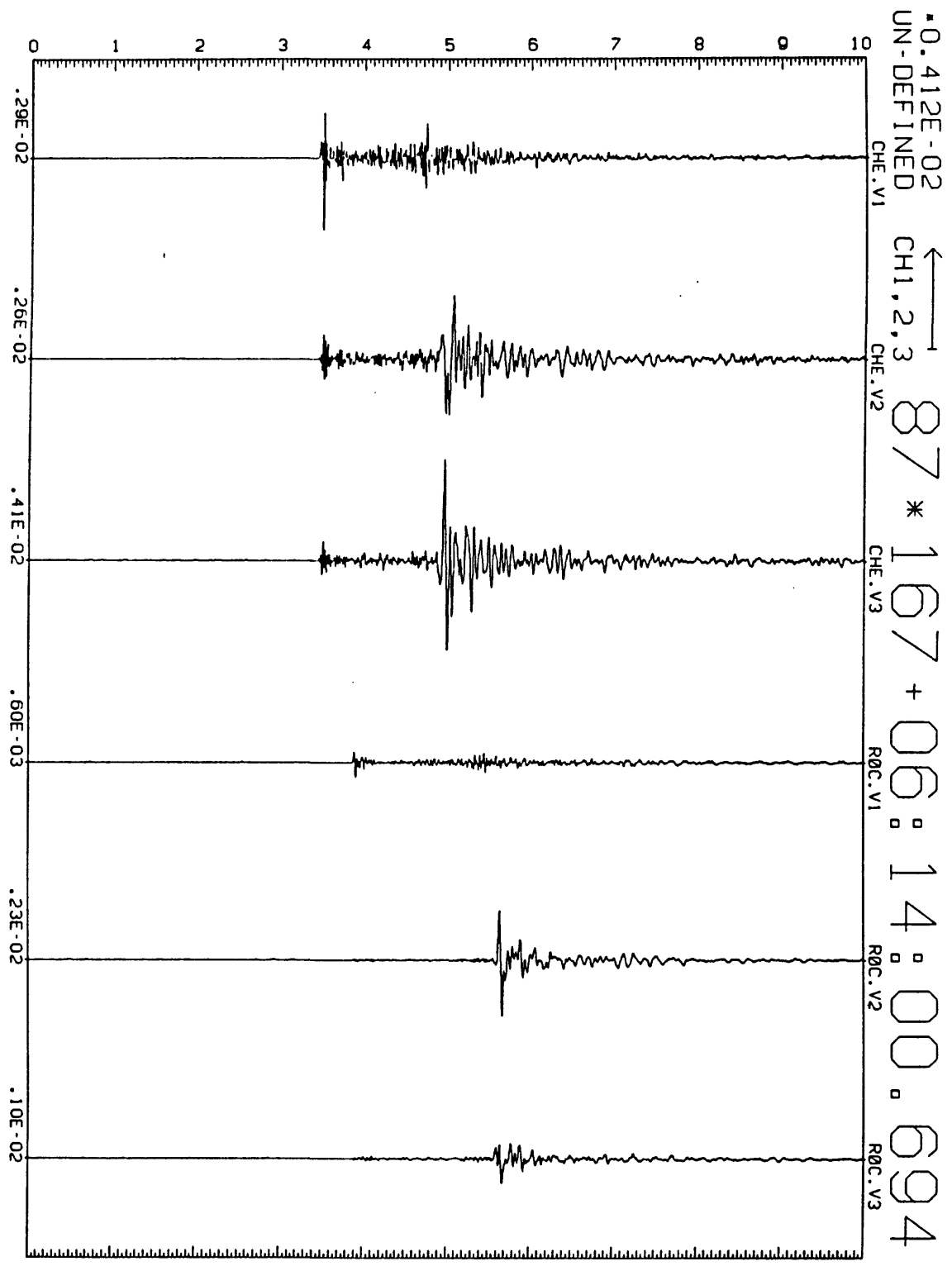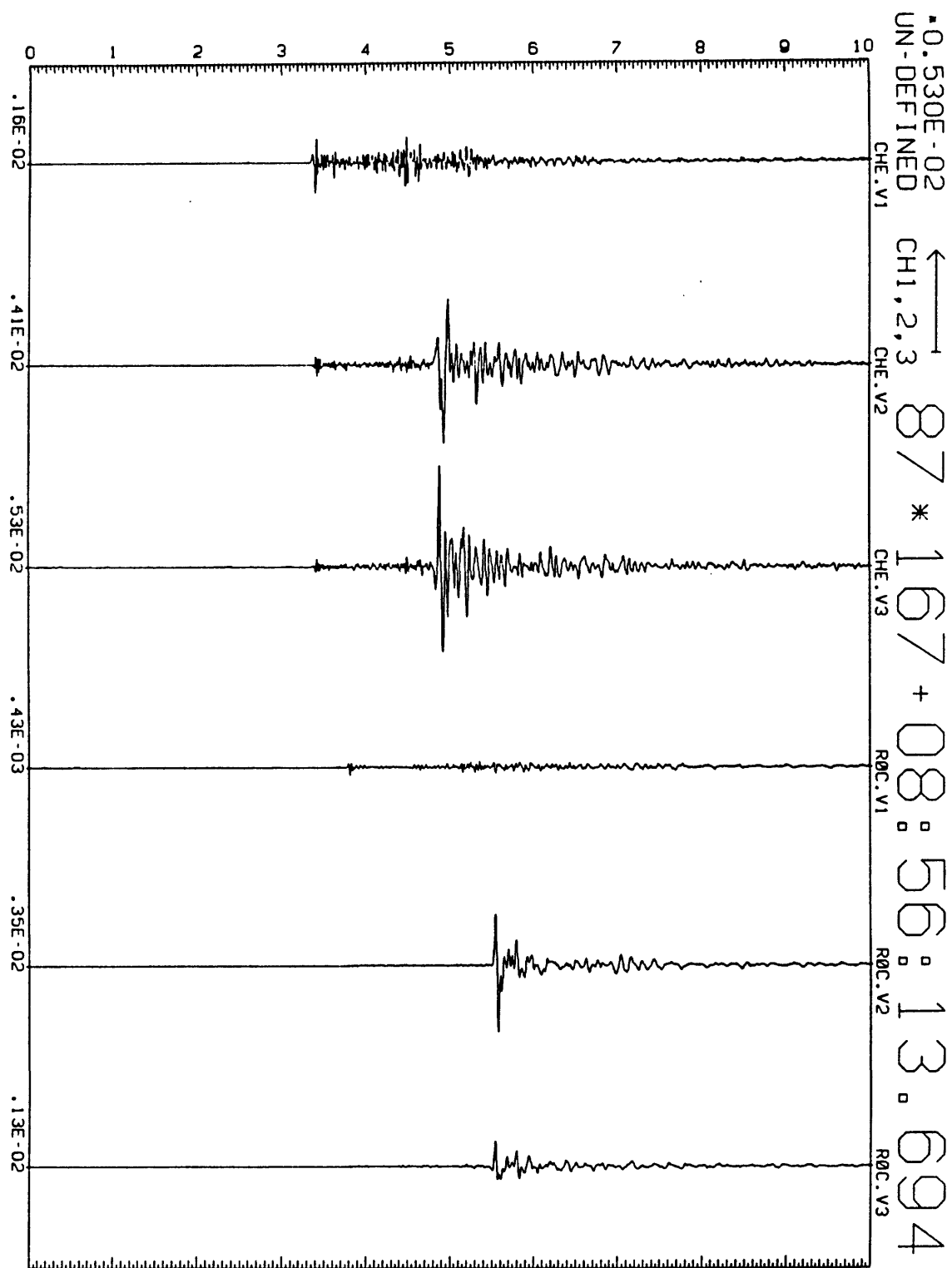
FIGURE 2 continued: See Figure 2 caption on page 29 for a description of labeling conventions.

FIGURE 2 continued: See Figure 2 caption on page 29 for a description of labeling conventions.

FIGURE 2 continued: See Figure 2 caption on page 29 for a description of labeling conventions.
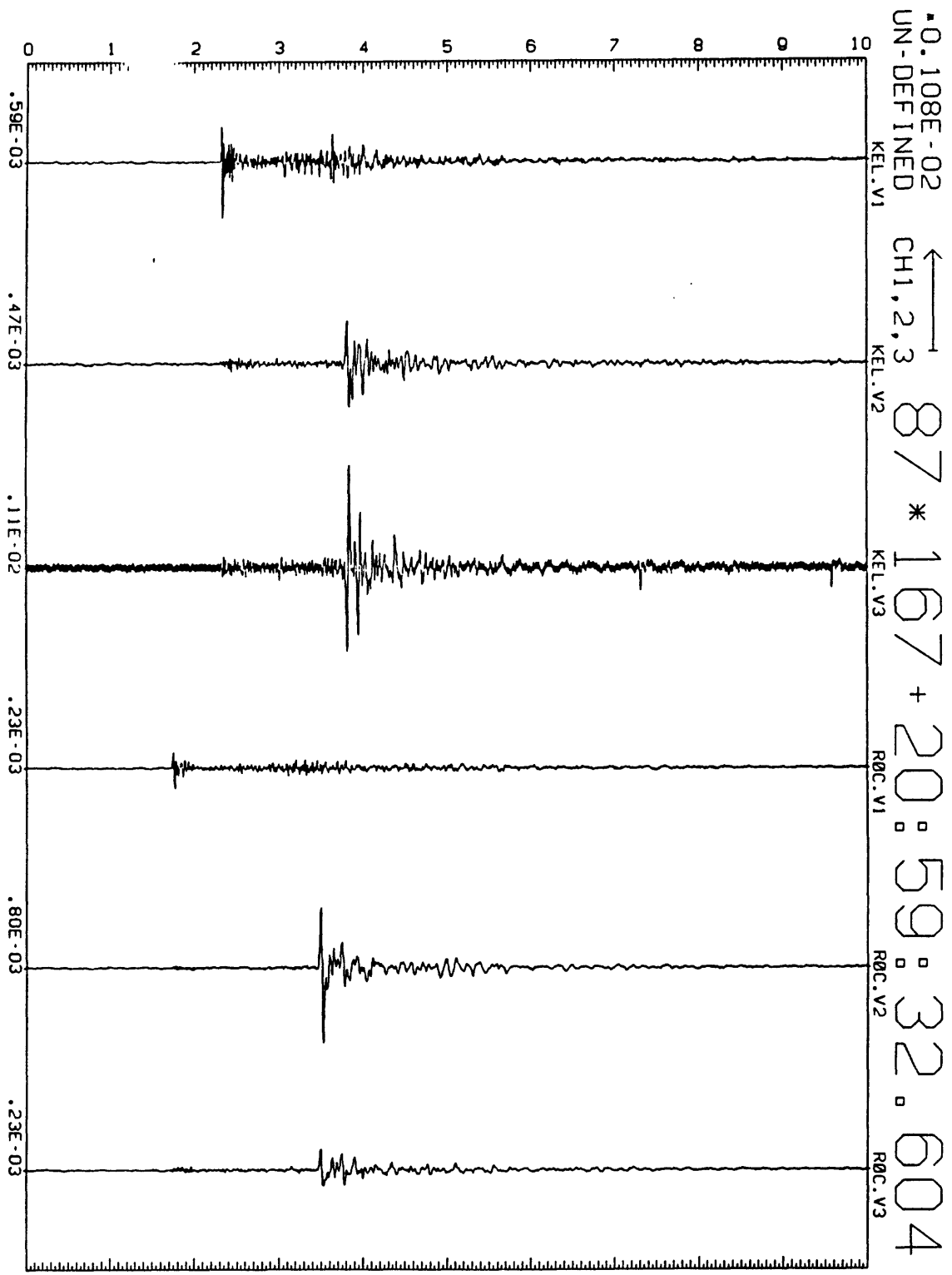
REGIONAL EARTHQUAKE

The 164+21:17 magnitude 4.1_{mbLg} regional earthquake generated the peak ground motion of the dataset as a whole --- 9×10^{-3} cm/s --- which is in the record of the S-wave arrival on the E-W horizontal component at Station RUS. The S-wave of this event was well-recorded by five PADS stations, and the vector time series are shown in Figure 3. Stations ART and ROC triggered on the P-wave as well but then turned off and subsequently retriggered on the S-wave when the other 3 stations also triggered. Thus an 8-second gap exists in the otherwise complete recording of the event at these two stations. The S-waves on the three components exhibit a significant variation between the five stations. The peak velocities which are annotated to the left of each trace (there are two values for each channel of stations ROC and ART which correspond to separate P- and S-wave arrivals respectively) exhibit a range of [3 - 9] $\times 10^{-3}$ cm/s, and these values quantify the variation of broad-band site-amplification.

The spectral response of the Olney, Illinois, area to an earthquake at regional epicentral distances is suggested by the spectra that are displayed in Figure 4. The figure depicts a source/receiver map of the regional event in the New Madrid Seismic Zone and five stations of the PADS array near Olney, Illinois, at f 270 km epicentral range. The three log-log velocity spectra which are inset in the center of the map are the raw (not corrected for transducer/recorder response) whole-record spectra of three components --- Z, N, and E --- of the S-wave arrival recorded at station ROC.

Because ROC was sited on outcrop, we have calculated the S-wave whole-record spectral ratios with respect to Station ROC (see Figure 4) of the other four stations which recorded the S-wave arrival of the 164+21:17 event. Smoothed versions of the Station ROC denominator spectra and the four spectral ratios are plotted in Figure 5 for each of the three components. The most significant feature of the ratios is that all the numerator stations (which are sited on glacial drift, i.e., a thin surficial layer of low-velocity material) exhibit site-amplifications that increase with frequency up to a maximum of +12 dB (factor of f4) in the octave 25-50 Hz.
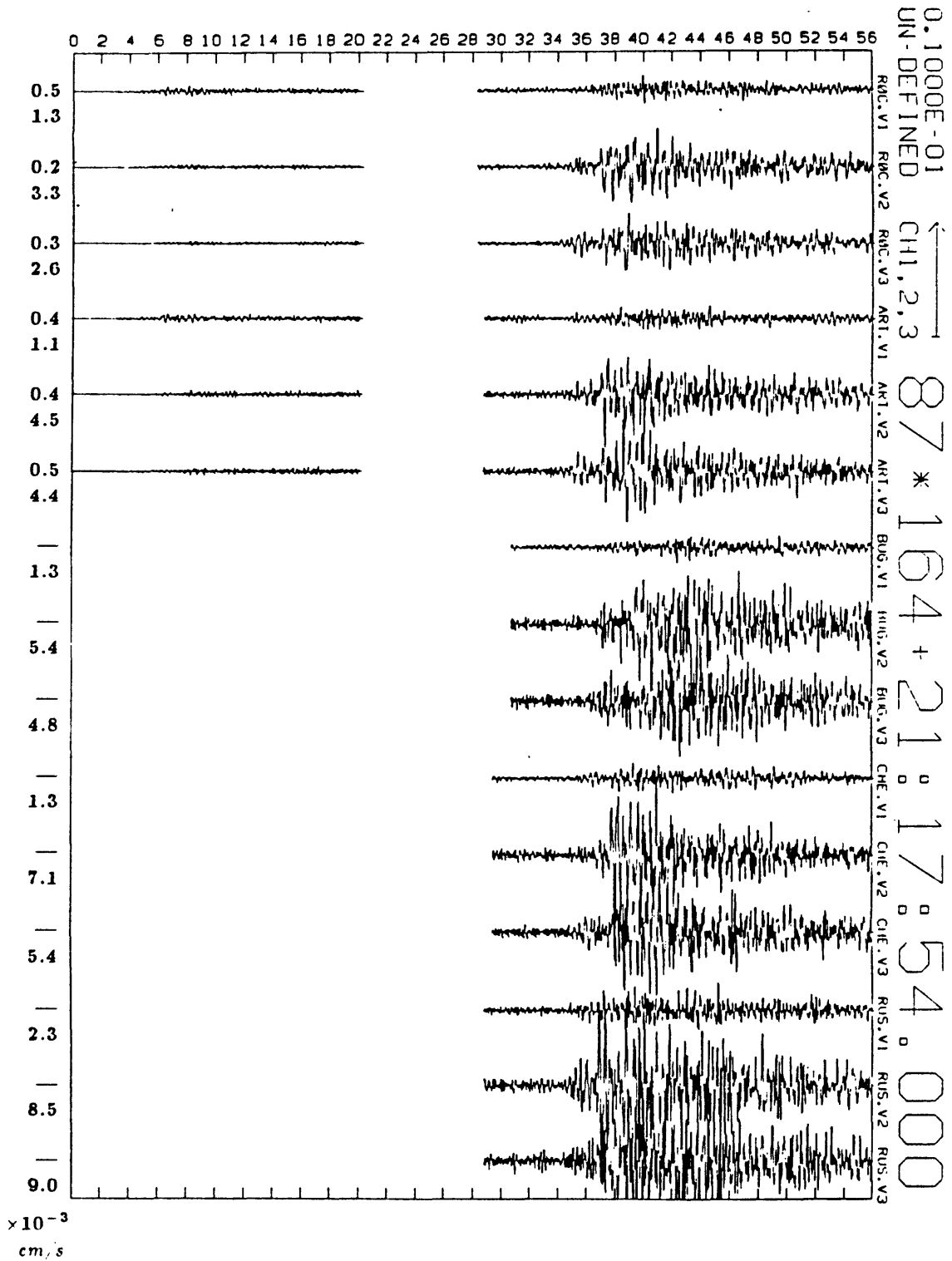
FIGURE 3: P- and S-waves of a magnitude 4.1_{mbLg} regional earthquake of the New Madrid Seismic Zone at ~ 270 km as recorded by 5 PADS stations of the Olney Aftershock Array. See Figure 2 caption on page 29 for a description of labeling conventions.
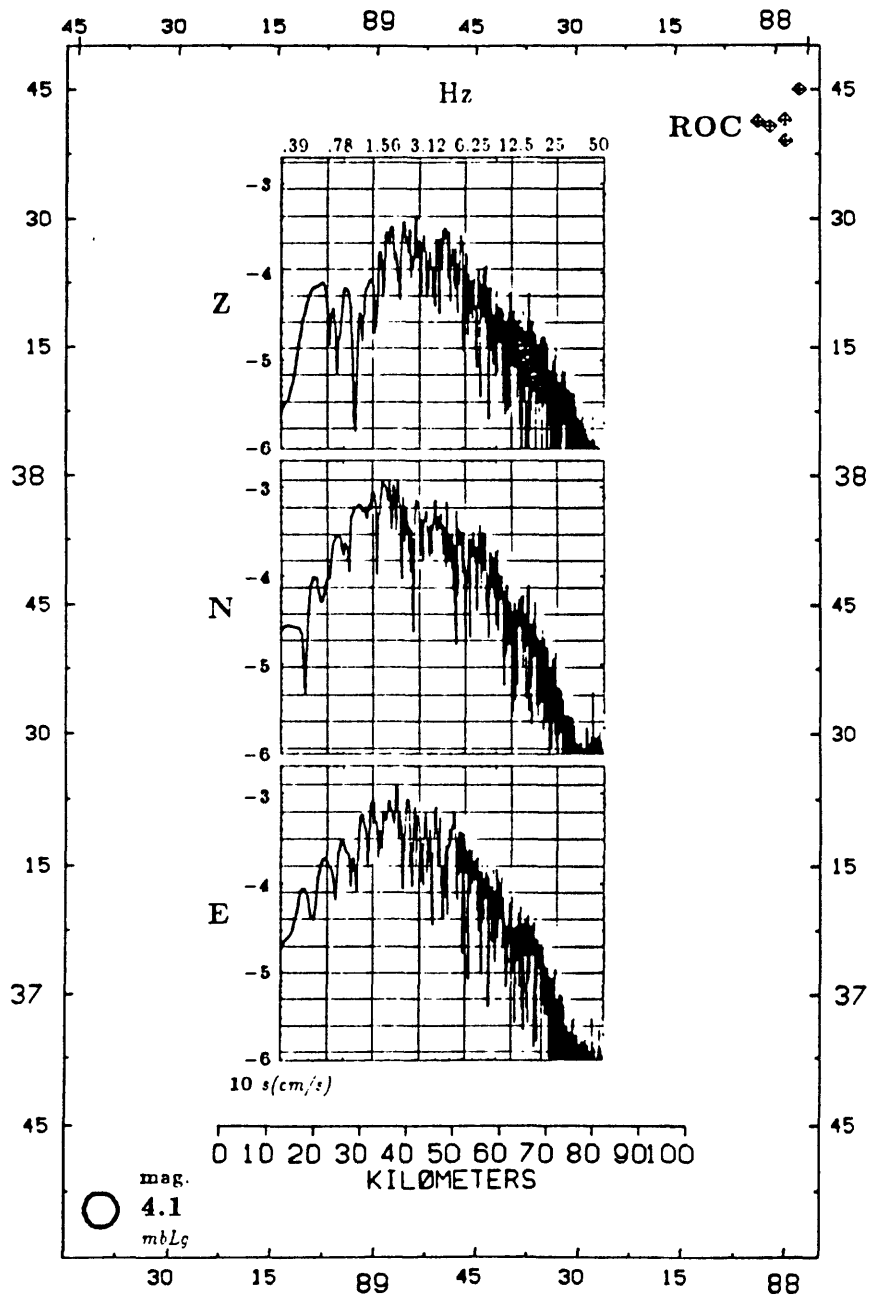
FIGURE 4: Source/Receiver map showing the locations of the 164+21:17 magnitude 4.1$_{mbLg}$ regional earthquake (*lower left corner*) and the 5 PADS stations (*upper right corner*; only Station ROC is labeled) of the USGS Olney Earthquake aftershock array which recorded S-waves from the regional event. The 3 log-log velocity spectra (*center* inset of map) are the 3 components respectively of the uncorrected whole-record spectra (see Figure 5 caption) of the S-wave vector-timeseries of the regional event recorded at Station ROC. In all spectra presented in this report, vertical lines are octaves and horizontal lines are power-of-2 (~ 6 dB) steps of spectral amplitude measured with respect to the peak spectral amplitude. In this figure, the frequencies of the octave divisions are marked in Hz at the top of the Z spectrum, and the 3 spectra are plotted on the same absolute scale and range which are defined by the power-of-10 exponents on the *left* (in units of pendulum motion).
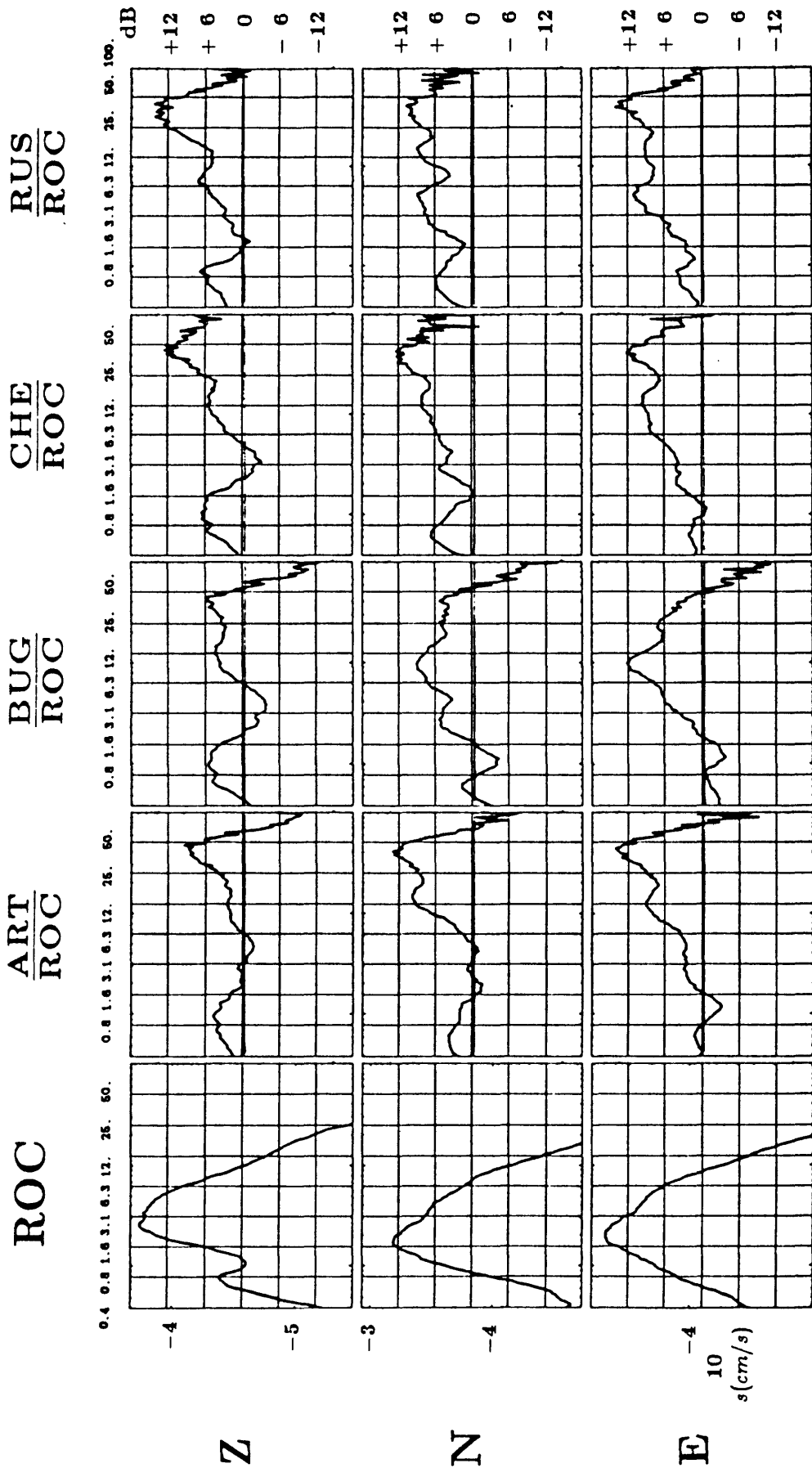
FIGURE 5 Log-log velocity spectra of Station ROC (a smoothed version of the spectra in Figure 4), and spectral ratios with respect to ROC of the other stations which also recorded the regional event. Both spectra and ratios have been smoothed after log-log transformation by averaging spectral amplitudes over octave-wide intervals (i.e., the division formed by two vertical lines; see Figure 4 caption for a description of spectrum labeling conventions). Each station's spectra were calculated from timeseries of the same duration which were created by truncating the originally recorded length to the length of the shortest timeseries (26 s at Station BUG). The bold horizontal lines define a ratio of 1.

63

APPENDIX

Computer Processing Procedures Applied to the Digital Seismograms Recorded
During The Olney, Illinois, Earthquake Aftershock Study

The USGS field program to monitor aftershocks of the Olney, Illinois, Earthquake generated a total of 24 digital tape cassettes. Commencing 21 Jun, within a week of the conclusion of the field program, the cassettes were played back and processed (by E.C.) on a microVAX operated by the BoGRA PADS/WFPS Project (Portable Autonomous Digital Seismograph/WaveForm Processing System). The suite of records that we present in this report represents a first-pass processing of the initial dataset which consists of more than 519 individual station/trigger records. This is a minimum value of the total number of trigger records potentially contained by the cassettes because an estimated 5-10% of the total have not been read due to hardware errors during playback (some portion of which may be subsequently recovered).

The primary function of the management aspect of the data processing is the separation of the waveform records into two categories: signal (containing useful seismic information) and noise (i.e., false triggers). After playback and transformation of the data into "DR-100 Format" files, an "ordered-arrival" list of all the corresponding "DR-100 Format" filenames ordered by trigger time was created. Two automatic computer methods were then used to distinguish scientifically useful earthquake records from the overall datamass. First, the list was analyzed for simultaneity of trigger within a 30 s time window (30 s was chosen so as to include both P- and S-phases of regional events from the New Madrid Seismic Zone which is roughly 300 km away), and the filenames of triggers which were coincident in that time were annotated with the number of simultaneous arrivals (station triggers; see Table II). Second, the trigger times of the ordered-arrival list were correlated (checked for the same minute) with a set of 43 event times determined from a first-pass inspection of the smoked-drum records, and the correlated trigger times were flagged (55 triggers were correlated with 24 event times). The time series of all records which were: EITHER members of an arrival group consisting of at least 2 triggers within a 30 s window, OR were correlated with an observed event time, OR both; were then automatically plotted. These plots were inspected to confirm that they represented seismic events and not coincidental false triggers or thunderclaps traveling across the array with a phase velocity of sound in air. The false trigger or uncorrelated filename entries were removed, and the resulting "verified ordered-arrival" list defined the first-pass suite of valid seismograms which is presented in this report.

As a model of the false triggers generated by the thunderstorms, assume tht each of 3 PADS is randomly triggering once a minute (60 s) when averaged over a 30-minute period of intense thunderstorm activity (i.e., 30 minutes represents the time until either the intensity of the storm abates or the cassette, which has a maximum capacity of 30-50 triggered records of 30 s

```
163+ 0
163+ 1
163+ 2
163+ 3
163+ 4
163+ 5   |1111
163+ 6
163+ 7
163+ 8
163+ 9   |1
163+10
163+11   |111
163+12
163+13
163+14
163+15   |1111
163+16
163+17   |1.
163+18   |1
163+19
163+20   |2211
163+21   |11111
163+22   |111
163+23   |111111122······1111111111122112222211111122333111111111
164+ 0   |111221111111111111
164+ 1
164+ 2   |1
164+ 3
164+ 4
164+ 5
164+ 6   |1
164+ 7
164+ 8   |1
164+ 9
164+10
164+11
164+12
164+13
164+14   |11
164+15   |1
164+16   |11
164+17   |1 1111
164+18   |1 1
164+19   |113331·4444
164+20   |11221 11
164+21   |55··555122112211111222222111221221 1
164+22   |1221 12233·322333.1:122122:2233311:111122:1113331122333:122221222222.122111:11111111111111111111:
164+23   |11111122111221
165+ 0   |11111111111111111:1
165+ 1   |11
165+ 2
165+ 3   |1
165+ 4   |111
165+ 5   |1
165+ 6
165+ 7   |1
165+ 8
165+ 9
165+10
165+11
165+12   |1
165+13   |111
165+14   |1.1
165+15   |1
165+16
165+17   |1333
165+18   |1 333
165+19   |1
165+20   |1
165+21   |11
165+22   |11
165+23   |1
166+ 0   |1
166+ 1   |1 1
166+ 2   |1
166+ 3   |333
166+ 4   |:
166+ 5   |55555
166+ 6
166+ 7   |2211
166+ 8   |1555551
166+ 9   |555554444
166+10
166+11   |1
166+12   |111
166+13   |1111
166+14   |111111111
166+15   |11111
166+16   |1444411111
166+17   |22111
166+18   |111111
166+19   |11··1144441113332211111
166+20   |11111
166+21   |11
166+22   |22111
166+23   |11.1122111111111111:111:111
167+ 0   |1111
167+ 1
167+ 2
167+ 3   |11122
167+ 4
167+ 5
167+ 6   |22
167+ 7
167+ 8   |22
167+ 9
167+10
167+11
167+12   |1
167+13   |111
167+14   |111
167+15   |11
167+16
167+17   |11111
167+18   |1
167+19   |1
167+20   |22
167+21   |11
167+22   |11111
167+23   |1
168+ 0   |111111
168+ 1   |11
168+ 2   |11
168+ 3
168+ 4   |1
168+ 5
168+ 6
168+ 7
168+ 8
168+ 9
168+10   |1
168+11   |11
168+12   |111
```

FIGURE A1: Histogram of total number of triggers per hour during the period of PADS deployment: 163+05:00 —→ 168+12:00. Each digit (1-5) or colon (:) represents a single PADS trigger at a single station. The values of the digits correspond to the number of distinct PADS stations which triggered within a 30 second time window. If the same PADS triggered more than once within a given 30 s window, its first trigger is assigned the appropriate digit, and subsequent triggers are assigned a colon. Note the two periods of intense thunderstorm activity, 163+23:00 —→ 164+00:00 and 164+22:00 —→ 165+00:00, which are followed by periods of few triggers because the cassettes had exhausted their tape capacity.